

NAVAL POSTGRADUATE SCHOOL
MONTEREY, CALIFORNIA

2

AD-A277 209



S DTIC
ELECTE
MAR 25 1994
F **D**

THESIS

*Original contains color
plates: All DTIC reproductions
will be in black and
white*

TRANSPORTABILITY ANALYSIS OF THE M119
HOWITZER IN THE FIRING CONFIGURATION

by

Ole Knudson

September, 1993

Thesis Advisor:

Anthony J. Healey

Approved for public release; distribution is unlimited



94-09255

94 3 24 086

REPORT DOCUMENTATION PAGE			Form Approved OMB No. 0704-0188	
<small>Public reporting burden for this collection of information is estimated to average 1 hour per response, including the time for reviewing instructions, searching existing data sources, gathering and maintaining the data needed, and completing and reviewing the collection of information. Send comments regarding this burden estimate or any other aspect of this collection of information, including suggestions for reducing this burden, to Washington Headquarters Services, Directorate for Information Operations and Reports, 1215 Jefferson Davis Highway, Suite 1204, Arlington, VA 22202-4302 and to the Office of Management and Budget, Paperwork Reduction Project (0704-0188), Washington, DC 20503.</small>				
1. AGENCY USE ONLY (Leave blank)		2. REPORT DATE SEPTEMBER 1993		3. REPORT TYPE AND DATES COVERED MASTER'S THESIS
4. TITLE AND SUBTITLE TRANSPORTABILITY ANALYSIS OF THE M119 HOWITZER IN THE FIRING CONFIGURATION			5. FUNDING NUMBERS	
6. AUTHOR(S) OLE KNUDSON				
7. PERFORMING ORGANIZATION NAME(S) AND ADDRESS(ES) NAVAL POSTGRADUATE SCHOOL MONTEREY, CA 93943-5000			8. PERFORMING ORGANIZATION REPORT NUMBER	
9. SPONSORING / MONITORING AGENCY NAME(S) AND ADDRESS(ES)			10. SPONSORING / MONITORING AGENCY REPORT NUMBER	
11. SUPPLEMENTARY NOTES The views expressed in this thesis are those of the author and do not reflect the official policy or position of the Department of Defense or the U.S. Government.				
12a. DISTRIBUTION / AVAILABILITY STATEMENT APPROVED FOR PUBLIC RELEASE; DISTRIBUTION IS UNLIMITED			12b. DISTRIBUTION CODE	
13. ABSTRACT (Maximum 200 words) This study was undertaken to determine if the US Army's M119 Howitzer could be safely towed in the "firing" position using the existing A-Frame brace to support the gun tube during movement. A computer model of the howitzer was developed that would predict motions of the howitzer and consequently, loads on critical components. The results obtained from this computer model were validated by comparing them to actual data obtained from an instrumented test done on the howitzer at Aberdeen Proving Grounds, Md. The validated model was used to predict the "worst case" loads on the howitzer's A-Frame and the T-Bar during movement in the "firing" position. The maximum predicted stresses in the A-Frame and the T-Bar from the "worst case" loads were compared to the yield stress. These comparisons showed that the A-Frame and T-Bar were strong enough to withstand the "worst case" predicted loads that would be caused by towing the M119 Howitzer in the "firing" position.				
14. SUBJECT TERMS HOWITZER AND TRANSPORTING TOWED VEHICLES			15. NUMBER OF PAGES 146	
			16. PRICE CODE	
17. SECURITY CLASSIFICATION OF REPORT UNCLASSIFIED	18. SECURITY CLASSIFICATION OF THIS PAGE UNCLASSIFIED	19. SECURITY CLASSIFICATION OF ABSTRACT UNCLASSIFIED	20. LIMITATION OF ABSTRACT UL	

Approved for public release; distribution is unlimited.

**TRANSPORTABILITY ANALYSIS OF THE M119
HOWITZER IN THE FIRING CONFIGURATION**

b y

OLE KNUDSON

Captain, United States Army
B.S. United States Military Academy, 1982


Submitted in partial fulfillment of the
requirements for the degree of

MASTER OF SCIENCE IN MECHANICAL ENGINEERING
from the

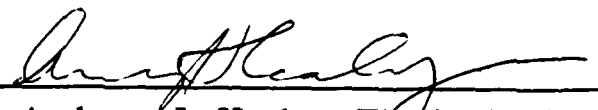
NAVAL POSTGRADUATE SCHOOL

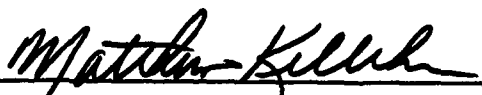
September 1993

Author:


Ole Knudson

Approved by:


Anthony J. Healey, Thesis Advisor


Matthew D. Kelleher, Chairman
Department of Mechanical Engineering

ABSTRACT

This study was undertaken to determine if the US Army's M119 Howitzer could be safely towed in the "firing" position using the existing A-Frame brace to support the gun tube during movement. A computer model of the howitzer was developed that would predict motions of the howitzer and consequently, loads on critical components. The results obtained from this computer model were validated by comparing them to actual data obtained from an instrumented test done on the howitzer at Aberdeen Proving Grounds, Md. The validated model was used to predict the "worst case" loads on the howitzer's A-Frame and the T-Bar during movement in the "firing" position. The maximum predicted stresses in the A-Frame and the T-Bar from the "worst case" loads were compared to the yield stress. These comparisons showed that the A-Frame and T-Bar were strong enough to withstand the "worst case" predicted loads that would be caused by towing the M119 Howitzer in the "firing" position.

Accession For	
NTIS CRA&I	<input checked="" type="checkbox"/>
DTIC TAB	<input type="checkbox"/>
Unannounced	<input type="checkbox"/>
Justification	
By	
Distribution /	
Availability Codes	
Dist	Avail and/or Special
A-1	

TABLE OF CONTENTS

I. INTRODUCTION.....	1
A. GENERAL.....	1
B. BACKGROUND.....	1
C. METHOD OF ANALYSIS.....	2
II. HUMMV/HOWITZER SYSTEM COMPUTER MODEL.....	4
A. HUMMV/HOWITZER SYSTEM PARAMETERS.....	4
1. HUMMV and Howitzer Tires.....	7
2. HUMMV Suspension System.....	7
3. Howitzer Suspension System.....	8
4. A-Frame/T-Bar Stiffness.....	17
5. Equilibrator Springs.....	17
6. Elevating Clutch.....	17
7. HUMMV Component Mass Properties.....	18
8. Howitzer Component Mass Properties.....	18
9. Length Properties.....	19
B. EQUATIONS OF MOTION (EOM).....	19
1. Generalized Coordinates (q_i).....	22
2. Kinetic Energy (T).....	26
3. Potential Energy (U).....	28
4. Generalized Power Lost Due to Damping Forces (F).....	30
5. External Forces (Q_i).....	31
6. Assembling Lagrange's Equation.....	32
C. HUMMV/HOWITZER NUMERICAL INTEGRATION.....	32
1. Transformation to 1st Order Equations.....	32
2. Integration Difficulties.....	34
III. ROADWAY INPUTS.....	36
A. WASHBOARD COURSE.....	36
B. "WORST CASE" POTHOLE COURSE.....	39

IV. MODEL RESULTS.....	41
A. WASHBOARD COURSE RESULTS.....	42
1. Results at 3.75 MPH.....	43
2. Results at 5.0 MPH.....	43
3. Results at 5.25 MPH.....	43
B. NATURAL FREQUENCIES AND MODE SHAPES.....	50
C. "WORST CASE" POTHOLE COURSE RESULTS.....	50
V. STRUCTURAL ANALYSIS.....	52
A. A-FRAME CALIBRATION.....	52
1. A-Frame Instrumentation.....	53
2. Support Equipment.....	53
3. Load Cells.....	56
4. Calibration Procedures.....	56
5. Calibration Factor.....	58
6. A-Frame Stiffness.....	60
7. Observations.....	61
B. STRESS ANALYSIS.....	61
1. T-Bar Stress.....	62
2. A-Frame Stress.....	64
3. Worst Case Stress and Factors of Safety.....	66
VI. INSTRUMENTED TEST.....	67
A. INSTRUMENTATION.....	67
1. Accelerometers.....	67
2. Single Strain Gages.....	69
3. Other Gages.....	69
B. TEST COURSES.....	72
1. Belgian Block Course.....	72
2. Six Inch Washboard Course.....	72
3. Cross Country Course Number 1.....	73
4. Cross Country Course Number 3.....	73
C. TEST PROCEDURES.....	74

D. TEST RESULTS AND DISCUSSION.....	74
1. Time History Results.....	75
2. Frequency Domain.....	84
3. Other Results.....	91
VII. CONCLUSIONS/RECOMMENDATIONS.....	96
A. CONCLUSIONS.....	96
B. RECOMMENDATIONS.....	97
APPENDIX A. SYSTEM PARAMETER VALUES.....	98
APPENDIX B. MATRICES FOR EQUATIONS OF MOTION.....	101
APPENDIX C. NUMERICAL INTEGRATION COMPUTER CODE	104
APPENDIX D. POT HOLE COURSE COMPUTER CODE.....	108
APPENDIX E. NATURAL FREQUENCIES AND MODE SHAPES.....	113
APPENDIX F. A-FRAME CALIBRATION DATA.....	114
APPENDIX G. HOWITZER ORIENTATION PICTURES AND DIAGRAMS.....	123
LIST OF REFERENCES.....	127
INITIAL DISTRIBUTION LIST.....	128

LIST OF FIGURES

2-1	HUMMV/Howitzer Model Components.....	6
2-2	Force vs Velocity Plot for the Front HUMMV Shock.....	9
2-3	Force vs Velocity Plot for the Rear HUMMV Shock.....	10
2-4	Torsional Spring Stiffness for Serial No. 22 (Upward Motion)....	12
2-5	Torsional Spring Stiffness for Serial No. 22 (Downward Motion).....	13
2-6	Torsional Spring Stiffness for Serial No. 27 (Upward Motion)....	14
2-7	Torsional Spring Stiffness for Serial No. 27 (Downward Motion).....	15
2-8	Force vs Velocity Plot for the Howitzer Shock.....	16
2-9	Length Properties for the HUMMV/Howitzer System.....	20
2-10	Generalized Coordinates for the HUMMV/Howitzer System.....	23
2-11	Key Locations for the HUMMV/Howitzer System.....	25
3-1	Six Inch Washboard Course Wheel Inputs.....	38
3-2	"Worst Case" Pothole Profile and Axle Trace.....	40
4-1	Model Results for A-Frame Force at 3.75 MPH (Time History)..	44
4-2	Model Results for A-Frame Force at 3.75 MPH (FFT).....	45
4-3	Model Results for A-Frame Force at 5.0 MPH (Time History)....	46
4-4	Model Results for A-Frame Force at 5.0 MPH (FFT).....	47
4-5	Model Results for A-Frame Force at 5.25 MPH (Time History)..	48
4-6	Model Results for A-Frame Force at 5.25 MPH (FFT).....	49

4-7	Model Results for A-Frame Force for "Worst Case" Pothole at 15 MPH	51
5-1	Location of A-Frame Strain Gages.....	53
5-2	Vertical Configuration for A-Frame Test.....	55
5-3	Lateral Configuration for A-Frame Test.....	55
5-4	A-Frame Connection to Test Mount.....	57
5-5	A-Frame Apex Clamping Device.....	57
5-6	Balance of Forces on the A-Frame.....	58
5-7	T-Bar and A-Frame Assembly.....	62
5-8	T-Bar Cantilevered Beam Model.....	63
5-9	Stress Concentration Due to a Circular Hole in a Pipe Section....	65
6-1	Howitzer Instrumentation for APG Test.....	68
6-2	Location of the Elevating Mass Accelerometer.....	70
6-3	Location of T-Bar Strain Gages.....	71
6-4	APG Belgian Block Course.....	72
6-5	APG Six Inch Washboard Course.....	73
6-6	A-Frame Force at 3.75 MPH on the Washboard Course.....	77
6-7	Trail Vertical Acceleration at 3.75 MPH on the Washboard Course.....	78
6-8	A-Frame Force at 5.0 MPH on the Washboard Course.....	79
6-9	Trail Vertical Acceleration at 5.0 MPH on the Washboard Course.....	80
6-10	A-Frame Force at 5.25 MPH on the Washboard Course.....	81

6-11	Trail Vertical Acceleration at 5.25 MPH on the Washboard Course.....	82
6-12	A-Frame Force at 15 MPH on Cross Country Course Number 3.....	83
6-13	FFT of A-Frame Force at 3.75 MPH on the Washboard Course.....	85
6-14	FFT of Trail Vertical Acceleration at 3.75 MPH on the Washboard Course.....	86
6-15	FFT of A-Frame Force at 5.00 MPH on the Washboard Course.....	87
6-16	FFT of Trail Vertical Acceleration at 5.00 MPH on the Washboard Course.....	88
6-17	FFT of A-Frame Force at 5.25 MPH on the Washboard Course.....	89
6-18	FFT of Trail Vertical Acceleration at 5.25 MPH on the Washboard Course.....	90
6-19	Lateral Force from the APG Washboard Course at 3.75 MPH...	92
6-20	Lateral Force from the APG Washboard Course at 5.0 MPH.....	93
6-21	Lateral Force from the APG Washboard Course at 5.25 MPH...	94
6-22	Lateral Force from Cross Country Course Number 3 at 15 MPH.....	95
G-1	Towing in the Firing Position.....	123
G-2	Towing in Stowed Position.....	124
G-3	A-Frame/ T-Bar Support.....	124
G-4	T-Bar (View from the Top Down).....	125
G-5	Howitzer Wheels and Suspension.....	126

LIST OF TABLES

A-1	COMPUTER MODEL PARAMETER VALUES.....	99
E-1	NATURAL FREQUENCIES AND MODE SHAPES.....	113
F-1	VERTICAL TEST #1 A-FRAME CALIBRATION DATA.....	115
F-2	VERTICAL TEST #2 A-FRAME CALIBRATION DATA.....	117
F-3	LATERAL TEST #1 A-FRAME CALIBRATION DATA.....	119
F-4	LATERAL TEST #2 A-FRAME CALIBRATION DATA.....	121

NOMENCLATURE

<u>SYMBOL</u>	<u>DESCRIPTION</u>
HUMMV	Abbreviation for the howitzer prime mover
CG	Center of gravity of component masses
K_1	The combined spring stiffness of the two front HUMMV tires
K_2	The combined spring stiffness of the two front HUMMV suspension springs
K_3	The combined spring stiffness of the two rear HUMMV tires
K_4	The spring combined stiffness of the two rear HUMMV suspension springs
K_6	The combined spring stiffness of the two howitzer tires
K_7	The combined spring stiffness of the two howitzer torsional springs
K_A	The combined spring stiffness of the A-Frame and T-Bar
B_1	The combined damping constant for the two front HUMMV shock absorbers
B_2	The combined damping constant for the two rear HUMMV shock absorbers
B_3	The combined damping constant of the two howitzer shock absorbers
B_4	The rotational damping constant for the elevating clutch

M_1	The combined mass of the two front HUMMV wheels and suspension components
M_2	The combined mass of the two rear HUMMV wheels and suspension components
M_3	The mass of the HUMMV body when it is fully combat loaded
M_4	The mass of the howitzer wheel
M_5	The total mass of the howitzer trail/saddle
M_6	The mass of the howitzer elevating mass
I_1	The mass moment of inertia of the HUMMV for pitch motion about its CG
I_2	The mass moment of inertia of the howitzer trail/saddle mass about its CG
I_3	The mass moment of inertia of the elevating mass about the trunion
R_w	The static weight carried by the rear HUMMV wheels with the howitzer attached
F_w	The static weight carried by the front HUMMV wheels with the howitzer attached
L_1	The distance from the HUMMV CG to the connecting point of HUMMV front shocks and suspension springs
L_2	The distance from the HUMMV CG to the connecting point of HUMMV rear shocks and suspension springs
L_3	The distance from the HUMMV/howitzer hitch connection point to the HUMMV CG
L_7	The distance between the center of the HUMMV front and rear axles

L_8	The distance from the front HUMMV axle center to the howitzer axle center
L_{11}	The distance from the howitzer axle to the CG of the howitzer trail/saddle mass (M5)
L_{12}	The distance from the howitzer suspension spring and shock to the HUMMV/howitzer hitch connecting point
L_{13}	The horizontal distance from the trunion to the A-Frame connection point on the T-Bar
L_{16}	The horizontal distance from trunion to the HUMMV/howitzer hitch connection point
L_A	The distance from where the point A-Frame attaches to the saddle, to the trunion
L_{CG}	The distance from CG of the gun tube to the trunion
θ_0	The static angle made between the horizontal plane and the gun tube
ϕ_A	The angle made between the A-Frame and the gun tube
Z_1	The vertical displacement for the CG of front HUMMV wheel mass
Z_2	The vertical displacement for the CG of rear HUMMV wheel mass
Z_3	The vertical displacement of HUMMV CG
Z_4	The vertical displacement of the CG of howitzer wheel mass
θ_1	The pitch angle of the HUMMV about its CG

- θ_2 The pitch angle of the howitzer trail/saddle mass about its CG
- θ_3 The rotation of gun tube about the trunion.

ACKNOWLEDGEMENT

I thank Professor Healey for all his help in preparing this study. LTC Melvin Miller and Mr. Jerome Nathan of AMCCOM, Rock Island Arsenal, IL, the study sponsors, provided the funding to the Naval Postgraduate School for the study. CPT Dave Anderson's and CPT Steve Roger's efforts were instrumental in developing an original simplified model of just the howitzer, that served as the basis for the complete HUMMV/Howitzer system model I developed later and used to predict loads on the howitzer.

I. INTRODUCTION

A. GENERAL

The purpose of this study was to determine the feasibility of transporting the M119 howitzer in the firing position over terrain and at speeds used during normal tactical operations. The end objective was to determine if costly design changes would be required to safely permit towing the M119 Howitzer in the firing position. The approach used was to model the vertical plane dynamics of the towing vehicle (HUMMV) and the howitzer, model representative terrain inputs to the wheels in the form of potholes, and to perform experiments to validate the model. It is proven that the simulation model is reasonable and it follows that stresses in the critical components are not expected to warrant redesign.

B. BACKGROUND

The M119 Howitzer is a British designed howitzer that is currently being built at Rock Island Arsenal (RIA), Illinois and fielded to US Army Field Artillery units. The M119 Howitzer operational manuals specify towing procedures that require the gun tube to be placed in the stowed position when moving the howitzer during tactical operations. These towing procedures are different and more difficult to implement than those used for all other towed howitzers in the US Army. All other US Army towed howitzers are towed during tactical operations with the gun tube in the firing

position, facilitating rapid emplacements and displacements that are required for successful tactical operations.

The M119 Howitzer has an existing A-Frame brace which can support the gun tube when the howitzer is towed in the firing position. The primary concern of this study was whether or not the A-Frame and the T-Bar structure on the howitzer's trail section, to which the bottom of the A-Frame brace connects, will be strong enough to support the loads generated when towing the howitzer over rough terrain. This study also addresses concerns about trail loads on the howitzer. This study does not evaluate rollover stability for the M119 Howitzer when towing in the firing position.

The terrain that the HUMMV/Howitzer system can traverse is clearly limited by the terrain the HUMMV can negotiate, therefore, the M119 Howitzer and HUMMV have been evaluated as a system. A dynamic simulation model of this system was seen to be a necessary tool to aid in making design decisions from a rational viewpoint and is the basis of this study.

C. METHOD OF ANALYSIS

To analyze the M119 Howitzer a computer model of the HUMMV/Howitzer system was developed to predict the response of the system to roadway inputs. This computer model treats the major mass elements of the HUMMV/Howitzer system as lumped masses to develop vertical plane heave and pitch equations of motion for the system. The development of this computer model is contained in Chapter II. To drive the computer simulation model, terrain models

were developed for both a "worst case" trench type pothole and a sinusoidal "washboard" roadway. Details on the development of these roadway inputs are contained in Chapter III. Chapter IV contains the results of driving the computer model over the roadway inputs. Chapter V explains the structural analysis that was used to determine the maximum stress in the A-Frame and the T-Bar. Chapter V also contains the procedures and results of calibrating an A-Frame that was used as a load cell for an instrumented dynamic test. Chapter VI explains the conduct and the results of the instrumented test on the M119 Howitzer/HUMMV system that was conducted at Aberdeen Proving Grounds, Maryland in April 1993. Also, in Chapter VI the results of the model are compared to the experimental results from the instrumented test. This comparison showed reasonable correlation between the model and experimental results. Conclusions and recommendations based on this study are contained Chapter VII. The final recommendation is that towing in the firing position should be allowed.

II. HUMMV/HOWITZER SYSTEM COMPUTER MODEL

The computer model developed is based only on the heave and pitch equations of motion (EOM) for the HUMMV/Howitzer system. The reason for this simplification is that the lateral, yaw, and roll motions are much less significant for determining the forces in the A-Frame for the type terrain inputs considered by this study. While horizontal plane motions are key elements for the analysis of turns and rolling during transit, the concerns of this study indicate that a vertical plane model is adequate. The major mass groups of the HUMMV/Howitzer were treated as lumped masses in the development of the equations of motion. The equations of motion were developed using Lagrange techniques.

A. HUMMV/HOWITZER SYSTEM PARAMETERS

The primary sources of information for system parameters for the HUMMV and howitzer were the US Army Tank-Automotive Command Research, Development & Engineering Center Technical Report No. 13337, [Ref. 1], for HUMMV data and US Army Combat Systems Test Activity, APG, Report No. P-83179, [Ref. 2], for the M119 Howitzer data. Additionally, many system parameters were determined from direct measurement on the HUMMV and howitzer or from design diagrams, or obtained from the study sponsor at Rock Island Arsenal (RIA). For readers of this study that are unfamiliar with the components of the M119 Howitzer, Appendix G contains

several diagrams that depict the howitzer components that are important for this study.

The system parameters used for the HUMMV are based on using the Model No. M1069 HUMMV as the prime mover for the M119 Howitzer. The cargo loading of the HUMMV significantly effects its center of gravity and consequently effects all of the HUMMV's system parameters which are dependent on its center of gravity. Modeling was therefore limited to using the same cargo loading configuration that was used in [Ref. 1] and other loading effects were ignored. These HUMMV simplifications are justified because for this computer model the HUMMV serves primarily as the driving force at the howitzer hitch causing pitching motions of the entire howitzer and we are not concerned with the loading of HUMMV components. The major components of the HUMMV/Howitzer system computer model are identified in Figure 2-1 below.

In the model, the tires act as linear springs which provide force inputs to the HUMMV and howitzer wheels, based on the terrain over which the model was "driven". The suspension systems for both the HUMMV and the howitzer are modeled as springs and dampers connected in parallel. The A-Frame and T-Bar are modeled as a set of stiff springs connected in series. The following paragraphs provide more detail on the modeling of the individual components and the determination of appropriate parameter values. Appendix A provides a listing of the numerical values, units, and the symbols used for each system parameter in the computer model. The parameter values for those components with identical components on

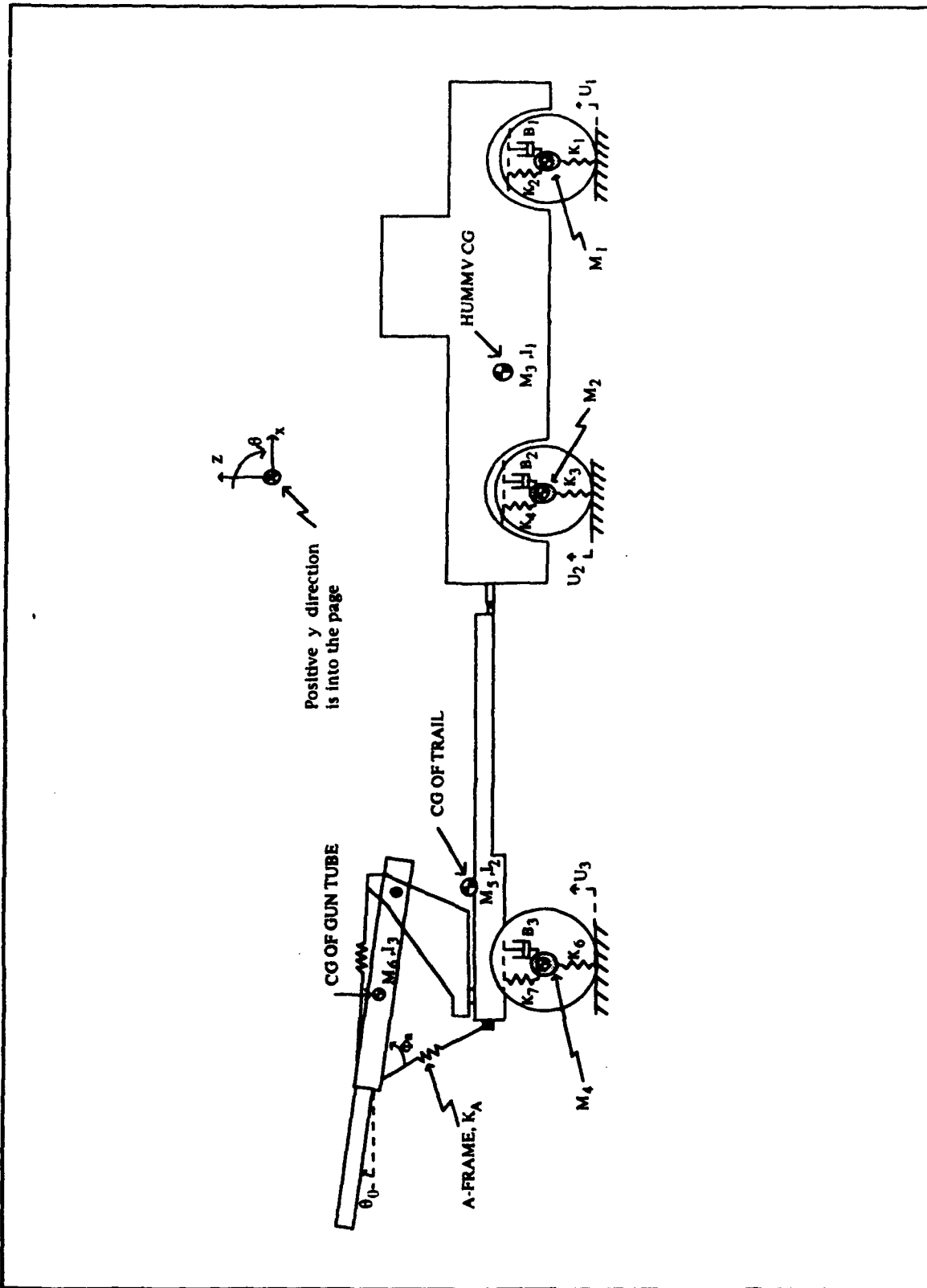


Figure 2-1 HUMMV/Howitzer Model Components

the right and left sides of the system (wheels and suspension components) are multiplied by two. The values in Appendix A for these components reflect the effects of both sides.

1. HUMMV and Howitzer Tires

The HUMMV has the same tires on the front and rear, however, the front and rear tire pressure is different (20 psi vs 30 psi) resulting in the rear tire spring being much stiffer. The stiffness used for the HUMMV tires was obtained from normal force vs tire deflection data [Ref. 1]. The stiffness of the howitzer tire used in the model was estimated because no measured data on the howitzer tire stiffness was available.

The tires are modeled as linear springs which transmit a vertical force to the respective wheel masses proportional to the amount that the springs are stretched or compressed. The amount of force is determined by the relative dynamic displacement between the terrain input for the wheel and the center of mass of the wheel. If the tire leaves contact with the ground there will be no input from the terrain until it again returns to contact. To account for this loss of contact situation in the computer model, the tire spring force is set to the static weight that the tire supports when the tensile (decompressive) spring force exceeds the static weight on the tire. The tire springs are turned back on in the computer model when the conditions are met for road surface contact to be re-established.

2. HUMMV Suspension System

The HUMMV suspension system consists of a shock absorber and coil spring for each wheel. The shock absorber passes

through the middle of the coil spring. The force in the spring is linearly proportional to the relative displacement between the center of mass of the wheel and the attachment point on the HUMMV body. The values for the spring constants were obtained from Table 5-13 of [Ref. 1]. Precise modeling of the shock absorbers is difficult because they have a mid-stroke region and a hydraulic bump stop region. In the mid-stroke region the shock absorber force is linearly dependent on the relative velocity of the center of mass of the wheel and the attachment point on the HUMMV. However, the linear damping constant changes depending on whether the force in the shock absorber is tensile or compressive. When the shock absorber is compressed or stretched into the hydraulic bump stop region the damping of the shock absorber greatly increases. This sudden increase in damping causes problems in the integration routine that was used for the computer model. To overcome these problems and still account for the energy loss due to the increased damping in the hydraulic bump stop region, the mid-stroke linear damping constant obtained from [Ref. 1] was increased by 20% for both the front and rear shock HUMMV absorbers. Figures 2-2 and 2-3 shows the force versus velocity plots that were obtained from [Ref. 1] for the front and rear shock absorbers, respectively.

3. Howitzer Suspension System

Modeling the howitzer suspension system is more complicated than the HUMMV because it consists of a torsional spring and a shock absorber that is not vertically oriented. The torsional spring is modeled as a linear vertical spring that is connected to the

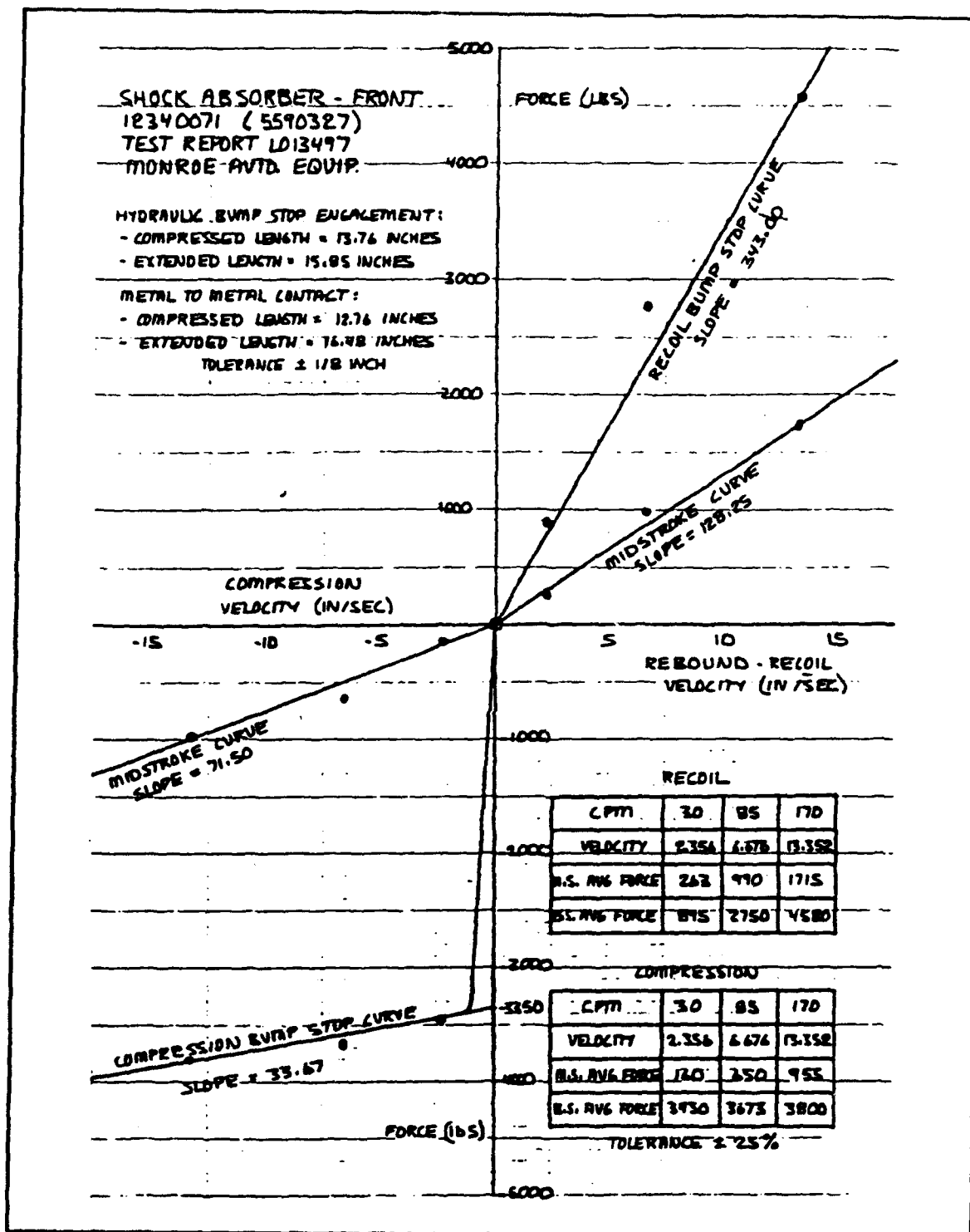


Figure 2-2 Force vs Velocity Plot for the Front HUMMV Shock

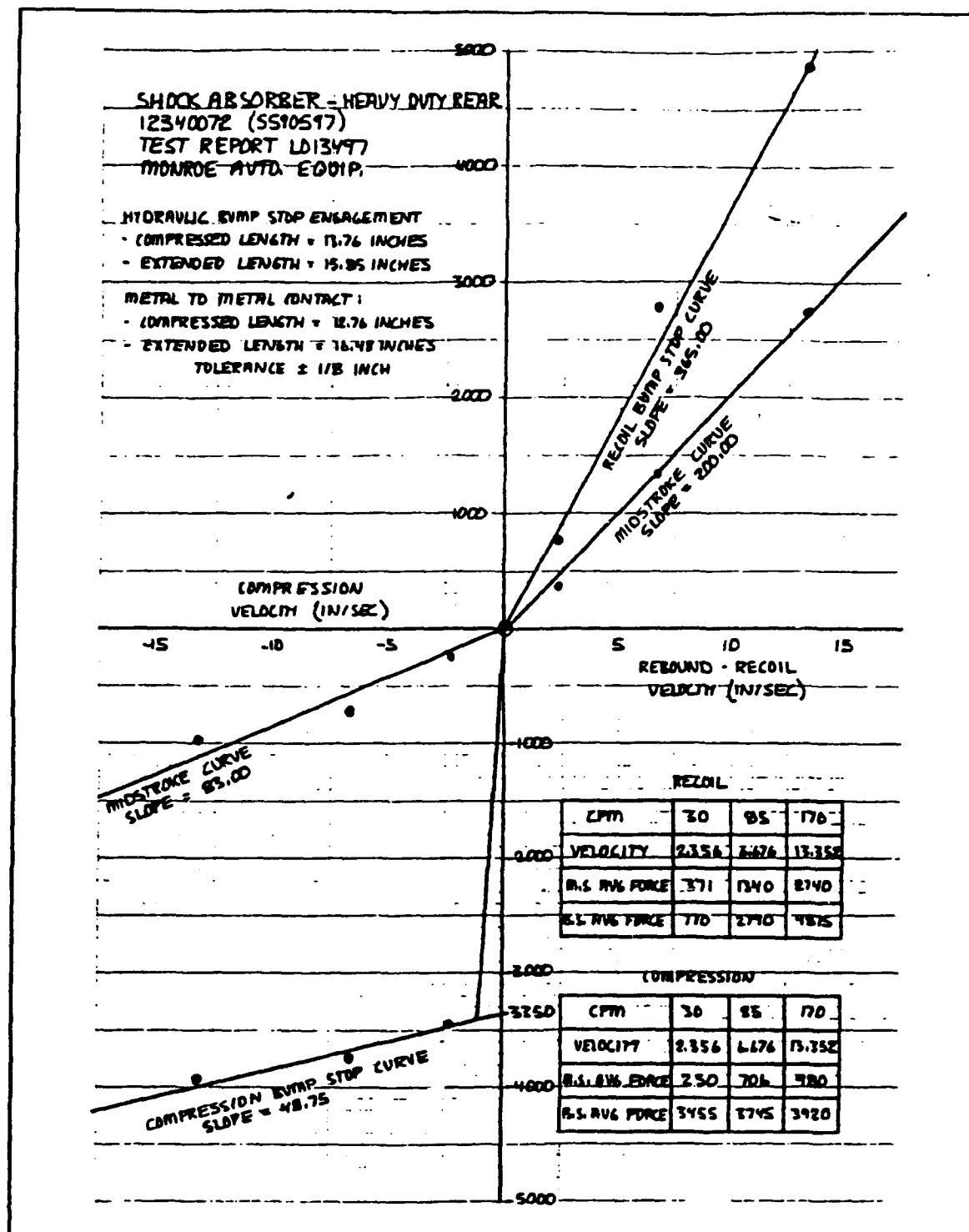


Figure 2-3 Force vs Velocity Plot for the Rear HUMMV Shock

center of mass of the howitzer wheel and attached to the howitzer trail directly above the wheel center of mass. The effective spring stiffness constant was calculated based on the measured data of the torsional spring stiffness. Figures 2-4 through 2-7 show the angular deflection versus vertical force plots that were contained in [Ref. 2]. Using the average torsional spring stiffness from this data and the length of the road arm, an angular rotation was converted to an equivalent vertical displacement at the end of the road arm. The spring constant for the model was then calculated by determining the constant value that must be multiplied times this vertical displacement at the end of the road arm, to produce a moment that is equivalent to that caused by the torsional spring for a specified angular rotation.

A similar procedure was used to model the howitzer's shock absorber as a vertical shock absorber with a linear damping constant that is velocity dependent. The attachment points for the ends of the shock absorbers in the model are the same as the modeled end points of the howitzer suspension spring. The actual non-vertical shock absorber force was transformed to a vertical force in the model by determining the amount of vertical force applied at the end of the road arm needed to produce an equivalent moment about the road arm pivot point. Like the HUMMV shock absorbers, the howitzer shock absorbers are non-linear and have different damping values for tension and compression that are accounted for in the computer model. This non-linear damping in the shock absorbers is a significant aspect of the computer model. The values

used for the shock absorber damping constants were determined from force versus velocity test data provided by RIA. Figure 2-8 shows the force versus velocity plot for the howitzer shock absorber.

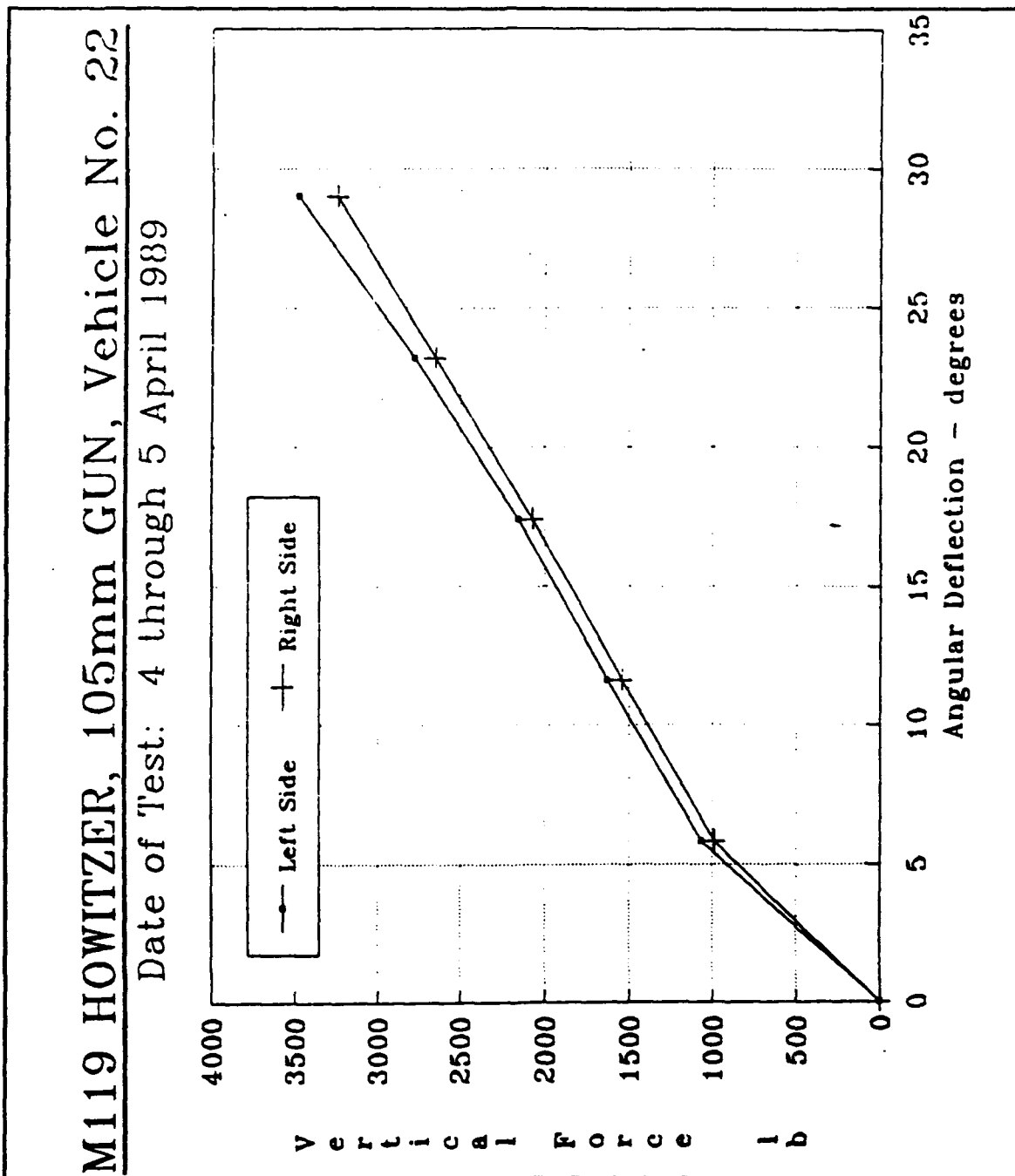


Figure 2-4 Torsional Spring Stiffness for Serial No. 22 (Upward Motion)

M119 HOWITZER, 105mm GUN, Vehicle No. 22

Date of Test: 4 through 5 April 1989

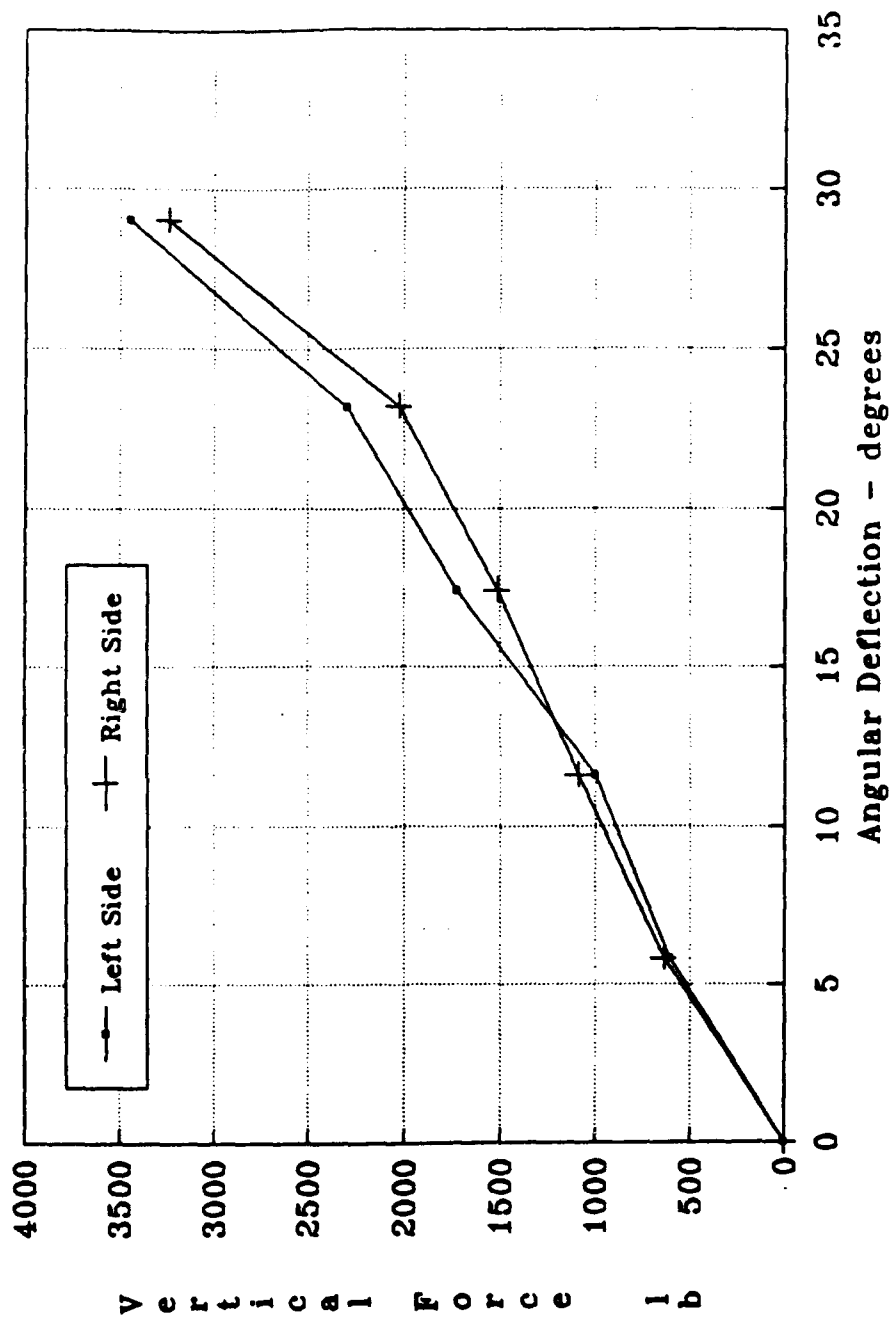


Figure 2-5 Torsional Spring Stiffness for Serial No. 22 (Downward Motion)

M119 HOWITZER, 105mm GUN, Vehicle No. 27

Date of Test: 25 April 1989

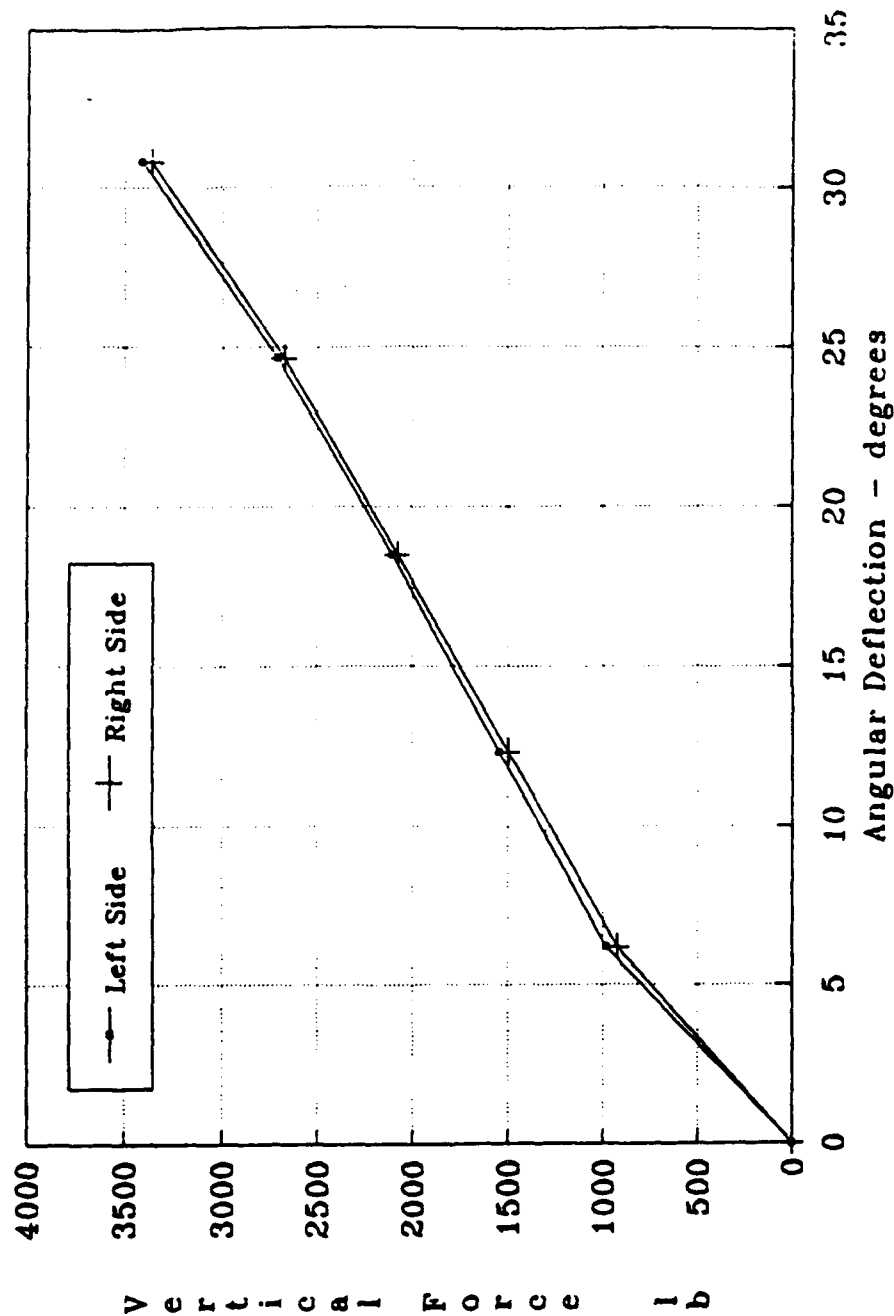


Figure 2-6 Torsional Spring Stiffness for Serial No. 27 (Upward Motion)

M119 HOWITZER, 105mm GUN, Vehicle No. 27

Date of Test: 25 April 1989

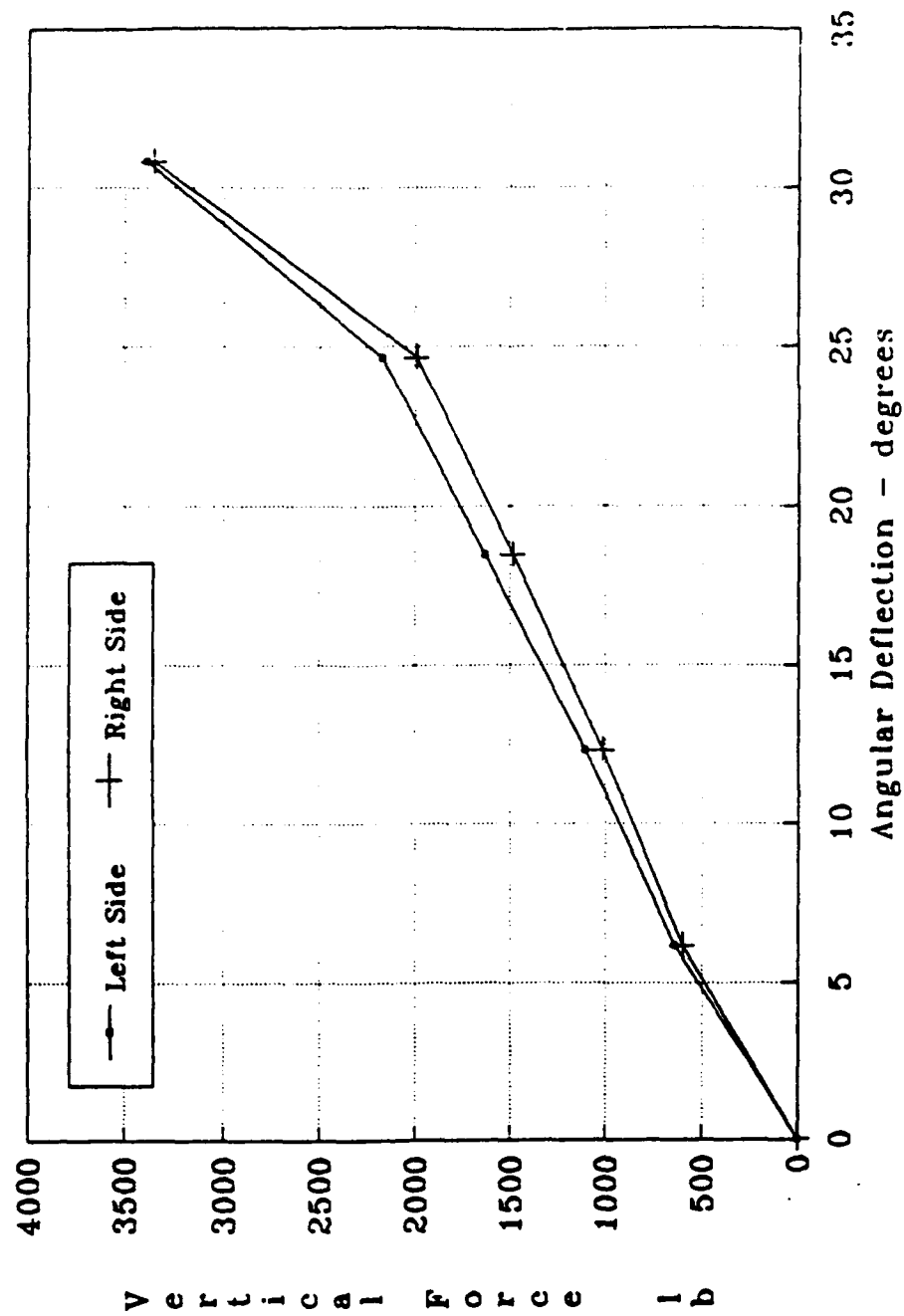


Figure 2-7 Torsional Spring Stiffness for Serial No. 27 (Downward Motion)

Howitzer Shock Absorber

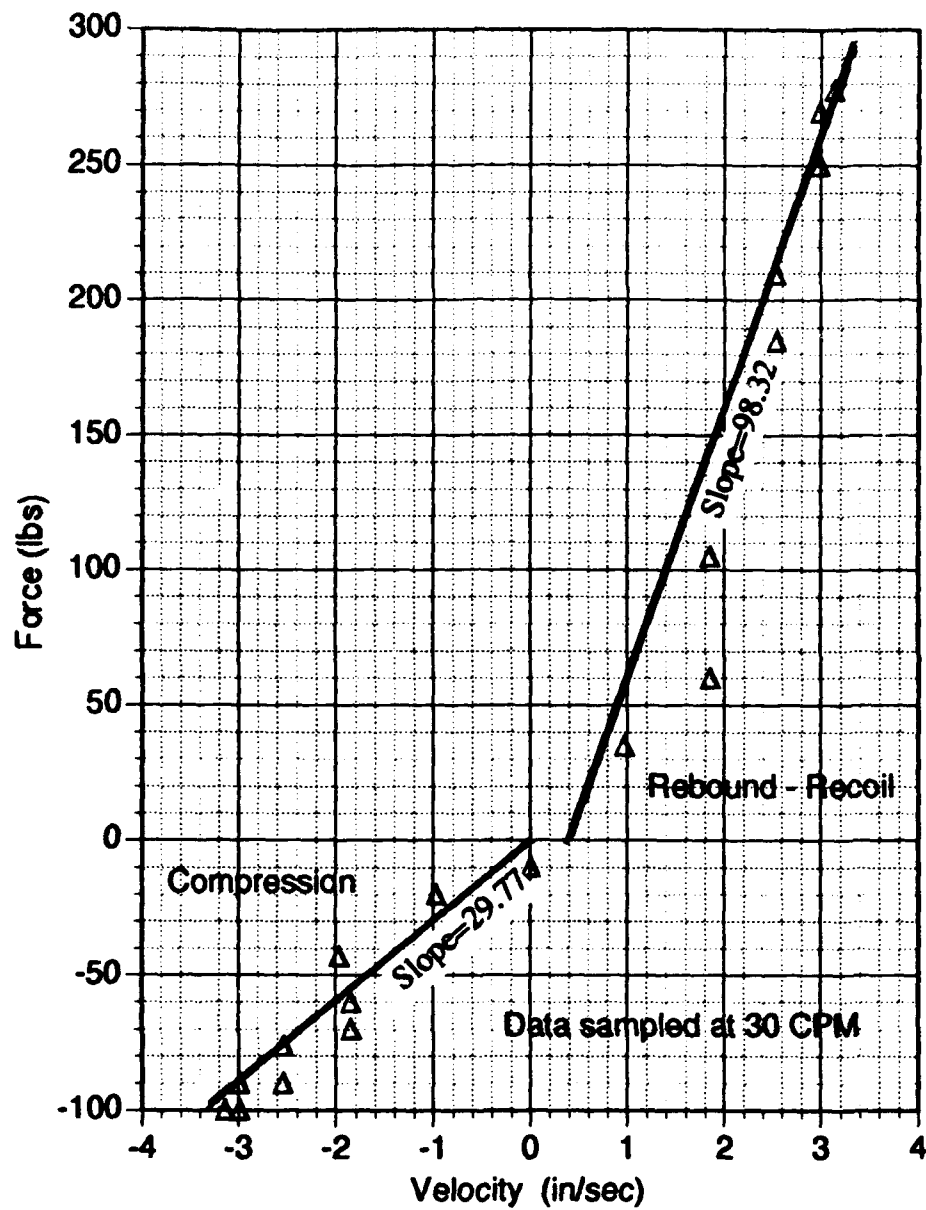


Figure 2-8 Force versus Velocity Plot for Howitzer Shock

4. A-Frame/T-Bar Stiffness

The A-Frame and T-Bar are modeled as stiff springs connected in series to determine a combined linear spring stiffness. The stiffness of the A-Frame was determined during the A-Frame calibration test (explained in Chapter V). The stiffness of the T-Bar was determined by using the principle of superposition of forces to determine the effective bending stiffness for the non-symmetric bending of the T-Bar that is caused by the A-Frame. This non-symmetric bending of the T-Bar results because the angle at which the A-Frame transmits forces and moments to the T-Bar is not perpendicular to an axis of symmetry of the T-Bar.

5. Equilibrator Springs

The equilibrator springs provide only small dynamic forces because their combined stiffness is nearly 1000 times less than the effective stiffness of the A-Frame/T-Bar assembly. Therefore, equilibrator springs are neglected in the computer model.

6. Elevating Clutch

The effects of the elevating clutch of the howitzer were neglected in the final computer model. It is believed backlash in the elevating mechanism gears will prevent the clutch from being activated while towing with the A-Frame attached because the relative rotation of the gun tube is very small. However, because of some uncertainty about the clutch several computer runs were made with clutch modeled as a linear torsional damper. The value of the torsional damper used in the model was estimated because no test data on the clutch was available. These model runs with the clutch

included, produced only slightly different results from the runs without the clutch included. Therefore, because of the previously mentioned belief that the clutch would not be activated, it was neglected in the final model.

7. HUMMV Component Mass Properties

The HUMMV is divided into three lumped masses, the HUMMV body mass and two wheel masses. The front and back HUMMV wheels are treated as having identical mass values in the model. Each wheel weight/mass includes the weight of the tire, wheel, shocks, suspension springs, and suspension support arms. The HUMMV body weight/mass varies dependent upon it's cargo load. The location of the center of gravity also can vary and is determined by the positioning of the cargo. Therefore, the values used in the computer model for the HUMMV mass, the mass moment of inertia for pitch, and lengths that are based dependent on the center of gravity, are estimated values. These estimated values are based on the same loading situation as was used in [Ref. 1]. The pitch mass moment of inertia for the HUMMV is about the center of gravity of the sprung HUMMV mass.

8. Howitzer Component Mass Properties

The howitzer is divided into three separate lumped masses in the model; the howitzer wheel masses, the elevating mass, and the combined trail/saddle mass. The wheel weight/mass includes the tire, rim, and approximately 30% of the road arm that rests on the wheel assembly. The elevating mass includes the gun tube, the cradle, the recoil system and all other parts that move the when the

gun is elevated about the trunion. The mass moment of inertia of the gun tube for rotation about the trunion was estimated using the approximate masses of all the elevating components. The center of gravity location for the elevating mass was estimated by RIA. The combined trail/saddle mass includes all of the gun mass except the elevating mass and the wheel mass. The center of gravity location for the trail/saddle mass and the pitching mass moment of inertia for the trail/saddle mass was estimated from design diagrams.

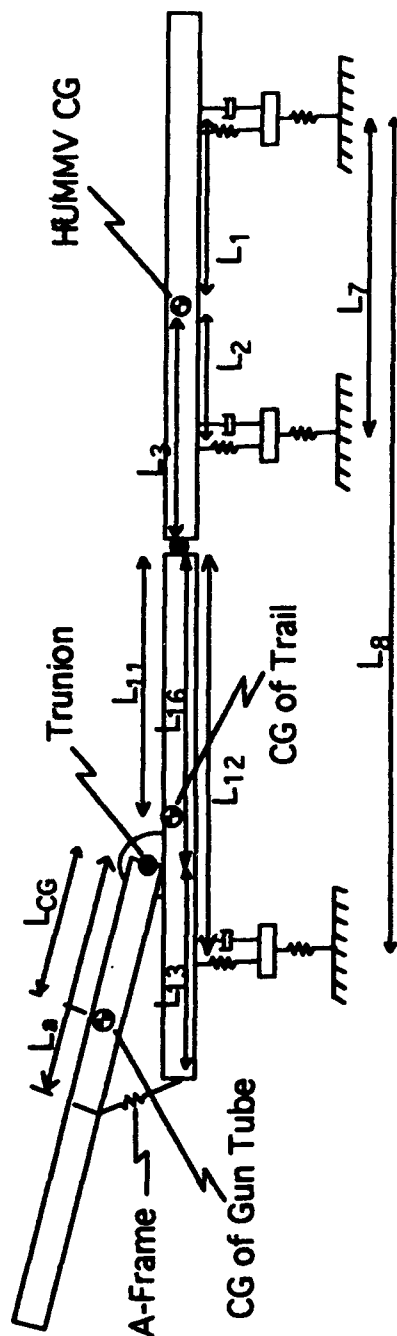
9. Length Properties

All lengths used in the computer model are identified in Figure 2-9 below. These length properties were determined either by direct measurements on the howitzer or by scaling from design diagrams.

B. EQUATIONS OF MOTION (EOM)

In this section the heave and pitch equations of motion (EOM) for the model are developed from Lagrange's equations using the HUMMV/Howitzer system parameters that were previously explained. Lagrange's equations require the determination of the system's total kinetic and potential energy and the power dissipated by the dampers, in terms of a set of generalized coordinates.

Throughout this development of the EOM, expressions are developed that are functions of generalized positions and velocities, angular displacements, angular velocities, and angular accelerations. To simplify the EOM with minimal loss of representational accuracy, these expressions are linearized using small angle approximations.



- L_1 : The distance from the CG of the HUMMV to the front suspension system
- L_2 : The distance from the CG of the HUMMV to the rear suspension system
- L_3 : The distance from the CG of the HUMMV to the howitzer hitch point
- L_7 : The distance from the front HUMMV wheel to the rear HUMMV wheel
- L_8 : The distance from the front HUMMV wheel to the howitzer wheel
- L_{11} : The distance from the howitzer hitch point to the CG of the howitzer trail
- L_{12} : The distance from the howitzer hitch point to the howitzer suspension
- L_{13} : The distance from the howitzer trunion to the howitzer T-Bar
- L_{16} : The distance from the howitzer hitch point to the howitzer trunion
- L_{CG} : The distance from the howitzer trunion to the CG of the Gun Tube
- L_a : The distance from the howitzer trunion to the A-Frame connection

Figure 2-9 Length Properties of HUMMV/Howitzer System

The sine of a small angle is approximated as just the angle ($\sin\theta=\theta$) and the cosine of a small angle is approximated as equal to one ($\cos\theta=1$). These approximations are valid because the pitch or angular rotations are predicted to be less than five degrees. Order of magnitude considerations are used to further simplify the EOM. Because the angular displacements are small their angular velocities and angular accelerations are also small. Therefore, any terms that contain an angular displacement, angular velocity, or angular acceleration multiplied times another angular displacement, angular velocity, or angular acceleration are neglected because these terms will be very small.

The general form of Lagrange's equations used is:

$$\frac{d}{dt}\left(\frac{\partial T}{\partial \dot{q}_i}\right) - \frac{\partial T}{\partial q_i} + \frac{\partial U}{\partial q_i} + \frac{\partial F}{\partial \dot{q}_i} = Q_i$$

where:

- q_i = generalized coordinates
- T = total kinetic energy of the system
- U = change in the potential energy of the system with respect to its potential energy in the static-equilibrium position
- F = the power dissipated by forces in dampers
- Q_i = the input force acting on the system.

The development of the above components of Lagrange's equation and the assembly of these components into the system's heave and pitch EOM follows. Due to the length of this development the reader is provided only the final results from each step. The intermediate multiplication's, differentiation's, and linearization's are omitted.

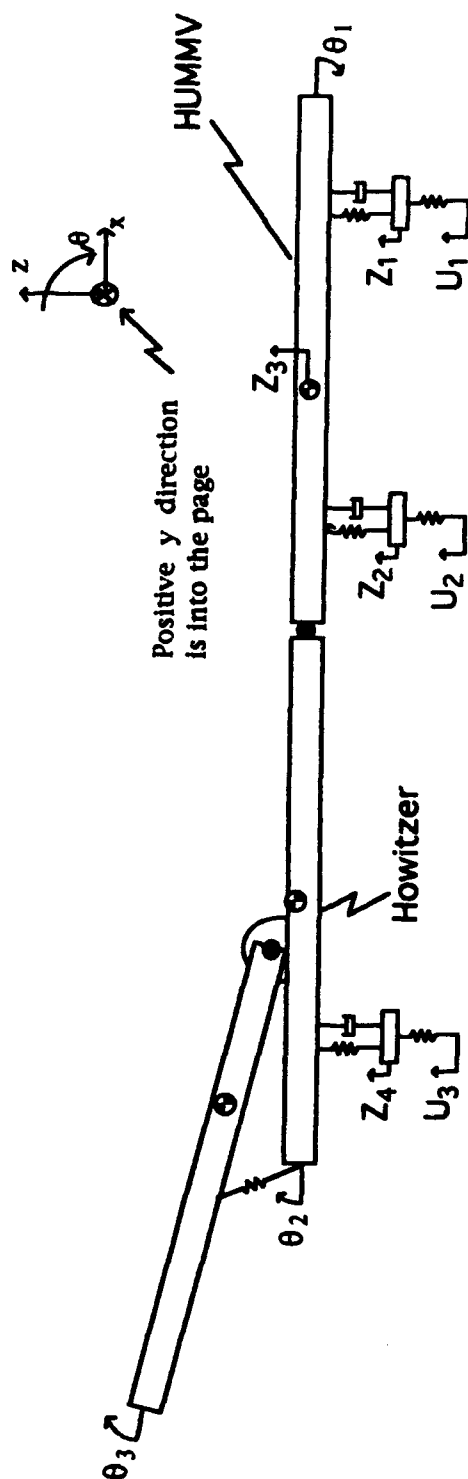
1. Generalized Coordinates (q_i)

The set of generalized coordinates, q_i , that was used to uniquely specify the motion of the HUMMV/Howitzer system are depicted on Figure 2-10 and are defined follows:

- * Z_1 & Z_2 : The vertical displacements for the front and rear HUMMV wheel masses, respectively.
- * Z_3 : The vertical displacement of the center of gravity of the HUMMV body.
- * Z_4 : The vertical displacements of the center of gravity of the howitzer wheel mass.
- * θ_1 : The pitch angle of the HUMMV body about its center of gravity.
- * θ_2 : The pitch angle of the howitzer trail/saddle mass about its center of gravity.
- * θ_3 : The absolute rotation of the gun tube.

As depicted on Figure 2-10, upward vertical motions and clockwise rotational motions are defined as positive. The equilibrium position for each of the generalized coordinates is the static equilibrium position for the respective components that are correlated to each of the generalized coordinates. In defining positions to key locations in the system unit vector notation of i , j , and k will be used corresponding to the x , y , and z axis directions of the Cartesian coordinate reference system shown on Figure 2-10.

The kinetic and potential energy of the system and the damping and input forces are all computed in terms of these



DEFINITION OF GENERALIZED COORDINATES:

- Z_1 & Z_2 : The vertical displacements for the front and rear HUMMV wheel masses.
- Z_3 : The vertical displacement of the center of gravity of the HUMMV body.
- Z_4 : The vertical displacements of the center of gravity of the howitzer wheel mass.
- θ_1 : The pitch angle of the HUMMV body about its center of gravity.
- θ_2 : The pitch angle of the howitzer trail/saddle mass about its center of gravity.
- θ_3 : The absolute rotation of the gun tube.

DEFINITION OF ROADWAY INPUTS:

- U_1 : The road input for the front HUMMV wheel
- U_2 : The road input for the rear HUMMV wheel
- U_3 : The road input for the howitzer wheel

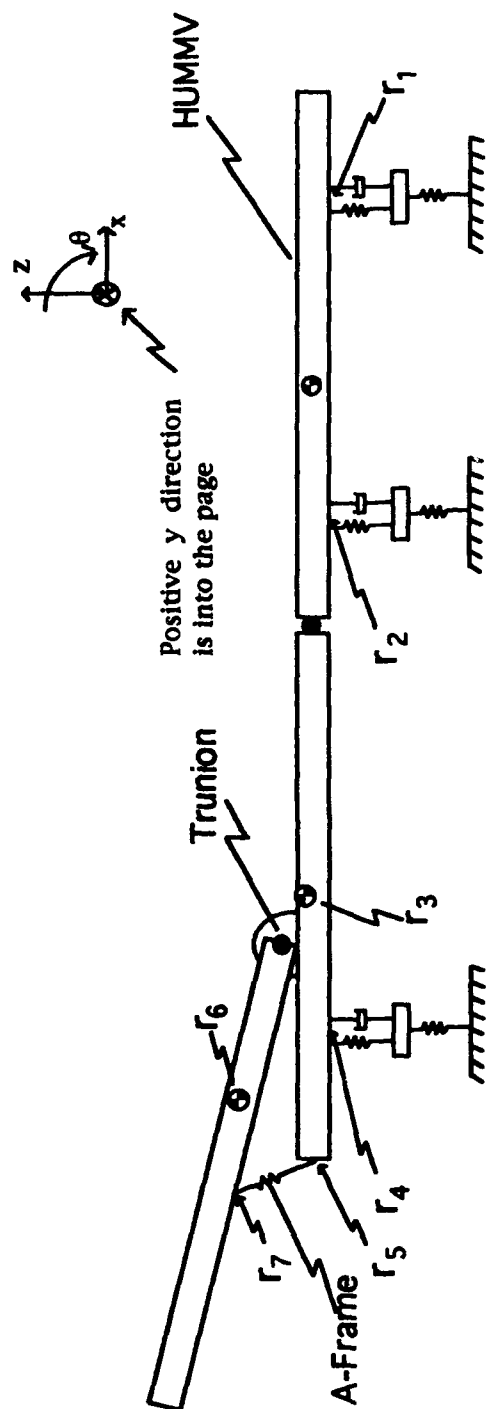
Figure 2-10 Generalized Coordinates for the HUMMV/Howitzer System

generalized coordinates and the road inputs U_1 , U_2 , and U_3 . To carry out the required computations, position vectors to key locations on the HUMMV and howitzer are defined in terms of the generalized coordinates. The position vectors to these key locations are depicted on Figure 2-11 and defined as follows:

- * r_1 & r_2 = the front and rear attachment points, respectively, for the suspension springs and shock absorbers on the HUMMV.
- * r_3 = the center of mass of the trail/saddle mass
- * r_4 = the modeled attachment location of the suspension spring and shock absorber of the howitzer
- * r_5 = the location where the A-Frame attaches to the T-Bar
- * r_6 = the location of the center of mass of the gun tube/elevating mass
- * r_7 = the location where the A-Frame attaches to the gun tube/elevating mass

These key locations that are defined above can be expressed as position vectors in terms of the above defined lengths (Figure 2-9), generalized coordinates (Figure 2-10), and the unit vectors i , j , and k of the Cartesian coordinate reference system (Figure 2-10) as follows:

- * $r_1 = (Z_3 - L_1 \sin(\theta_1))k + (L_1 \cos(\theta_1))i$
- * $r_2 = (Z_3 + L_2 \sin(\theta_1))k - (L_2 \cos(\theta_1))i$
- * $r_3 = (Z_3 + L_3 \sin(\theta_1) + L_{11} \sin(\theta_2))k - (L_3 \cos(\theta_1) + L_{11} \cos(\theta_2))i$
- * $r_4 = (Z_3 + L_3 \sin(\theta_1) + L_{12} \sin(\theta_2))k - (L_3 \cos(\theta_1) + L_{12} \cos(\theta_2))i$
- * $r_5 = (Z_3 + L_3 \sin(\theta_1) + (L_{13} + L_{16}) \sin(\theta_2))k - (L_3 \cos(\theta_1) + (L_{13} + L_{16}) \cos(\theta_2))i$



DEFINITION OF KEY LOCATIONS ON THE HUMMV & HOWITZER:

- r_1 & r_2 = the front and rear attachment points for the suspension springs and shock absorbers on the HUMMV.
- r_3 = the center of mass of the howitzer trail/saddle mass
- r_4 = the modeled attachment location of the suspension spring and shock of the howitzer
- r_5 = the location where the A-Frame attaches to the T-Bar
- r_6 = the location of the center of mass of the gun tube/elevating mass
- r_7 = the location where the A-Frame attaches to the gun tube/elevating mass

Figure 2-11 Key Locations for the HUMMV/Howitzer System

$$\begin{aligned}
* \mathbf{r}_6 &= (Z_3 + L_3 \sin(\theta_1) + L_{16} \sin(\theta_2) + L_{CG} \sin(\theta_0 + \theta_3)) \mathbf{k} - \begin{pmatrix} L_3 \cos(\theta_1) + L_{16} \cos(\theta_2) \\ + L_{CG} \cos(\theta_0 + \theta_3) \end{pmatrix} \mathbf{i} \\
* \mathbf{r}_7 &= (Z_3 + L_3 \sin(\theta_1) + L_{16} \sin(\theta_2) + L_A \sin(\theta_0 + \theta_3)) \mathbf{k} - \begin{pmatrix} L_3 \cos(\theta_1) + L_{16} \cos(\theta_2) \\ + L_A \cos(\theta_0 + \theta_3) \end{pmatrix} \mathbf{i}
\end{aligned}$$

The velocities of these key locations can be determined by taking the time derivatives of the position vectors. However, only the velocities of locations where there are velocity dependent actions occurring in Lagrange's equations need to be determined. The required velocities of the key locations on the HUMMV and howitzer are as follows:

$$\begin{aligned}
* \dot{\mathbf{r}}_1 &= (\dot{Z}_3 - L_1 \cos(\theta_1) \dot{\theta}_1) \mathbf{k} - (L_1 \sin(\theta_1) \dot{\theta}_1) \mathbf{i} \\
* \dot{\mathbf{r}}_2 &= (\dot{Z}_3 + L_2 \cos(\theta_1) \dot{\theta}_1) \mathbf{k} + (L_2 \sin(\theta_1) \dot{\theta}_1) \mathbf{i} \\
* \dot{\mathbf{r}}_3 &= (\dot{Z}_3 + L_3 \cos(\theta_1) \dot{\theta}_1 + L_{11} \cos(\theta_2) \dot{\theta}_2) \mathbf{k} + (L_3 \sin(\theta_1) \dot{\theta}_1 + L_{11} \sin(\theta_2) \dot{\theta}_2) \mathbf{i} \\
* \dot{\mathbf{r}}_4 &= (\dot{Z}_3 + L_3 \cos(\theta_1) \dot{\theta}_1 + L_{12} \cos(\theta_2) \dot{\theta}_2) \mathbf{k} + (L_3 \sin(\theta_1) \dot{\theta}_1 + L_{12} \sin(\theta_2) \dot{\theta}_2) \mathbf{i} \\
* \dot{\mathbf{r}}_6 &= \begin{pmatrix} \dot{Z}_3 + L_3 \cos(\theta_1) \dot{\theta}_1 + L_{16} \cos(\theta_2) \dot{\theta}_2 \\ + L_{CG} \cos(\theta_0 + \theta_3) \dot{\theta}_3 \end{pmatrix} \mathbf{k} + \begin{pmatrix} L_3 \sin(\theta_1) \dot{\theta}_1 + L_{16} \sin(\theta_2) \dot{\theta}_2 \\ + L_{CG} \sin(\theta_0 + \theta_3) \dot{\theta}_3 \end{pmatrix} \mathbf{i}
\end{aligned}$$

In addition to the above velocities, the vertical velocity of the CG of the HUMMV, \dot{Z}_3 , and each of the wheel masses, \dot{Z}_1 , \dot{Z}_2 , & \dot{Z}_4 are needed in Lagrange's equation.

2. Kinetic Energy (T)

The velocities defined above are used to calculate the kinetic energy of the system. The kinetic energy is calculated by summing the linear and rotational kinetic energy for each of the

system's masses. The total kinetic energy of the system is given by:

$$\sum T_i = \sum (\frac{1}{2} m_i v_i^2 + \frac{1}{2} I_j \dot{\theta}_j^2) \quad i = 1,6; \quad j = 1,3$$

where:

T_i = the kinetic energy of each mass in the system

m_i = the mass of each lumped mass

v_i = the linear velocity of the each mass

I_j = the heave mass moment of inertia of each rotating mass about its center of gravity

θ_j = the angular velocity of each rotating mass

Therefore, the total kinetic energy of the HUMMV/howitzer system was determined by summing the kinetic energy components as follows:

$$T = \frac{1}{2} M_1 (\dot{Z}_1)^2 + \frac{1}{2} M_2 (\dot{Z}_2)^2 + \frac{1}{2} M_3 (\dot{Z}_3)^2 + \frac{1}{2} M_4 (\dot{Z}_4)^2 + \frac{1}{2} M_5 (\dot{r}_3)^2 \\ + \frac{1}{2} M_6 (\dot{r}_6)^2 + \frac{1}{2} I_1 (\dot{\theta}_1)^2 + \frac{1}{2} I_2 (\dot{\theta}_2)^2 + \frac{1}{2} I_3 (\dot{\theta}_3)^2$$

In the above expression the square of the velocities is determined by substituting in the appropriate velocity expression as defined above, and taking the dot product of the velocity with itself. This substitution and dot product operation is left for the reader. When taking this dot product all of the k dot i and i dot k cross product terms drop out because the i and k unit vectors are orthogonal. Having determined the total kinetic energy, the time derivative of the partial derivative of the total kinetic energy with respect to the velocity of each of the generalized coordinates, $\frac{d}{dt} \frac{\partial T}{\partial \dot{q}_i}$ can be determined. Carrying out this differentiation and linearizing yields the following:

$$\begin{aligned}
* \frac{d}{dt} \frac{\partial T}{\partial \dot{Z}_1} &= M_1 \ddot{Z}_1 \\
* \frac{d}{dt} \frac{\partial T}{\partial \dot{Z}_2} &= M_2 \ddot{Z}_2 \\
* \frac{d}{dt} \frac{\partial T}{\partial \dot{Z}_3} &= (M_3 + M_5 + M_6) \ddot{Z}_3 + (M_5 L_3 + M_6 L_3) \ddot{\theta}_1 + (M_5 L_{11} + M_6 L_{16}) \ddot{\theta}_2 \\
&\quad + M_6 L_{CG} \cos(\theta_0) \ddot{\theta}_3 \\
* \frac{d}{dt} \frac{\partial T}{\partial \dot{Z}_4} &= M_4 \ddot{Z}_4 \\
* \frac{d}{dt} \frac{\partial T}{\partial \dot{\theta}_1} &= (M_5 L_3 + M_6 L_3) \ddot{Z}_3 + (I_1 + M_5 L_3^2 + M_6 L_3^2) \ddot{\theta}_1 \\
&\quad + (M_5 L_3 L_{11} + M_6 L_3 L_{16}) \ddot{\theta}_2 + M_6 L_3 L_{CG} \cos(\theta_0) \ddot{\theta}_3 \\
* \frac{d}{dt} \frac{\partial T}{\partial \dot{\theta}_2} &= (M_5 L_{11} + M_6 L_{16}) \ddot{Z}_3 + (M_5 L_3 L_{11} + M_6 L_3 L_{16}) \ddot{\theta}_1 \\
&\quad + (I_2 + M_5 L_{11}^2 + M_6 L_{16}^2) \ddot{\theta}_2 + M_6 L_{16} L_{CG} \cos(\theta_0) \ddot{\theta}_3 \\
* \frac{d}{dt} \frac{\partial T}{\partial \dot{\theta}_3} &= M_6 L_{CG} \cos(\theta_0) \ddot{Z}_3 + M_6 L_3 L_{CG} \cos(\theta_0) \ddot{\theta}_1 + M_6 L_{16} L_{CG} \cos(\theta_0) \ddot{\theta}_2 \\
&\quad + (I_3 + M_6 L_{CG}^2) \ddot{\theta}_3
\end{aligned}$$

The total kinetic energy, T , must also be differentiated with respect to each of the generalized positional coordinates, however, for this system this differentiation is equal to zero for all coordinates.

3. Potential Energy (U)

The potential energy for this system results from the strain energy that is developed in the suspension springs and the A-Frame spring. The gravitational potential energy that arises from changes in vertical positions is ignored because the resulting terms drop out of the dynamic equations of motion. The potential energy in any spring is determined as follows:

$$U_i = \frac{1}{2} K_i (\Delta x_i)^2$$

where:

U_i = the potential strain energy in each spring

K_i = the spring stiffness for spring

Δx_i = the change in length of the spring.

Since locations to the attachment points of the ends of all the springs have been defined above in a common inertial coordinate reference system, taking the difference of the position vectors of the end points of each spring will yield the change in length of the spring. Thus for this system, the total potential energy is found by summing the potential energy in each of the springs as follows:

$$U = \frac{1}{2} K_1 (Z_1 - U_1)^2 + \frac{1}{2} K_2 (r_1 - Z_1)^2 + \frac{1}{2} K_3 (Z_2 - U_2)^2 + \frac{1}{2} K_4 (r_2 - Z_2)^2 \\ + \frac{1}{2} K_6 (Z_4 - U_3)^2 + \frac{1}{2} K_7 (r_4 - Z_4)^2 + \frac{1}{2} K_A (r_7 - r_5)^2$$

Therefore, the partial derivative of the total potential energy with respect to each of the generalized coordinates, $\frac{\partial U}{\partial q_i}$, after linearizing

results in the following:

$$\begin{aligned} * \frac{\partial U}{\partial Z_1} &= K_1 Z_1 + K_2 Z_1 - K_2 Z_3 + K_2 L_1 \theta_1 - K_1 U_1 \\ * \frac{\partial U}{\partial Z_2} &= K_3 Z_2 + K_4 Z_2 - K_4 Z_3 - K_4 L_2 \theta_1 - K_3 U_2 \\ * \frac{\partial U}{\partial Z_3} &= -K_2 Z_1 - K_4 Z_2 + (K_2 + K_4 + K_7) Z_3 - K_7 Z_4 \\ &\quad + (K_2 L_1 + K_4 L_2 + K_7 L_3) \theta_1 + K_7 L_{12} \theta_2 \\ * \frac{\partial U}{\partial Z_4} &= -K_7 Z_3 + (K_6 + K_7) Z_4 - K_7 L_3 \theta_1 - K_7 L_{12} \theta_2 - K_6 U_3 \end{aligned}$$

$$\begin{aligned}
* \frac{\partial U}{\partial \theta_1} &= K_2 L_1 Z_1 - K_4 L_2 Z_2 + (-K_2 L_1 + K_4 L_2 + K_7 L_3) Z_3 - K_7 L_3 \\
&\quad (K_2 L_1^2 + K_4 L_2^2 + K_7 L_3^2) \theta_1 + K_7 L_3 L_1 \theta_2 \\
* \frac{\partial U}{\partial \theta_2} &= K_7 L_1 Z_3 - K_7 L_2 Z_4 + K_7 L_3 L_1 \theta_1 + K_7 L_1^2 \theta_2 \\
&\quad + K_A L_A L_{13} \cos(\theta_0) \theta_2 - K_A L_A L_{13} \cos(\theta_0) \theta_3 \\
* \frac{\partial U}{\partial \theta_3} &= -K_A L_A L_{13} \cos(\theta_0) \theta_2 + K_A L_A L_{13} \cos(\theta_0) \theta_3
\end{aligned}$$

4. Generalized Power Lost Due to Damping Forces (F)

The amount of generalized power that is dissipated by each of the dampers in the system given by the equation:

$$F_i = \frac{1}{2} B_i (\Delta \dot{x}_i)^2$$

where:

F_i = the generalized power dissipated in each damper

B_i = the damping constant for each damper

$\Delta \dot{x}_i$ = the difference in velocity of the attaching points of each damper.

The total amount of generalized power dissipated in the system is found by summing the energy dissipated in each dampers. Summing the energy dissipated by the damping forces yields the following:

$$F = \frac{1}{2} B_1 (\dot{r}_1 - \dot{Z}_1)^2 + \frac{1}{2} B_2 (\dot{r}_2 - \dot{Z}_2)^2 + \frac{1}{2} B_3 (\dot{r}_4 - \dot{Z}_3)^2 + \frac{1}{2} B_4 (\dot{\theta}_3 - \dot{\theta}_2)^2$$

In Lagrange's equation this total dissipated energy, F , must be differentiated with respect to the velocities of each of the generalized coordinates, $\frac{\partial F}{\partial \dot{q}_i}$.

Carrying out this differentiation and again linearizing results in the following:

$$\begin{aligned}
 * \frac{\partial F}{\partial \dot{Z}_1} &= B_1 \dot{Z}_1 - B_1 \dot{Z}_3 + B_1 L_1 \dot{\theta}_1 \\
 * \frac{\partial F}{\partial \dot{Z}_2} &= B_2 \dot{Z}_2 - B_2 \dot{Z}_3 - B_2 L_2 \dot{\theta}_1 \\
 * \frac{\partial F}{\partial \dot{Z}_3} &= -B_1 \dot{Z}_1 - B_2 \dot{Z}_2 + (B_1 + B_2 + B_3) \dot{Z}_3 - B_3 \dot{Z}_4 + (-B_1 L_1 + B_2 L_2) \dot{\theta}_1 \\
 * \frac{\partial F}{\partial \dot{Z}_4} &= B_3 \dot{Z}_4 - B_3 \dot{Z}_3 - B_3 L_3 \dot{\theta}_1 - B_3 L_{12} \dot{\theta}_2 \\
 * \frac{\partial F}{\partial \dot{\theta}_1} &= B_1 L_1 \dot{Z}_1 - B_2 L_2 \dot{Z}_2 + (B_1 L_1 + B_2 L_2 + B_3 L_3) \dot{Z}_3 - B_3 L_3 \\
 &\quad + (B_1 L_1^2 + B_2 L_2^2 + B_3 L_3^2) \dot{\theta}_1 + B_3 L_3 L_{12} \dot{\theta}_2 \\
 * \frac{\partial F}{\partial \dot{\theta}_2} &= B_3 L_{12} \dot{Z}_3 - B_3 L_{12} \dot{Z}_4 + B_3 L_3 L_{12} \dot{\theta}_1 + (B_3 L_{12}^2 + B_4) \dot{\theta}_2 - B_4 \dot{\theta}_3 \\
 * \frac{\partial F}{\partial \dot{\theta}_3} &= -B_4 \dot{\theta}_2 + B_4 \dot{\theta}_3
 \end{aligned}$$

5. External Forces (Q_i)

The external forces acting on the system are the roadway inputs that are transmitted through the tire springs. For the computer model these input forces are treated as purely vertical forces. The forces result from the road inputs causing a change in length of the tire springs. These road inputs are depicted on Figure 2-10 and defined as follows :

- * U_1 = the road input for the front HUMMV wheel
- * U_2 = the road input for the rear HUMMV wheel
- * U_3 = the road input for the howitzer wheel.

6. Assembling Lagrange's Equation

Combining the parts of Lagrange's equations that were developed in the above paragraphs results in a system of equations of motion in the form:

$$[M]\{\ddot{x}\} + [C(\dot{x})]\{\dot{x}\} + [K]\{x\} = [f]$$

where:

$[M]$ = the 7 x 7 system mass matrix

$[C(\dot{x})]$ = the 7 x 7 system damping matrix that is a function of whether the shock absorbers are in tension or compression

$[K]$ = the 7 x 7 system stiffness matrix

$\{\ddot{x}\}$, $\{\dot{x}\}$, & $\{x\}$ = 7 x 1 column vectors that contain accelerations, velocities and positions of all coordinates, respectively.

$[f]$ = the 7x1 forcing vector that results from the road inputs.

The $[M]$, $[C(\dot{x})]$, and $[K]$ matrices for this system are contained in Appendix B. This completes the development of the heave and pitch EOMs. The resulting EOMs were numerically integrated to determine the time history for motions of the component masses of the system.

C. HUMMV/HOWITZER MODEL NUMERICAL INTEGRATION

The following section describes the procedures that were used to numerically integrate the previously developed equations of motion.

1. Transformation to 1st Order Equations

In order to numerically solve the equations of motion, the formulated system of second order ordinary differential equations must be transformed into a system of first order differential

equations. This equation transformation was performed using matrix algebra and results in the following expression for the system of first order differential equations:

$$[\dot{x}] = \begin{bmatrix} [0] & [I] \\ [-M^{-1}K] & [-M^{-1}C(\dot{x})] \end{bmatrix} \begin{bmatrix} [x] \\ [\dot{x}] \end{bmatrix} + \begin{bmatrix} [0] \\ [M^{-1}f] \end{bmatrix}$$

where:

$[\dot{x}]$ = a 14 x 1 column vector of which the first seven elements are the velocities of all the generalized coordinates and the last seven elements are the accelerations of the generalized coordinates.

$\begin{bmatrix} [x] \\ [\dot{x}] \end{bmatrix}$ = a 14 x 1 column vector of which the first seven elements are the positions in terms of the generalized coordinates and the last seven elements are the velocities of the generalized coordinates.

$[0]$ = a 7 x 7 zero matrix

$[I]$ = a 7 x 7 identity matrix

$[-M^{-1}C(\dot{x})]$ & $[-M^{-1}K]$ = these are 7 x 7 matrices that result from multiplying the negative inverse of the system mass matrix, $[M]$, times the damping matrix, $[C]$, and the stiffness matrix, $[K]$, respectively

$\begin{bmatrix} [0] \\ [M^{-1}f] \end{bmatrix}$ = a 14 x 1 vector which the first seven elements are zero and the last seven elements are the matrix product of multiplying the inverse of the mass matrix, $[M]$, times the forcing vector, $[f]$.

For the integration the system was started from rest, thus, all seven of the system's displacement, $\{x\}$, and velocity, $\{\dot{x}\}$, state variables had a value of zero for initial conditions.

2. Integration Difficulties

The equations of motion were numerically integrated using the Matlab ODE 45 integration routine. This is a variable time step 4th order Runge-Kutta integration routine. Integrating these equations of motion using ODE 45 was complicated by the non-linear damping of the shock absorbers and the required shutoff of the tire springs when they leave contact with the road surface.

When the damping values of the shock absorbers would abruptly change from compression to tension and vice versa, there would be a corresponding abrupt change in the shock absorber force. Determining when the shock absorber damping value should change is built into the integration code by checking for each time step if each of the shock absorber forces are compressive or tensile. An "if" statement ensures that the correct damping value is used for the condition that exists. The abrupt changes in force in the shock absorbers slowed down the tolerance based ODE 45 routine. A similar situation occurred when the tire spring forces would abruptly change to the respective static weights when contact with the road was lost for a particular wheel.

To increase the speed of the ODE 45 routine the integration was divided into one second time segments so the solution matrix that contains the state variables remains relatively small. The displacements and velocity states at the end of the previous time segment are used as the initial conditions for the next one second time segment.

The resulting time histories for the displacements and velocities allowed post-processing to be completed determine accelerations, forces,

and stress in key system components. The computer code developed for this numerical integration is contained in Appendix C.

III. ROADWAY INPUTS

This chapter explains the road inputs that were used to drive the computer model. The roadway inputs are defined in terms of the vertical change upward or downward of the values of the road inputs U_1 , U_2 , and U_3 that are shown on Figure 2-10. These are independent vertical displacement inputs to tires for each of the wheels in the computer model. As defined in Chapter II, there is one input for the front HUMMV wheels, (U_1), a second input for the rear HUMMV wheels, (U_2), and a third input for the howitzer wheels, (U_3). The model can be driven over any terrain that can be defined in terms of the road inputs U_1 , U_2 , and U_3 . The road inputs are functions of time which allows the user to control the speed at which the model is driven by using the time, velocity, and distance relationships. For this design study the road inputs used were a washboard course that was like one of the courses used in the actual test at Aberdeen Proving Grounds, MD (see Chapter VI), and a predicted "worst case" pothole road.

A. WASHBOARD COURSE

The washboard course that was used to drive the model was constructed to be similar to the Six Inch Washboard Course at APG. During the instrumented test at APG there were several data runs taken on the Six Inch Washboard Course (again, see Chapter VI). Comparing the model results for this type of washboard course to the

actual instrumented data from the APG test for a similar washboard provided a means of validating the output results of the computer model.

To model the APG Six Inch Washboard Course a sinusoidal input was used with an amplitude of three inches and a distance from peak to peak of 72 inches. However, because the distance between the front HUMMV wheels and both the rear HUMMV wheels and also the howitzer wheels does not correspond to even multiples of the 72 inch peak to peak distance, a lag had to be built into the input sinusoid for both the rear HUMMV wheels and the howitzer wheels. This lag was necessary, to get the correct timing of the bump wheel inputs for all the wheels in the system.

Additionally, in order to prevent difficulties in the integration routine that would occur if the wheel inputs were all turned on at the start of the integration run, the rear HUMMV and howitzer wheel inputs were not turned on initially. These inputs were turned on at the time when the respective wheels would start hitting the washboard course bumps if the HUMMV/howitzer system entered the course from level terrain. In other words, the front HUMMV wheels entered the washboard and started taking road input, U_1 , while the rear HUMMV wheels and the howitzer wheels remained on level terrain which provided zero input to them. Then the rear HUMMV wheels entered the washboard and started taking road input, U_2 , while the front HUMMV wheels continued to have the input, U_1 , and the howitzer wheels continued to have zero input.

Finally, the howitzer wheels entered the washboard and at this point all three wheels had their separate inputs U_1 , U_2 , and U_3 .

This sinusoidal input, for which the wavelength was defined in terms of horizontal distance between peaks, was converted into a function of time by using time, velocity, and distance relationships. To calculate the time between successive peaks for a specified velocity the inputs U_1 , U_2 , and U_3 were then defined in terms of time which allowed the computer model to be "driven" at any desired speed. Making the input a function of time was required for using the time based ODE 45 integration routine of Matlab to solve the equations of motion. Figure 3-1 depicts the wheel inputs U_1 , U_2 , and U_3 for the washboard course being driven at 5.0 MPH.

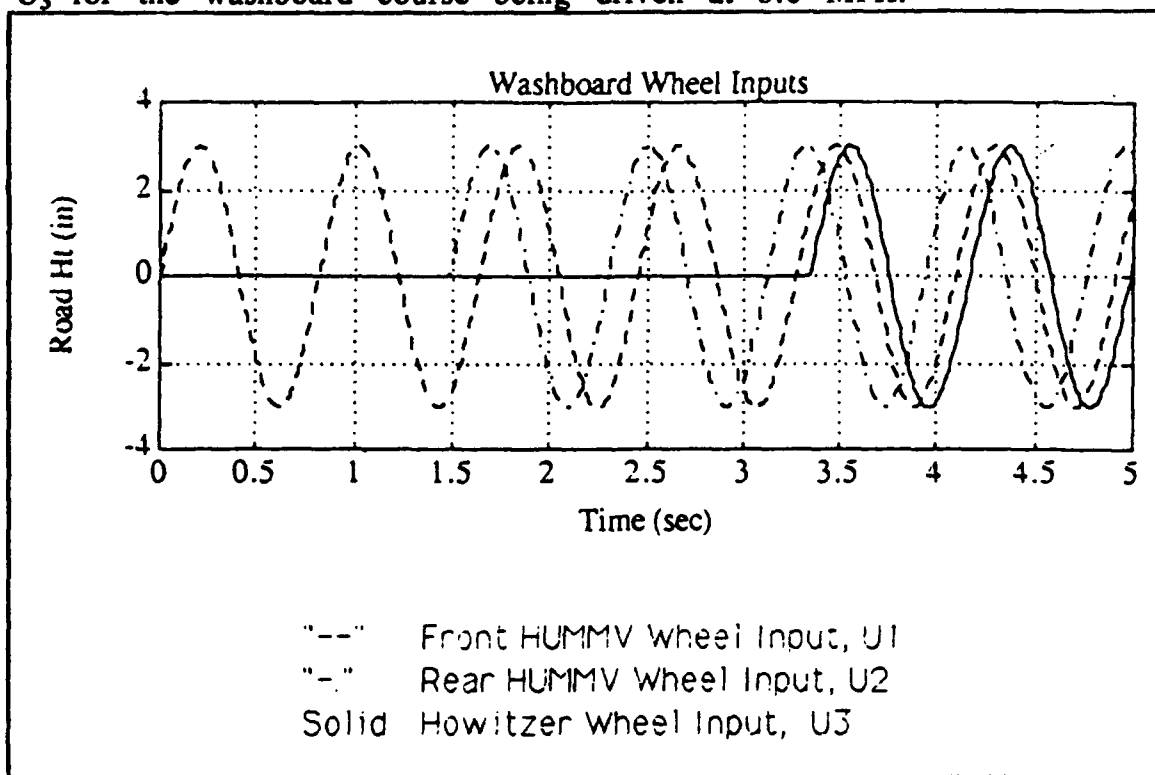


Figure 3-1 Six Inch Washboard Course Wheel Inputs

B. "WORST CASE" POTHOLE COURSE

The model was also "driven" over a trench type pothole to simulate some of the most severe road conditions that the howitzer would be subjected to during tactical operations. The model results for A-Frame force from this terrain were used to predict if the A-Frame and T-Bar were strong enough to handle this "worst case" terrain. The pothole course road inputs, U_1 , U_2 , and U_3 , are determined by a separate computer program (see Appendix D) that computes the changes in axle height as each of the HUMMV wheels and the howitzer wheels roll through the pothole. The road inputs are based on the path that would be traced out by the center of a 17 inch radius wheel rolling through the specified pothole. The computer program that was developed to determine the road inputs allows the user to specify the desired dimension of the pothole for driving the computer model. For this design study the "worst case" pothole was determined to be 20 inches deep and 30 inches across with 85 degree slopes on each edge. This size was selected because it was judged to be the largest pothole that the HUMMV driver would traverse without stopping the HUMMV. Thus, the "worst case" pothole dimensions were selected based on what was judged to be the most severe terrain the HUMMV/howitzer would encounter while traveling during tactical operations. The "worst case" pothole selected was slightly larger than the dimensions of the pothole that was used in an informal test conducted at RIA in June 1992. Figure 3-2 shows the pothole profile, and the axle path traced for the howitzer or HUMMV wheel rolling through this "worst case" situation.

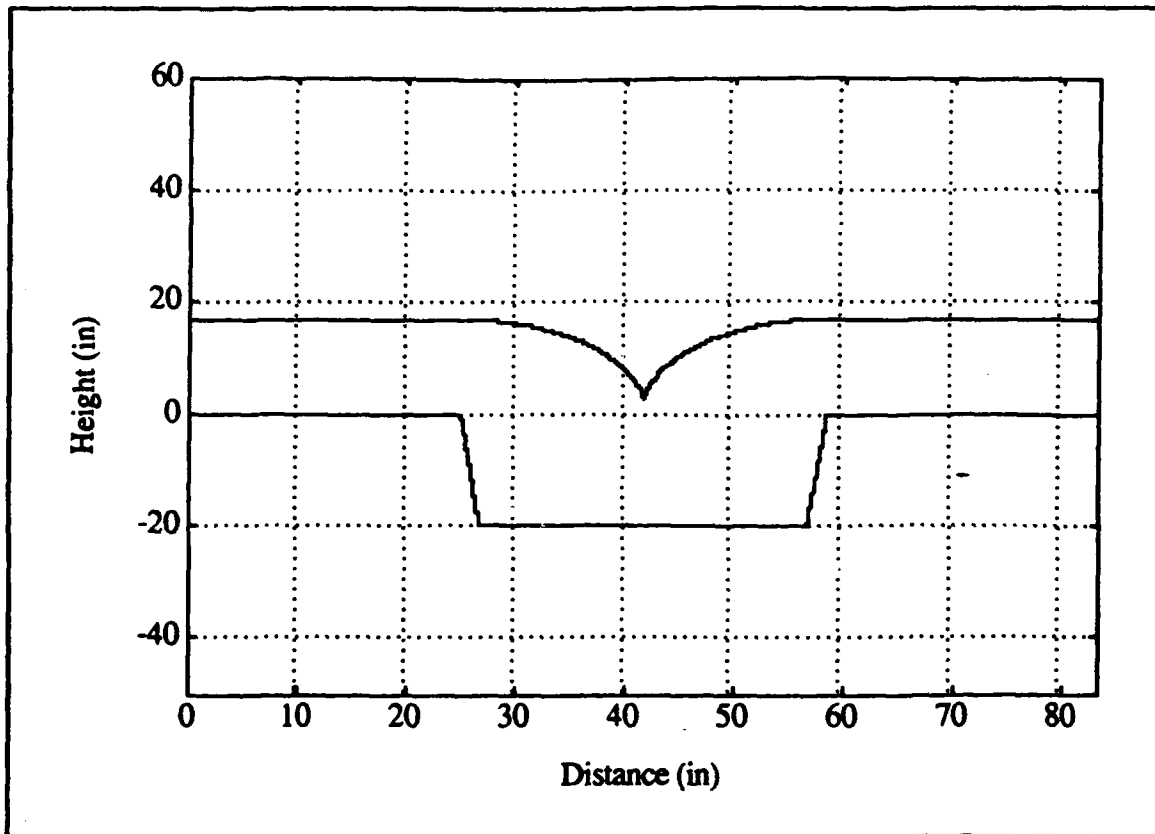


Figure 3-2 "Worst Case" Pothole Profile and Axle Trace

IV. MODEL RESULTS

This chapter contains the results of driving the computer model over the terrain that was explained in Chapter III. The results from driving the model over the washboard course show close agreement actual results obtained from the APG test. A detailed comparison of the model results to the actual results is contained in Chapter VI. The model's results from the "worst case" pothole were used to predict the maximum value of A-Frame force for the howitzer. From this predicted maximum force the stress in the A-Frame and T-Bar was calculated and compared to the yield stress for the material (see Chapter V).

The predicted A-Frame force is calculated by multiplying the combined spring stiffness of the A-Frame/T-bar times the change in length of A-Frame. The change in length of the A-Frame is a function of the difference in the angular displacements of the gun tube mass and the howitzer trail/saddle mass at a given time. The angular displacements of the gun tube and the trail were determined from numerically integrating the equations of motion.

In addition to determining results in terms of A-Frame force, the system's mass and stiffness matrices (see Appendix B) were used to determine natural frequencies and mode shapes of the system. These natural frequencies and mode shapes were used to gain physical insight into the system's performance. The natural frequencies and mode shapes for the system are shown in Appendix E.

The Matlab "FFT" function was used to perform the frequency analysis on the A-Frame force results from the washboard course to determine the frequencies at which the A-Frame force occurred in the model results. This frequency analysis used a 1250 Hz data sampling rate. This sampling rate yielded a time increment, dt , that equals $1/1250$ or the inverse of the sampling rate. In order to have a frequency increment that was sufficiently small, 8192 data points were used for the "FFT". The record length, T , equals dt times the number of points or $8192/1250$. The frequency increment, df , was the inverse of the record length or $1250/8192$.

A. WASHBOARD COURSE RESULTS

The time histories of the computer model's predictions for A-Frame force from the Six Inch Washboard Course are periodic with a period that corresponds to the period of the washboard input. But unlike the sinusoidal washboard input the A-Frame force output predictions are not sinusoidal. These non-sinusoidal A-Frame force outputs most likely result from the effects of the non-linear shock absorber damping that was incorporated into the model (see Chapter II).

The frequency analysis of the computer model's predictions for A-Frame force shows that as expected the largest component of output force occurs at the same frequency as the washboard input frequency. In all cases, there is also a significant but lesser force component that occurs at a frequency that is twice the input frequency.

The computer model was driven over the six inch washboard course at speeds of 3.75, 5.0 MPH, and 5.25 MPH. These speeds

correspond to the speeds for which actual data was taken during the APG test. The A-Frame force levels were relatively low at 3.75 MPH. The force levels in the A-Frame reached a maximum at 5.25 MPH because this speed for the washboard course corresponds to a natural frequency of the system. Driving the model at speeds higher than 5.25 MPH resulted in decreasing A-Frame force levels. The time histories and frequency analysis of the model's predicted results for A-Frame force are shown in Figures 4-1 through 4-6.

1. Results at 3.75 MPH

The time domain model results at 3.75 MPH are shown in Figure 4-1. The predicted A-Frame forces are approximately 1500 lbs in tension and 1200 lbs in compression. Figure 4-2 shows the frequency analysis at this speed. As expected, there is a large force component at the input of 3.75 MPH or a frequency of 0.92 Hz and there is smaller force spike at twice this frequency, 1.84 Hz.

2. Results at 5.0 MPH

The time domain results are shown in Figure 4-3. The A-Frame force levels reach 2800 lbs in tension and 4800 lbs in compression. Figure 4-4 shows the frequency analysis results. Again, a large force component at the input, 5.0 Hz, and another force spike at twice this frequency, 2.42 Hz.

3. Results at 5.25 MPH

The time domain results are shown in Figure 4-5. The A-Frame force levels reach 2900 lbs in tension and 4700 lbs in compression. Figure 4-6 shows the frequency analysis results. A large force component exists at the input frequency, 1.28 Hz, and smaller force component exists at twice this frequency, 2.56 Hz.

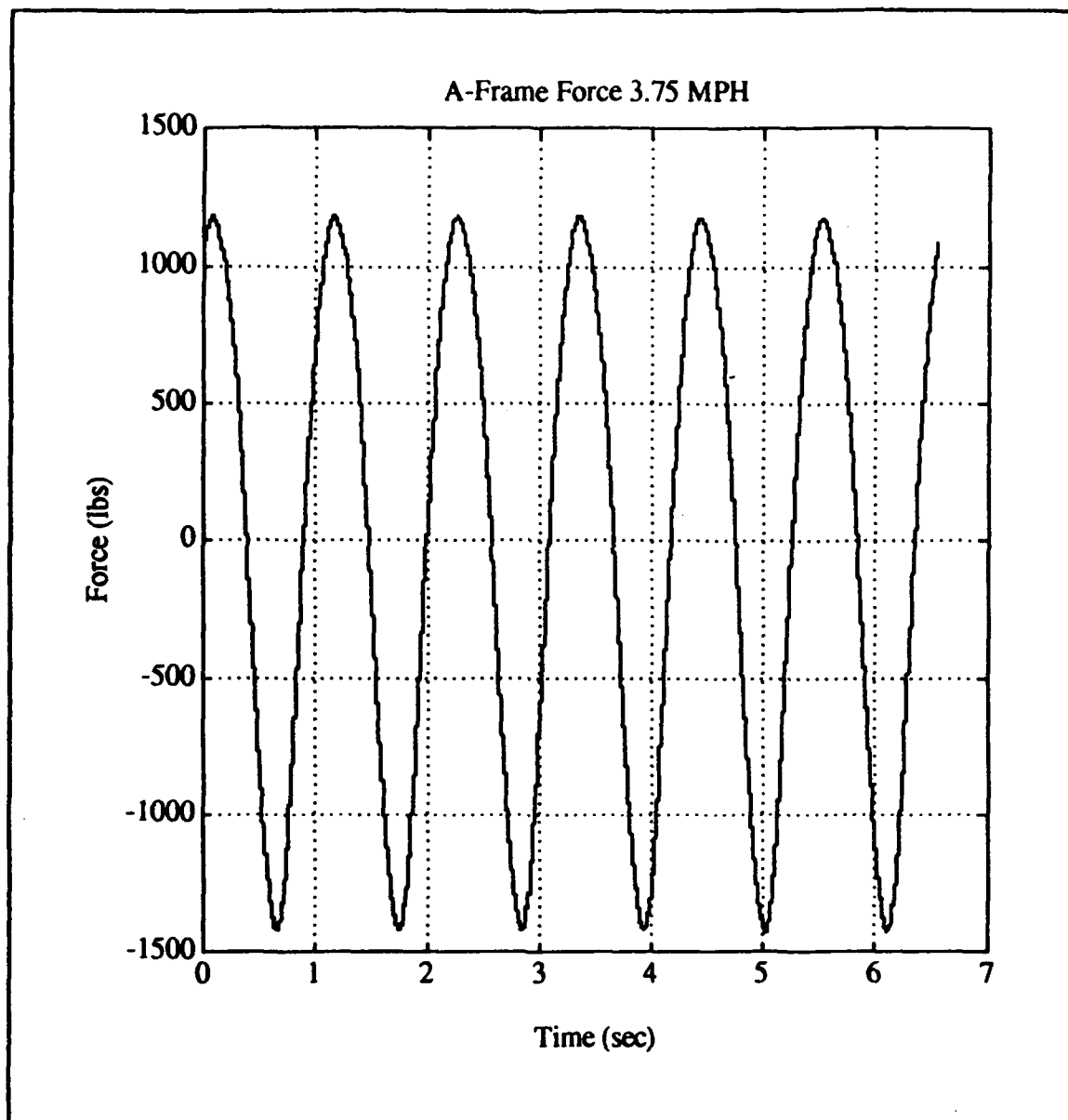


Figure 4-1 Model Results for A-Frame Force at 3.75 MPH (Time History)

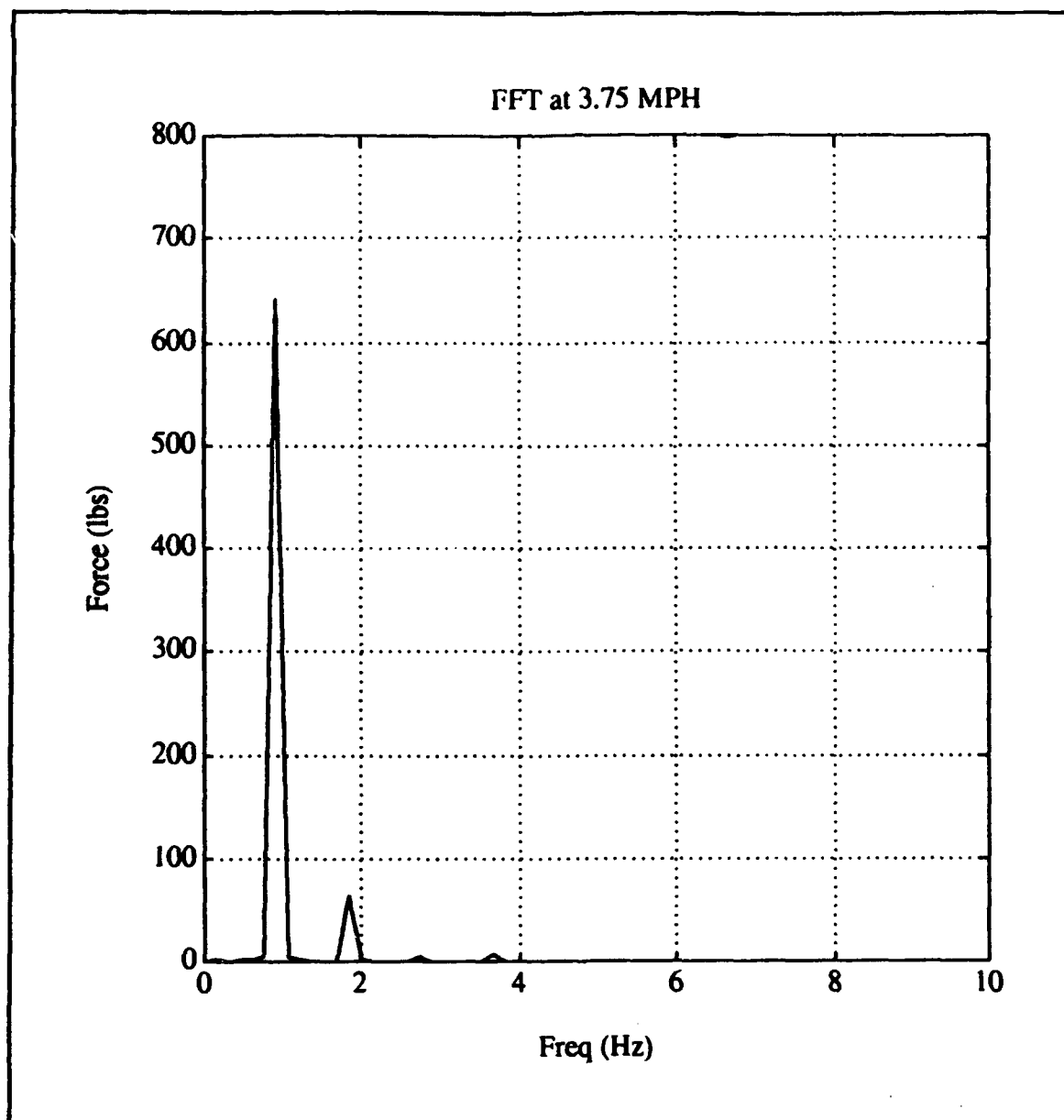


Figure 4-2 Model Results for A-Frame Force at 3.75 MPH (FFT)

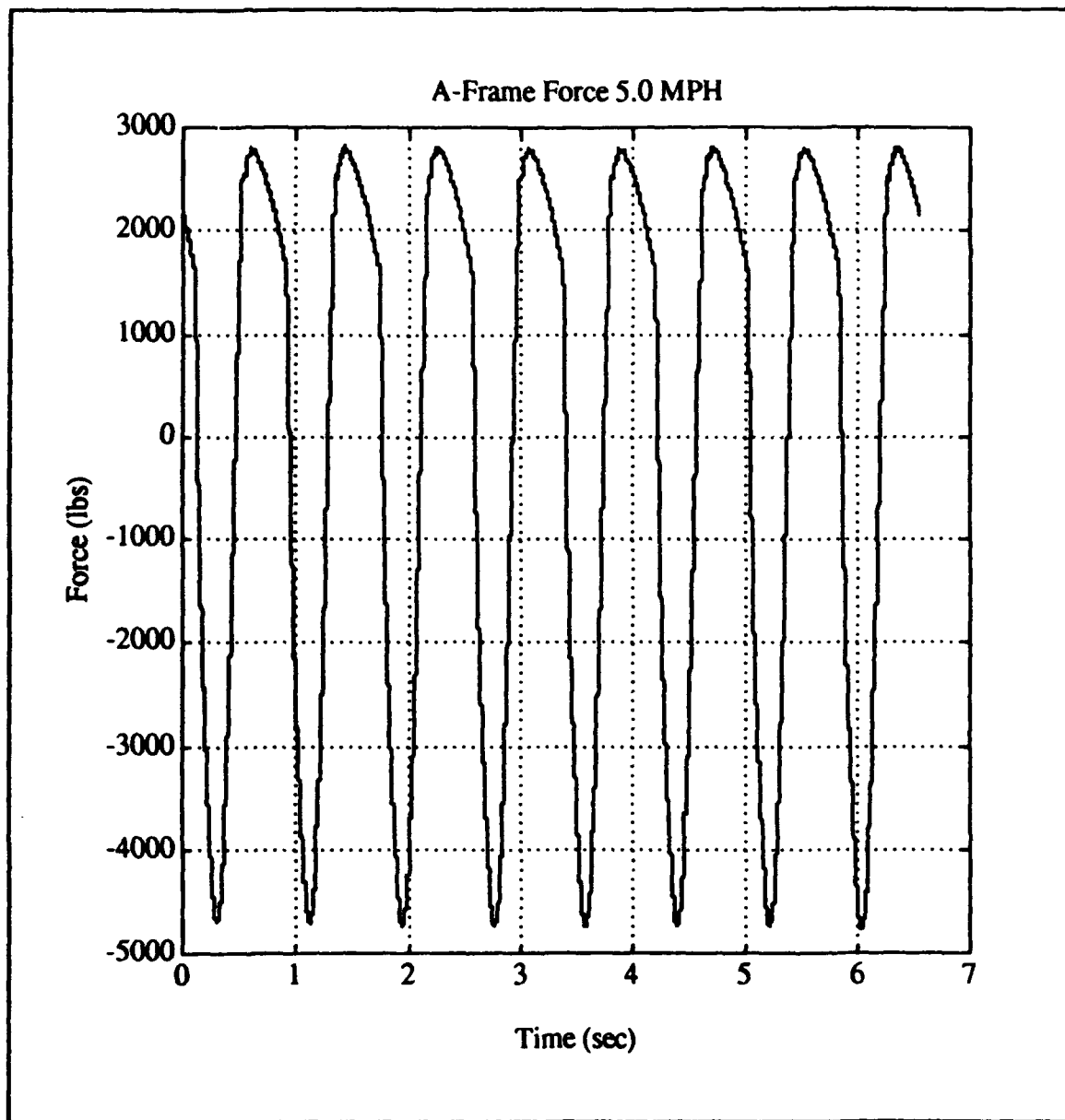


Figure 4-3 Model Results for A-Frame Force at 5.0 MPH (Time History)

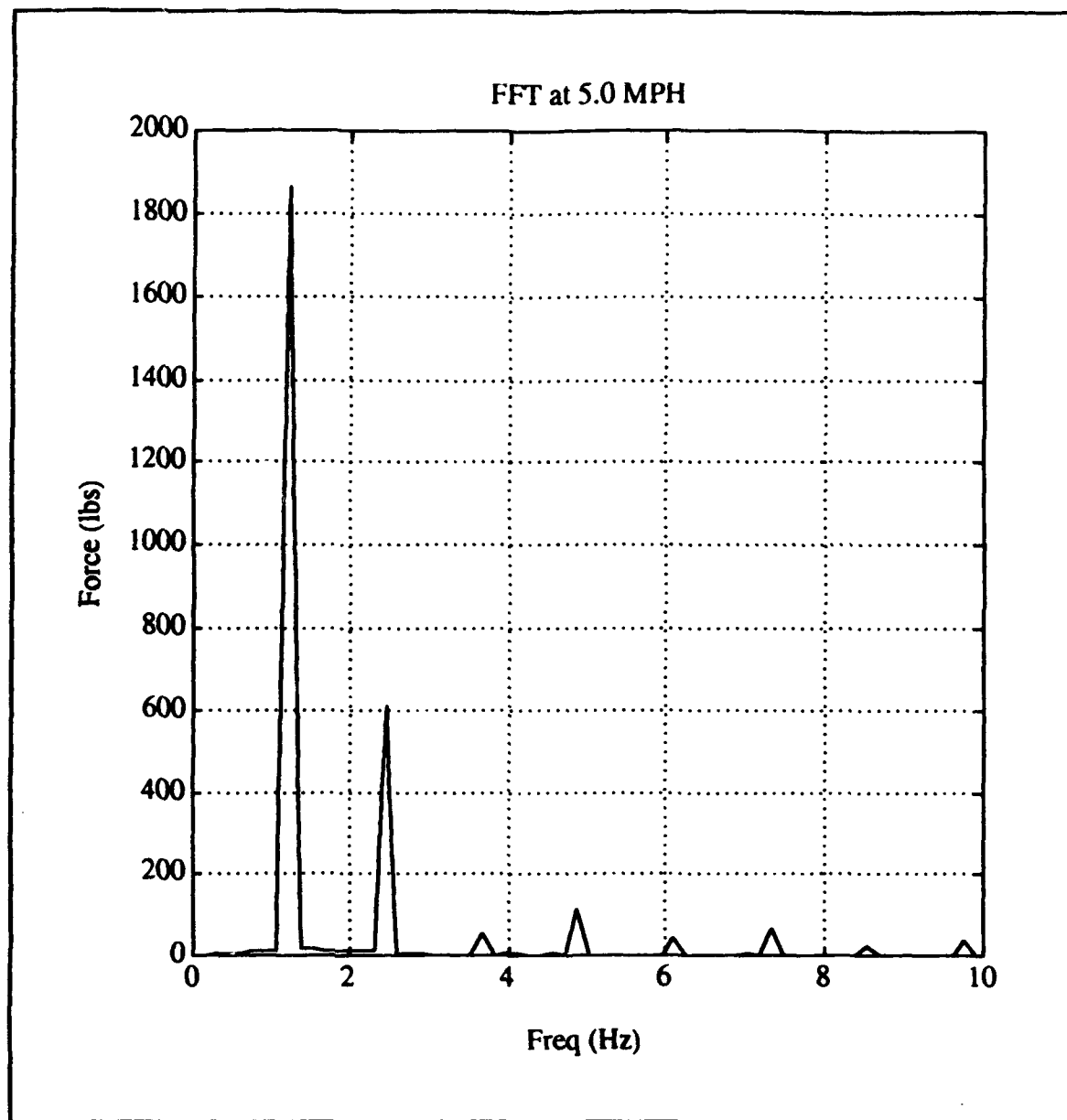


Figure 4-4 Model Results for A-Frame Force at 5.0 MPH (FFT)

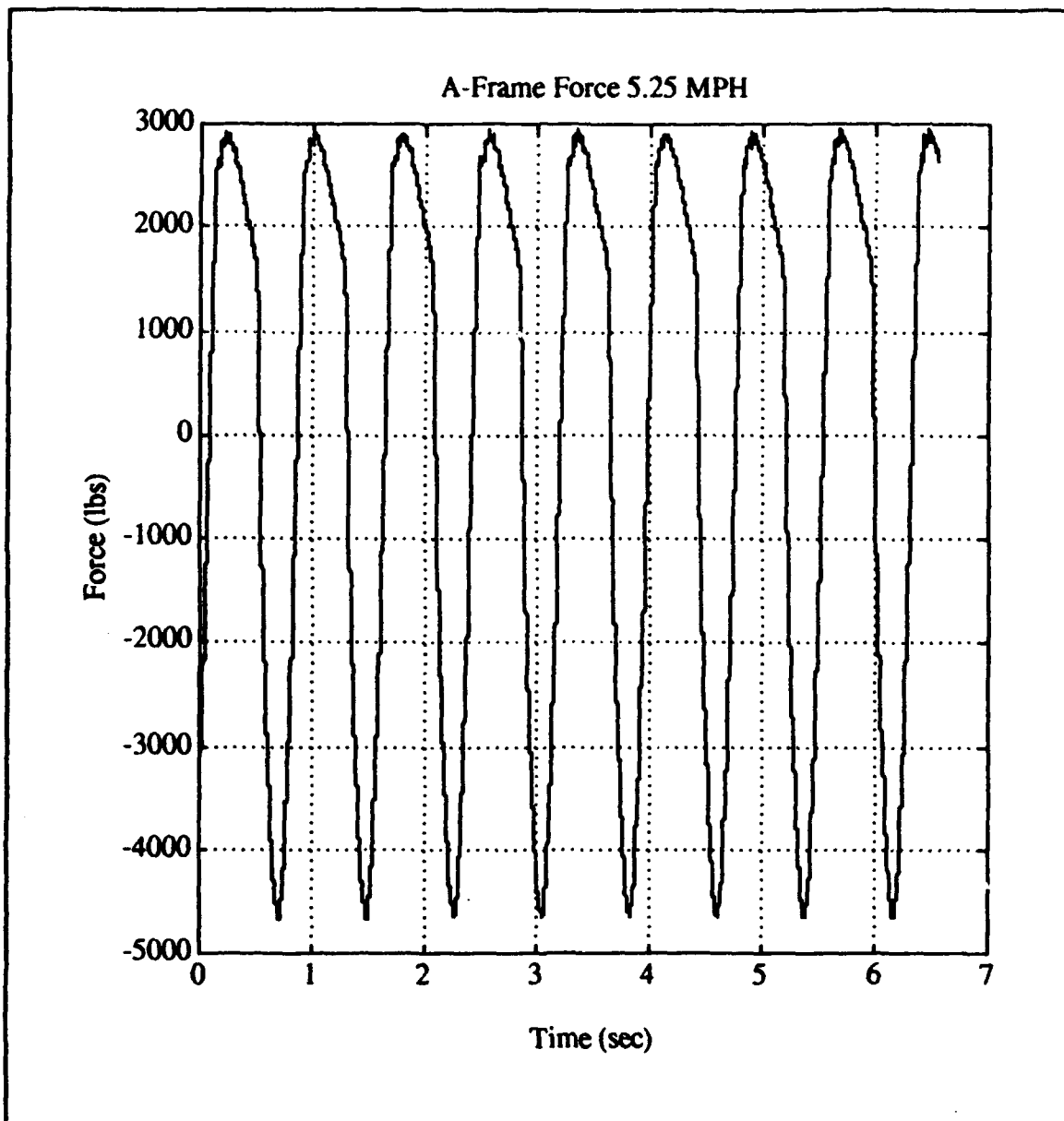


Figure 4-5 Model Results for A-Frame Force at 5.25 MPH (Time History)

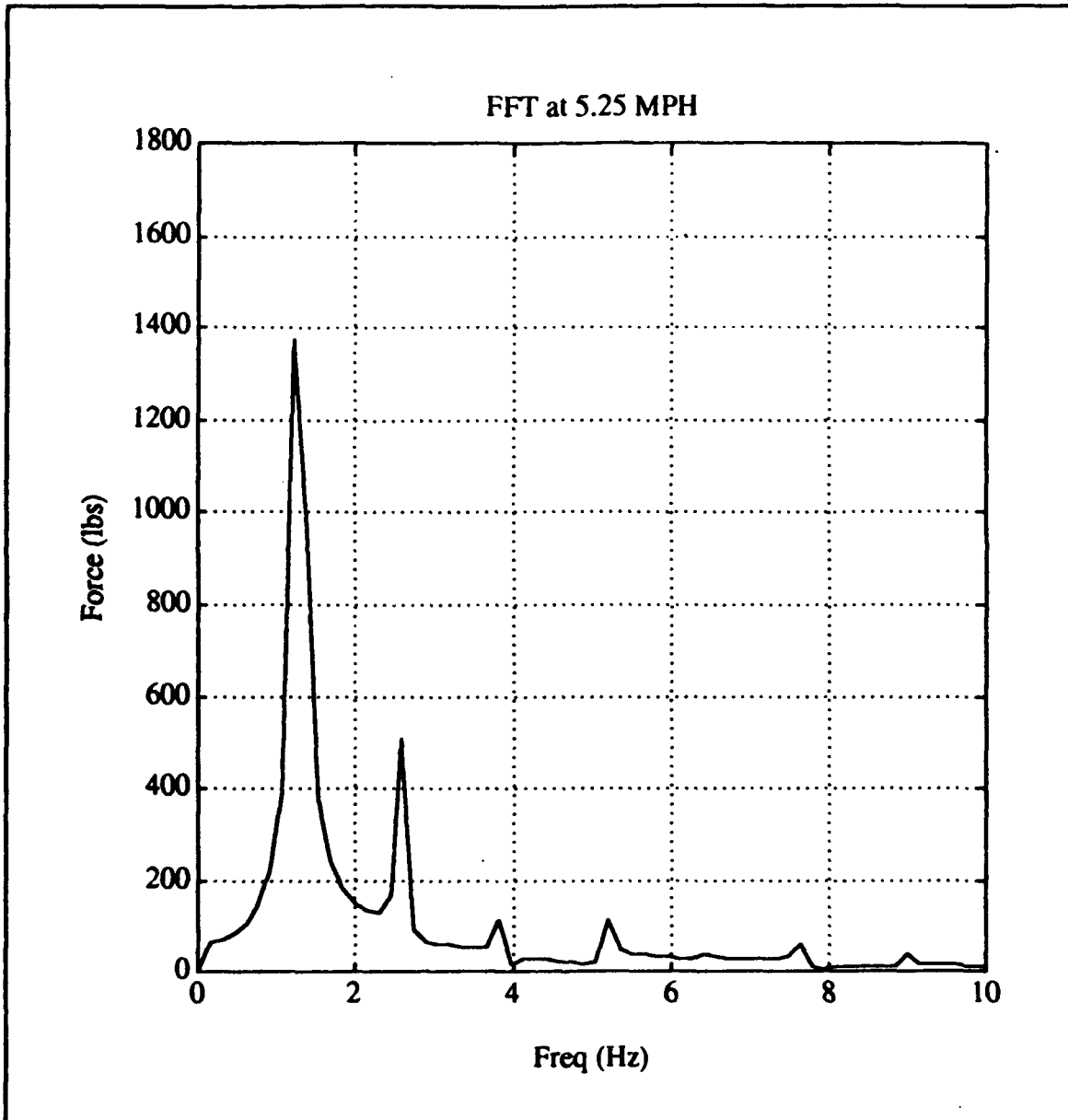


Figure 4-6 Model Results for A-Frame Force at 5.25 MPH (FFT)

B. NATURAL FREQUENCIES AND MODE SHAPES

The natural frequencies and mode shapes of the system were determined by using the mass and stiffness matrices that were developed in Chapter II. The eigenvalues and eigenvectors of the system are determined from the matrix that results from multiplying the inverse of the mass matrix, $[M^{-1}]$, by the stiffness matrix, $[K]$. The system's natural frequencies are the square root of the eigenvalues. The system's mode shapes are the eigenvectors that correspond to these natural frequencies. Analysis of these natural frequencies and mode shapes shows that the howitzer's bounce mode occurs at a natural frequency of 1.28 Hertz which corresponds to a speed of 5.25 MPH for the howitzer traveling over the washboard. By providing an excitation at a natural frequency of the system (1.28 Hz) the maximum A-Frame force that could possibly be developed for this particular washboard input resulted.

C. "WORST CASE" POTHOLE COURSE RESULTS

The model results from the "worst case" pothole that was identified in Chapter III show that maximum A-Frame force occurs lbs at 15 MPH. At speeds slower or faster than this speed the model results showed lower levels of A-Frame force for this pothole. Figure 4-7 shows the A-Frame force for the "worst case" pothole at 15 MPH. There are spikes in the A-Frame force when the wheels of the system hit the pothole. On Figure 4-7, at 0.1 seconds the front HUMMV wheels hit, at 0.6 seconds the rear HUMMV wheels hit, and at 1.2 seconds the howitzer wheels hit the pothole. When the

howitzer wheels hit at 15 MPH the maximum A-Frame force is 8,500 lbs.

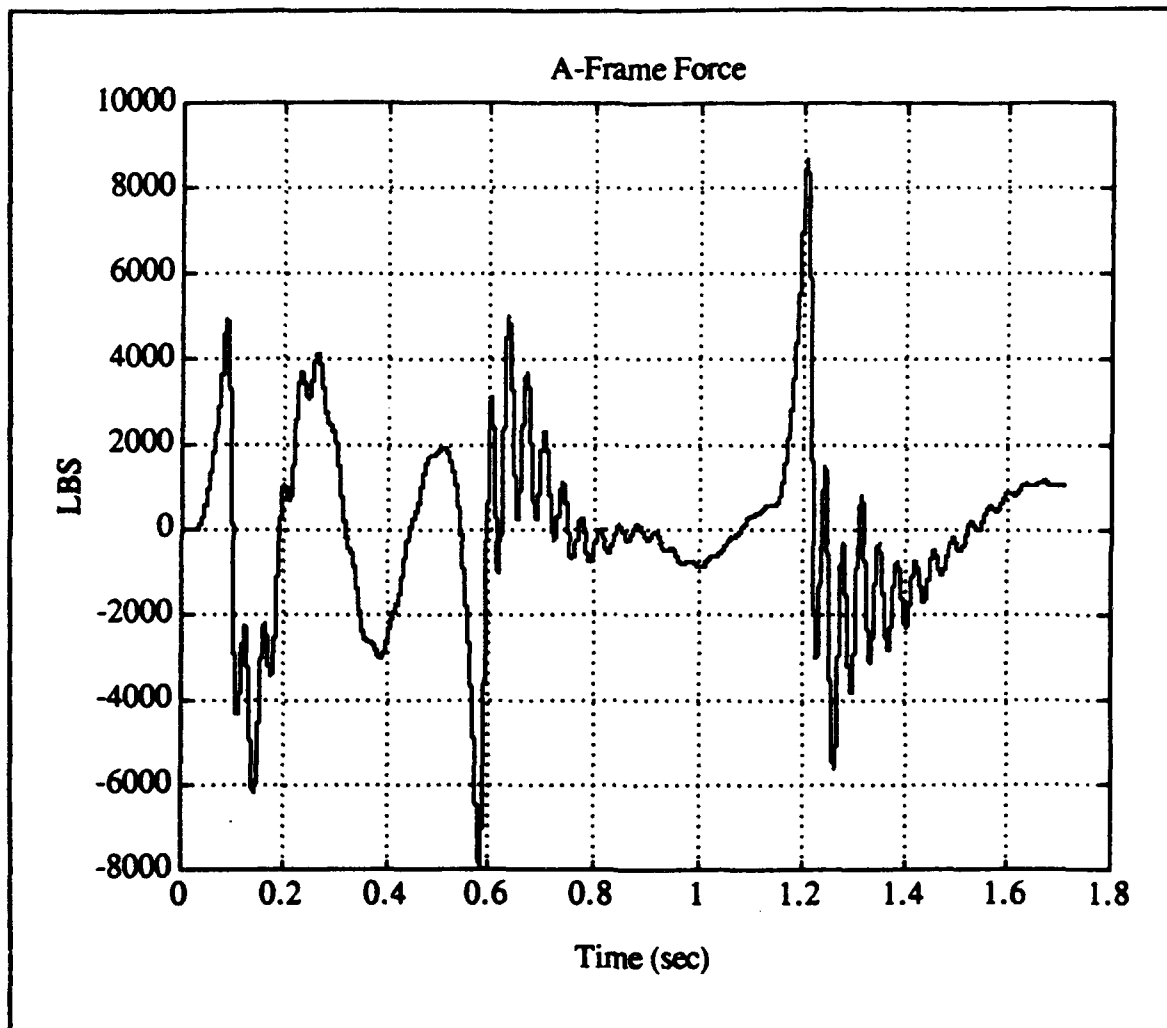


Figure 4-7 Model Results of A-Frame Force for "Worst Case" Pothole at 15 MPH

V. STRUCTURAL ANALYSIS

This chapter explains the structural analysis that was performed on the howitzer in order to determine both the force levels in the A-Frame and the stress on the howitzer's components. To determine the actual force levels in the A-Frame, the A-Frame was instrumented with strain gages as shown in Figure 5-1. This instrumented A-Frame was then calibrated to determine a calibration factor which would correlate strain gage readings to A-Frame force levels. This calibrated A-Frame was used during the dynamic test (see Chapter VI) at Aberdeen Proving Grounds (APG) to measure the actual force levels in the A-Frame.

A. A-FRAME CALIBRATION

The primary purpose of calibrating the A-Frame was to develop a reliable means to correlate dynamic strain gage measurements on the legs to the amount of force that causes the strain. Additionally, the strain measurements obtained during calibration were used to determine the value of the equivalent linear spring stiffness of the A-Frame for the computer model. During the calibration extra strain gages were attached to help identify levels of stress at key locations other than the locations needed for the force versus strain calibration. These extra gages provided information that was used to form conclusions about the stress in the A-Frame, discussed later.

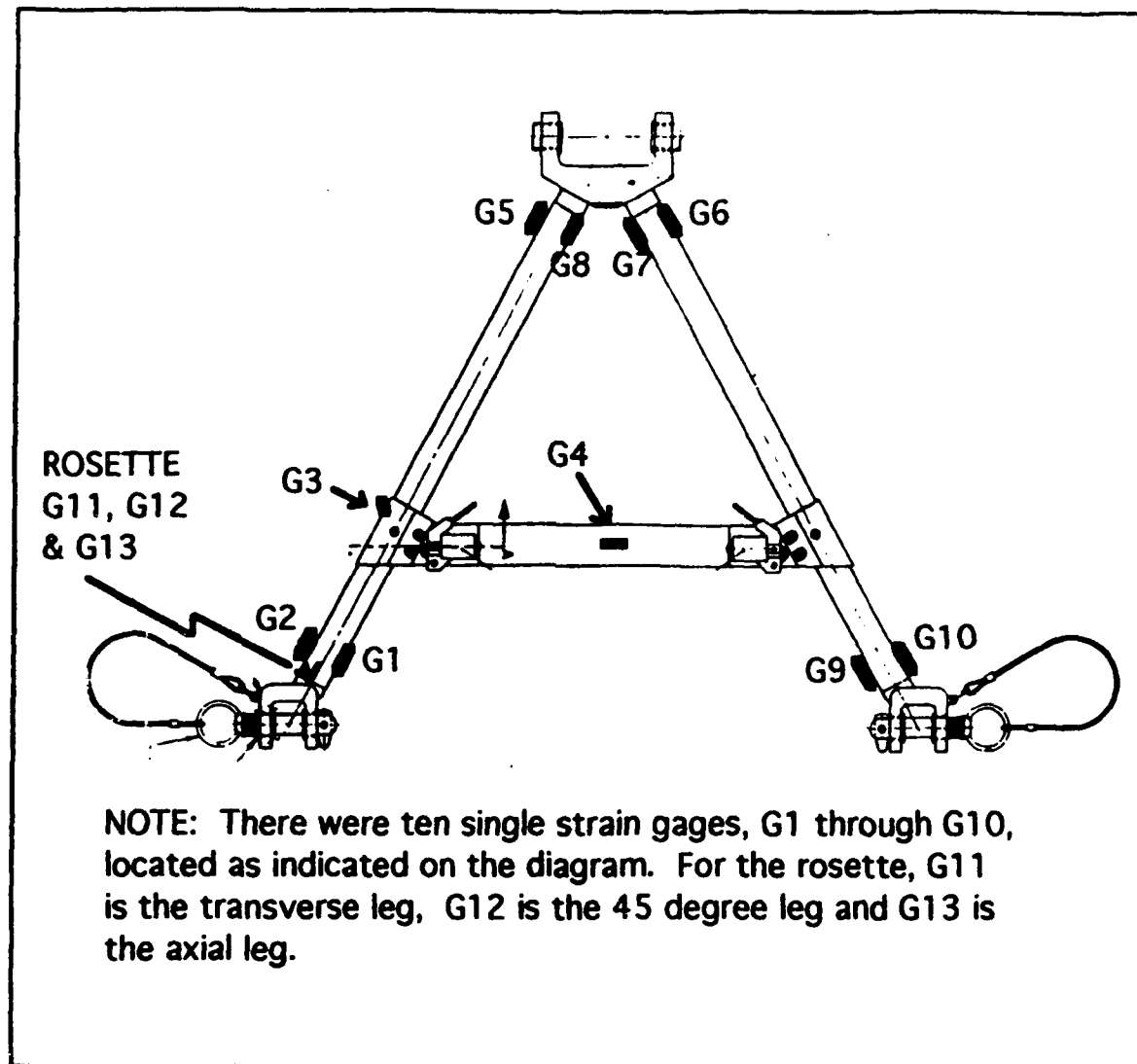


Figure 5-1 Location of A-Frame Strain Gages

The A-Frame was loaded in both a vertical and lateral load configuration to determine if there were any significantly different effects between the two loading configurations. Figures 5-2 & 5-3 show the test setup for both these configurations.

1. A-Frame Instrumentation

To conduct the calibration, the A-Frame was instrumented with 13 strain gages (Figure 5-1). The data taken from the pair of single strain gages located on the bottom of each leg was used for the development of the calibration curve. The pair of single strain gages on the top of each leg were used to verify that loads in the legs were mainly axial loads as opposed to bending loads. The single gage on the A-frame cross support brace and the single gage on the attaching clamp for this brace were used to identify stress levels in these members. The latter two strain gages were used because there were some known cases where the cross support brace clamps had cracked, and it was unknown whether these cracks were the result of high load levels or caused by manufacturing defects.

2. Support Equipment

The calibration was conducted using the lab facilities of the Department of Mechanical Engineering at the Naval Postgraduate School. To hold the A-Frame during the calibration a test support structure was built. The main objective of this support stand was to closely match the mechanical effects that occur in the A-Frame when it is loaded while connected to the T-Bar. The test support used was constructed out of heavy steel and used actuator eyebolts from a M119 Howitzer to connect the bottom of the A-Frame legs to the test

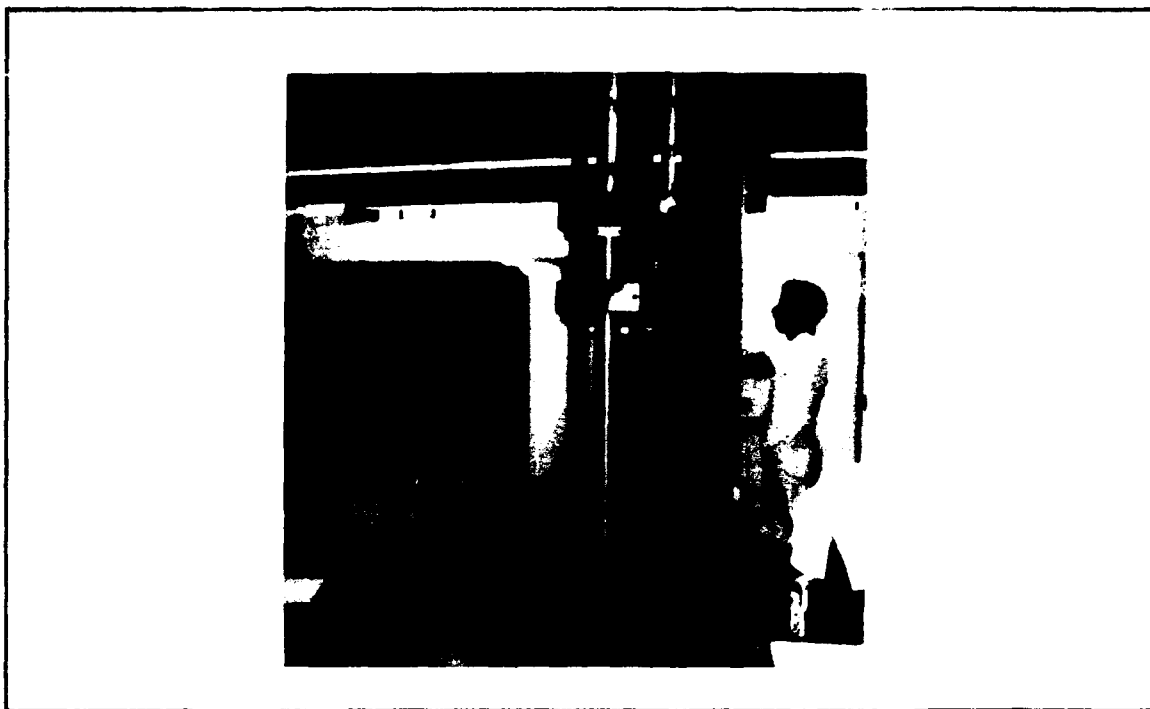


Figure 5-2 Vertical Configuration for A-Frame Test

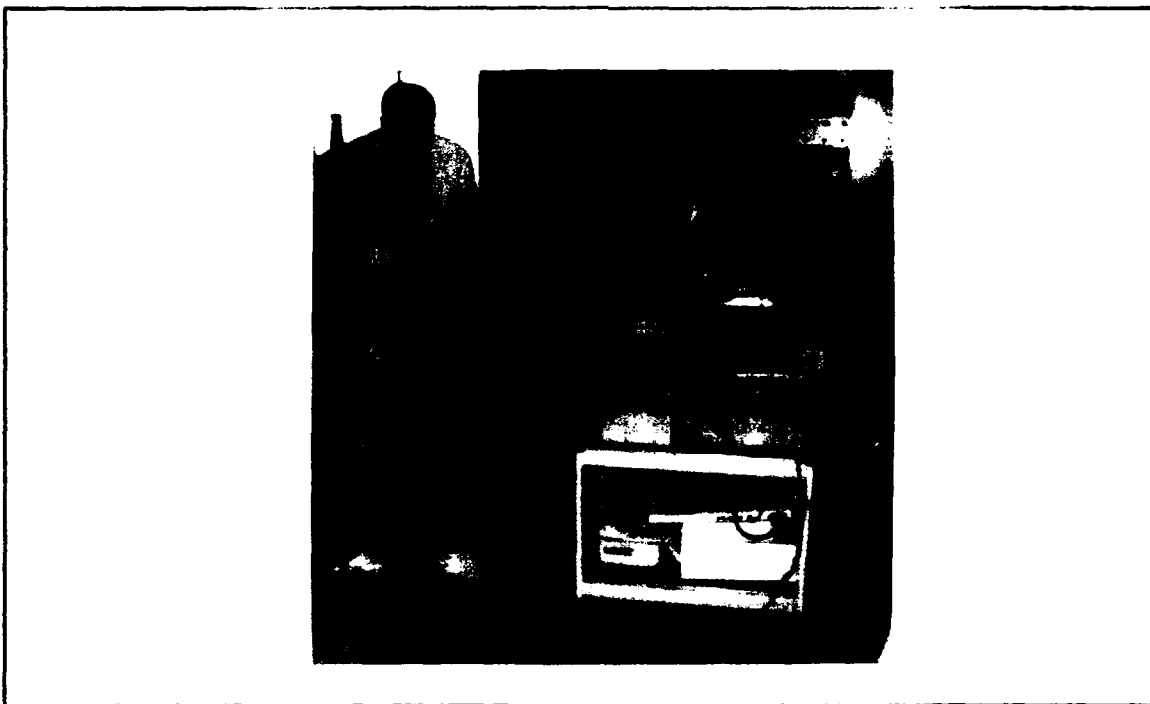


Figure 5-3 Lateral Configuration for A-Frame Test

support (Figure 5-4). A clamping device to attach the apex of the A-Frame to the load cell was also designed which simulated the loading effects of the actual clamping device on the howitzer (Figure 5-5). The test support structure achieved the goal of simulating the A-Frame being attached to the T-Bar of the howitzer.

3. Load Cells

The vertical loads were applied using a Riehe Testing machine as shown in Figure 5-2. This loading device was used to apply vertical loads up to 12,000 lbs. The lateral loads were applied using a turn-buckle that was connected to a 5,000 pound rated capacity dynamometer. This dynamometer and turn-buckle system is shown in Figure 5-3.

4. Calibration Procedures

Two data runs were recorded for both the vertical and lateral configurations. A data run consisted of loading the A-Frame in increments to the maximum load for that particular data run and then unloading it in the same manner. All strain gages were zeroed before the start of each run. At each load increment, strain gage readings were recorded for all of the strain gages. Tables F-1 through F-4 contain the strain gage readings and load data obtained from these calibration procedures.

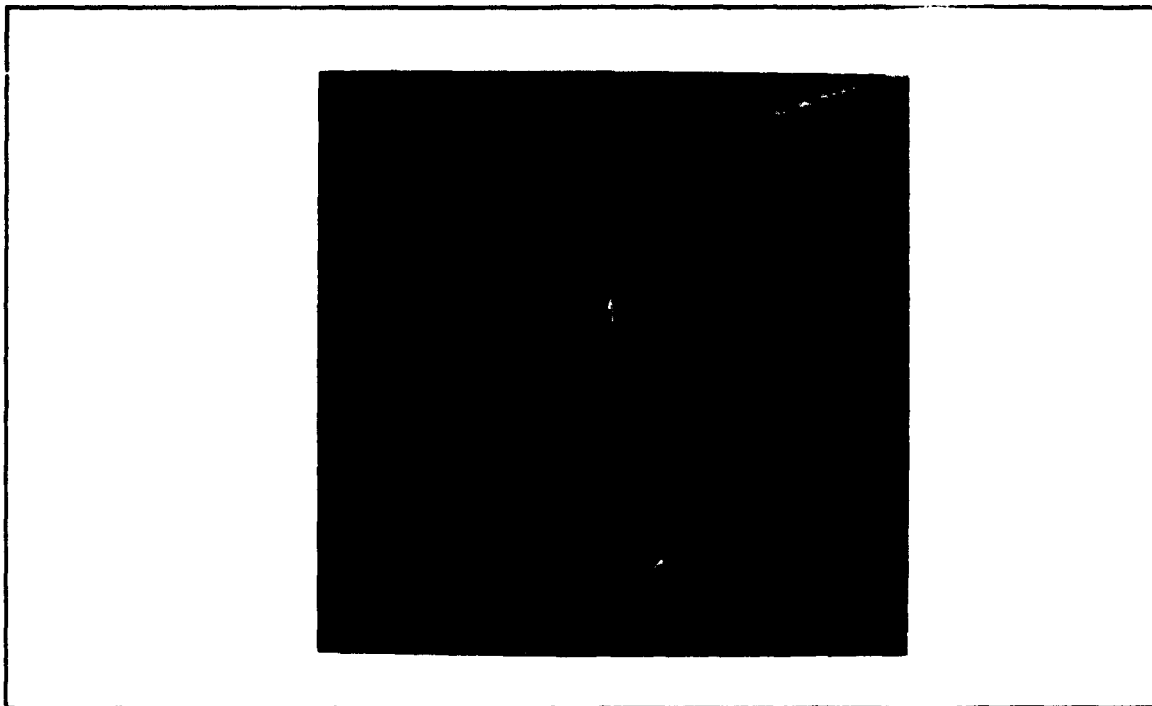


Figure 5-4 A-Frame Connection to Test Mount

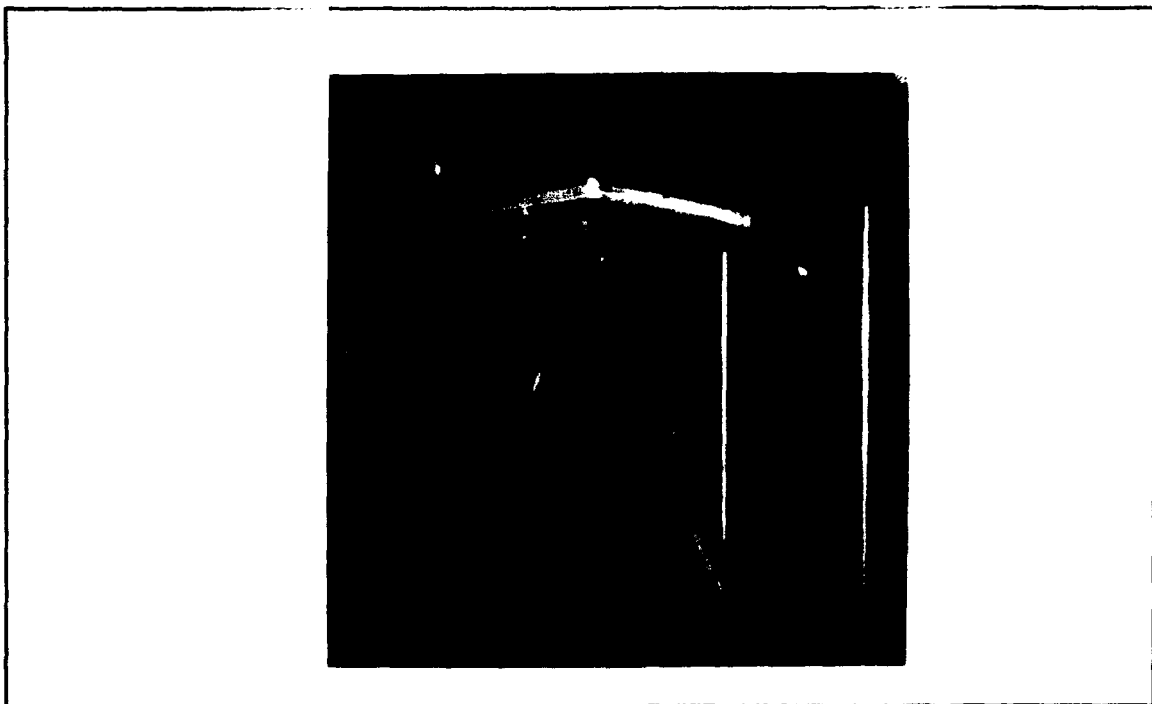


Figure 5-5 A-Frame Apex Clamping Device

5. Calibration Factor

From the vertical test strain gage data in Appendix F the A-Frame vertical force versus strain calibration factor was determined. Since the A-Frame vertical load test was a static test the vertical force loading at the apex of the A-Frame must be balanced by the sum of the vertical reaction forces in the legs of the A-Frame (Figure 5-6).

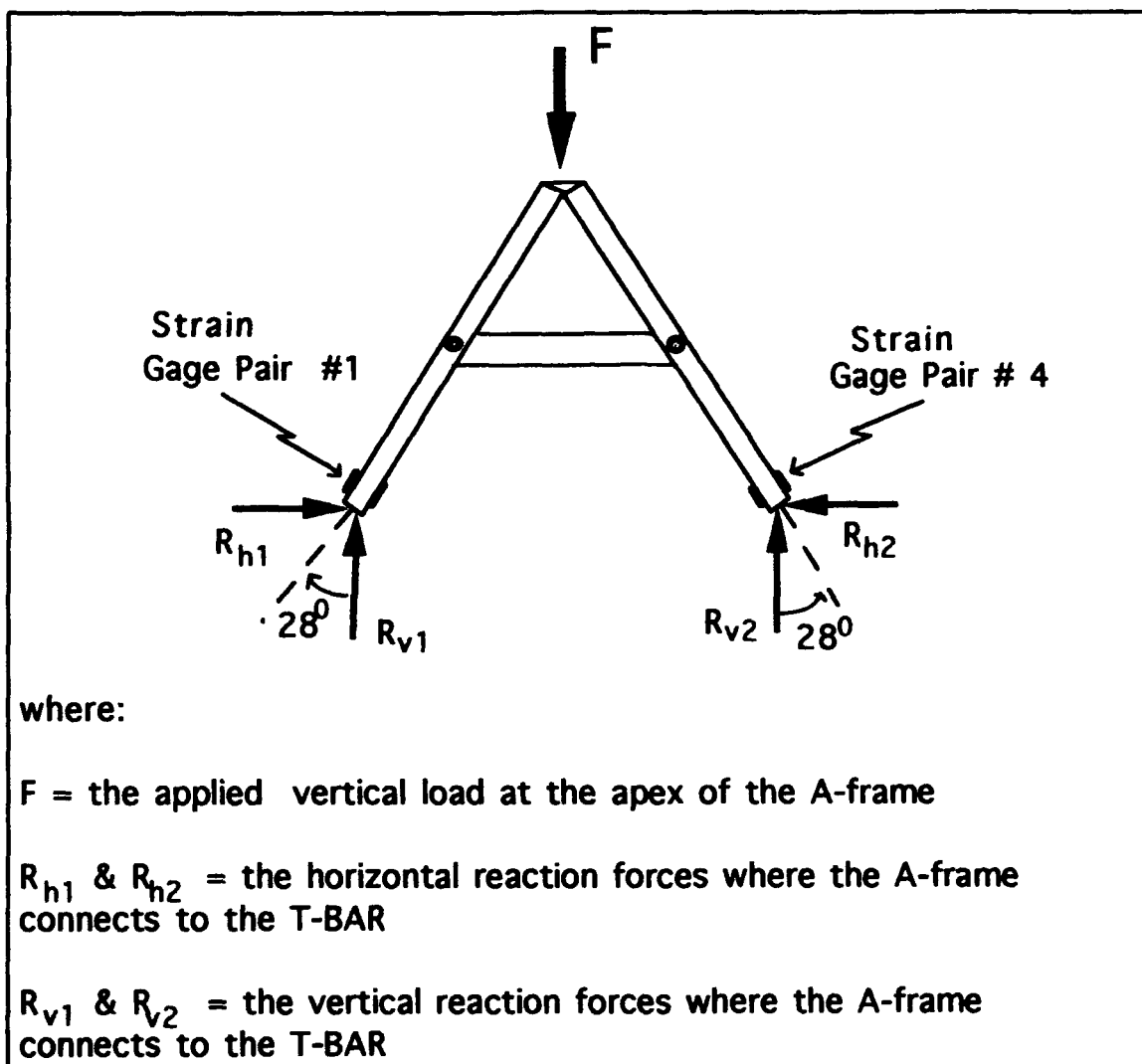


Figure 5-6 Balance of Forces on the A-Frame

The reaction forces (R_{v1} & R_{v2}) at the bottom of each leg of the A-Frame were determined by using the strain gage readings from Gage Pair 1 (gages 1 & 2) and Gage Pair 4 (gages 9 & 10) that are identified in Figure 5-6. The average value of the strain for either of the strain gage pairs was multiplied by the Modulus of Elasticity of the A-Frame (10×10^6 psi) which yields the axial stress in the A-Frame leg. This axial stress value was then multiplied by the cross sectional area of the A-Frame legs (0.6107 in^2) to determine the axial force. To calculate the vertical component of this axial force the above value for axial force was multiplied times the cosine of 28° . A sample calculation is shown below using the 10,000 lb load increment of Vertical Test #1 (see Table F-1 for strain gage data):

$$\text{Strain Gage Pair 1} \Rightarrow \text{Avg Strain} = 988 \times 10^{-6}$$

$$\therefore \text{Stress} = \text{Strain} \times \text{Modulus of Elasticity}$$

$$= (988 \times 10^{-6})(10 \times 10^6 \text{ psi}) = 9,880 \text{ psi}$$

$$\Rightarrow \text{Force} = \text{Stress} \times \text{Area} = (9,880 \text{ psi})(0.6107 \text{ in}^2) = 6,033 \text{ lbs}$$

$$\therefore \text{The vertical reaction force: } R_{v1} = (6,033 \text{ lbs})(\cos(28)) = 5,327 \text{ lbs}$$

$$\text{Strain Gage Pair 4} \Rightarrow \text{Avg Strain} = 1,095 \times 10^{-6}$$

$$\therefore \text{Stress} = \text{Strain} \times \text{Modulus of Elasticity}$$

$$= (1,095 \times 10^{-6})(10 \times 10^6 \text{ psi}) = 1,095 \text{ psi}$$

$$\Rightarrow \text{Force} = \text{Stress} \times \text{Area} = (10,950 \text{ psi})(0.6107 \text{ in}^2) = 6,687 \text{ lbs}$$

$$\therefore \text{The vertical reaction force: } R_{v2} = (6,687 \text{ lbs})(\cos(28)) = 5,904 \text{ lbs}$$

$$\sum \text{Vertical Forces} \Rightarrow R_{v1} + R_{v2} = 5,327 + 5,904 = 11,231 \text{ lbs}$$

To determine the calibration factor for vertical loading, the percentage difference between the known apex load and the sum of the calculated vertical force components at the bottom of the A-Frame was determined. The average percent difference for all the load increments is equal to the calibration factor. This calibration factor can then be used to compare measured loads in the A-Frame legs to the applied load at the apex of the A-Frame. An average calibration factor of 0.88 was determined over all of the load increments from both vertical tests. A sample calculation of the calibration factor for the 10,000 lb force increment of Vertical Test #1 (see Table F-1) is shown below:

Actual Vertical Force \rightarrow 10,000 lbs

Measured Vertical Force \rightarrow 11,231 lbs

Calibration Factor $\rightarrow \frac{10,000}{11,231} = 0.89$

6. A-Frame Stiffness

The measured strain data was also used to determine an effective linear spring stiffness for the A-Frame. To determine this stiffness the applied vertical load for a specified load increment was divided by the corresponding amount of vertical deflection in the A-Frame. The average axial deflection in the A-Frame legs was calculated from the average strain at the bottom of each leg. The average axial deflection was then multiplied by the cosine of 28° to calculate the amount of vertical deflection. A sample calculation for the 10,000 lb load increment of Vertical Test #1 (see Table F-1) is shown below:

Strain Gage Pair 1 = 998; Strain Gage Pair 4 = 1095

Avg axial strain = $\frac{998 + 1095}{2} = 1042 \times 10^{-6}$; Multiply by leg length

→ Avg axial deflection = $(28 \text{ in})(1042 \times 10^{-6}) = 0.029 \text{ in}$

Convert to vertical deflection = $(0.029 \text{ in})(\cos(28)) = 0.0257 \text{ in}$

∴ A - Frame Stiffness = $\frac{10,000 \text{ lbs}}{0.0257 \text{ in}} = 388,400 \text{ lbs/in}$

7. Observations

From analyzing the results of both the vertical and lateral A-Frame loadings the following conclusions were reached regarding A-Frame loading:

- * The strain measurements in both the cross member brace and the attaching clamp for this brace on the A-Frame (strain gages 3 & 4, in Figure 5-1) were very low regardless of the force at which the A-Frame was loaded. This indicates that these members are not critical components of the A-Frame in regards to failure.
- * The A-Frame loads are carried mostly through axial loads in the A-Frame legs as opposed to bending loads. This means that the bottom connection joints where the A-Frame attaches to the T-Bar act as pinned joints. However, because there was some bending in the A-frame legs at lower force levels the bottom joints do not act as perfect pin joints. The higher force levels break the static friction effects in the joints causing the joints to act more as perfect pin joints.

B. STRESS ANALYSIS

The stress analysis focused on determining the highest stress levels in the T-Bar and the A-Frame. To determine if mechanical failure will occur due to exceeding the yield stress, the stress at the

probable points of highest stress in the A-Frame and T-Bar were compared to the yield stress values for the respective materials.

1. T-Bar Stress

The T-Bar and A-Frame assembly are shown below in Figure 5-7. Point A on this figure is identified as the point of highest stress. This is where the geometry of the T-Bar assembly changes and the stronger built up portion of the T-Bar ends. To simplify the stress analysis the T-Bar is modeled as a cantilevered beam. Figure 5-8 below depicts the cantilevered beam modeling of the T-Bar as viewed from the end of the T-Bar and the rear of the howitzer. The point of highest stress was determined to be at the corner of the T-Bar at the base of the modeled cantilevered beam. One of these corners is identified as Point A in Figure 5-8.

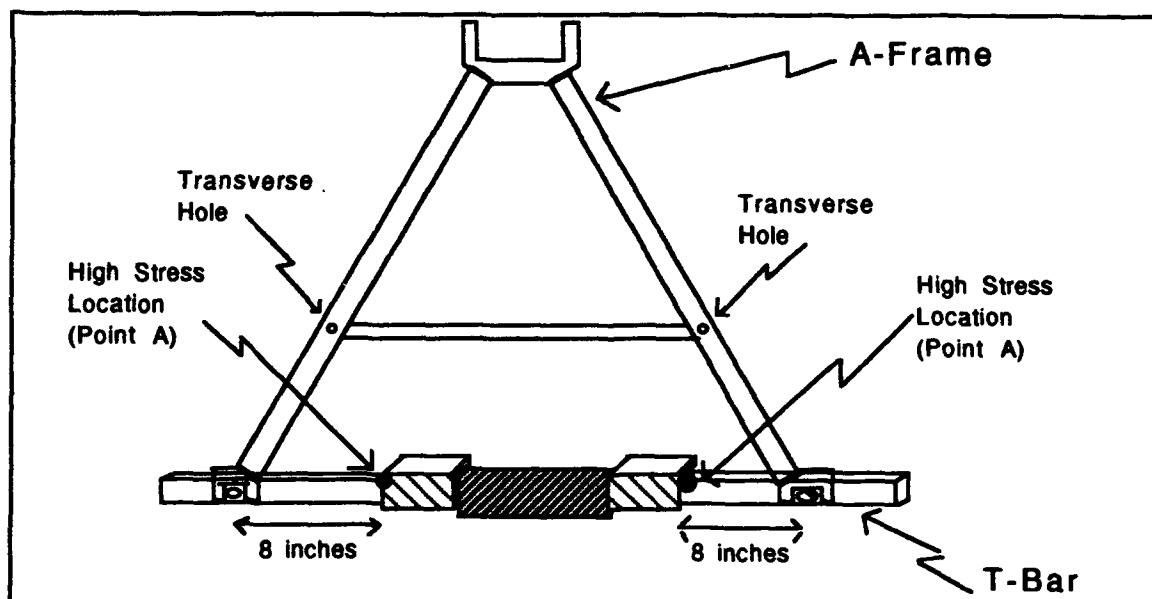


Figure 5-7 T-Bar and A-Frame Assembly

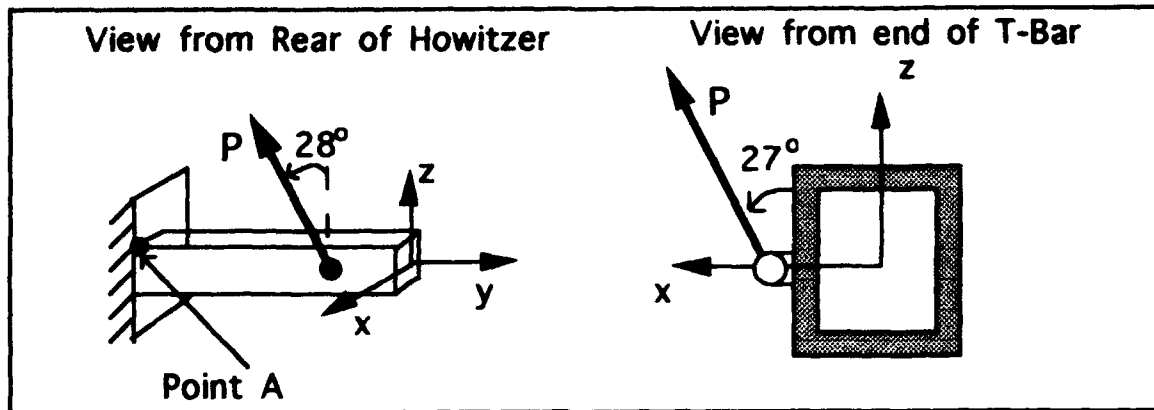


Figure 5-8 T-Bar Cantilevered Beam Model

To calculate the stress at Point A, the normal stress components that result when the axial force in the A-Frame leg, P , was resolved into components in the x , y , and z directions as shown on Figure 5-8. The stress at Point A is the sum of these normal stress components using the principle of superposition of stress. To find the normal stress components first the A-Frame leg force, P , was projected into a force component along the axis of the T-Bar in the y direction, $P_y = \sin(28)P$, and a second force component in the xz plane, $P_{xz} = \cos(28)P$. The P_{xz} component was further broken up into components in the x and z directions: $P_x = \cos(27)P_{xz}$ and $P_z = \sin(27)P_{xz}$. To calculate the normal stress that was caused by these force components P_x , P_y , and P_z well known strength of materials formulas for stress in a beam are applied. Therefore, applying these formulas the expression for the maximum stress in the T-Bar is:

$$\sigma = \left(\frac{P_y}{A} \right) + \left(\frac{P_z L_z}{I_x} \right) + \left(\frac{P_x L_x}{I_z} \right) \quad (\text{Eqn 5-1})$$

where:

P_x , P_y , and P_z : are defined in the above paragraph.

$L=8$ inches: The distance from the base of the cantilever to the point of application.

$A=.9240$ in²: The cross sectional area of the T-Bar.

$I_x=.8962$ in⁴: The bending moment of inertia about the x axis.

$I_z=.5979$ in⁴: The bending moment of inertia about the z axis.

$x =1.300$ in: The distance in the x direction from the geometric center of the T-Bar to the outer edge of the T-Bar.

$z =1.005$ in: The distance in the z direction from the geometric center of the T-Bar to the outer edge of the T-Bar.

2. A-Frame Stress

The probable point of highest stress in the A-Frame will occur around the 0.375 inch diameter transverse circular hole that positions the cross member attaching clamps. This hole is identified in Figure 5-7 above. At the location of this hole a stress concentration will exist. Figure 5-9 below contains the empirical formula from page 601 of [Ref. 4] that was used to determine the stress concentration in a pipe section with a transverse hole.

From the above formula the stress concentration factor for axial loads was determined to be 3.73. Additional stress concentrations due to the effects of bending and torsional loads were neglected. The justification for neglecting the effects of bending

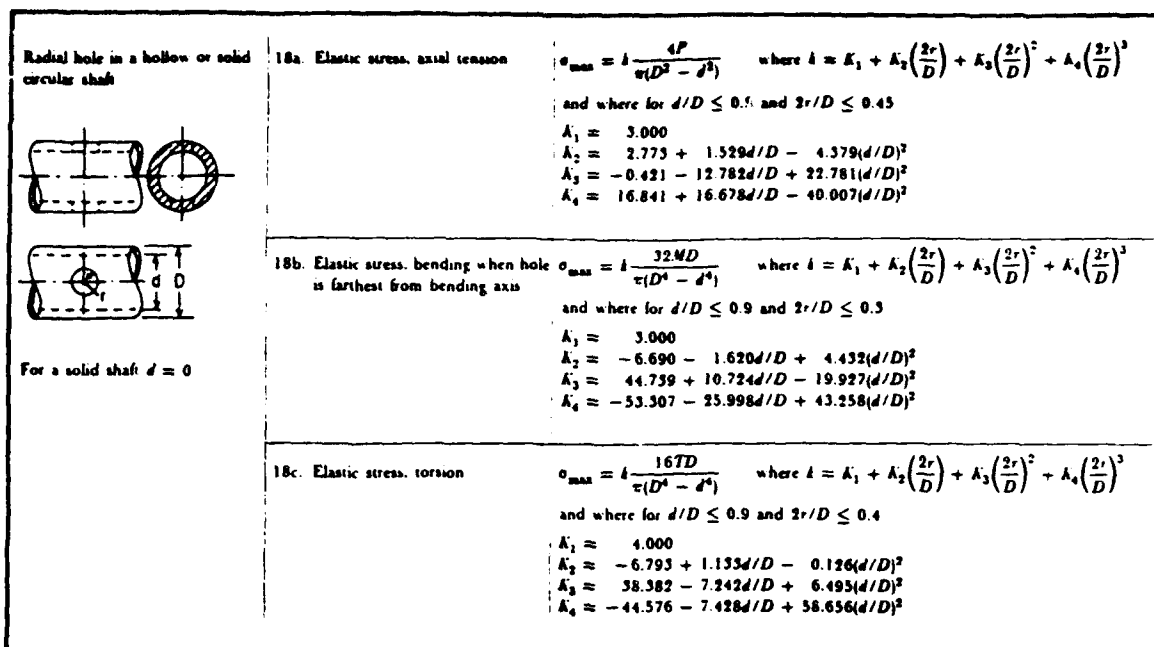


Figure 5-9 Stress Concentration Due to a Circular Hole in a Pipe Section

loads was that both the A-Frame calibration results (see Appendix F) and the results of the instrumented test (see Chapter VI) show that the joint where the A-Frame connects to the T-Bar acts as a nearly perfect pin joint at higher load levels. Any stress concentration reduction due to the spring pin that is driven into the hole were neglected because this stress reduction was assumed to be small. Therefore, maximum total stress in the A-Frame was based on only the axial stress component in the legs and was determined using the following formula:

$$\sigma = \frac{PK}{A} \quad (\text{Eqn 5-2})$$

where:

P = the axial load in the A-Frame leg.

$K = 3.73$: the stress concentration factor for axial loading that is caused by the hole in the A-Frame leg.

$A = 0.6107 \text{ in}^2$: the cross sectional area of the A-Frame leg.

Without this hole in the A-Frame the maximum allowable stress would be increased by the amount of the stress concentration factor, 3.73. This hole appears to only aid in assembling the A-Frame and serves no other function. Elimination of this hole would make the factor of safety more than three times greater.

3. Worst Case Stress and Factors of Safety

Using Eqn 5-1 and Eqn 5-2 above, the maximum stress was calculated for the T-Bar and the A-Frame. The maximum predicted A-Frame force of 8,500 lbs from driving the computer over the "worst case" pothole described in Chapter II was divided by two to calculate the force in each leg of the A-Frame. The resulting axial force, P, in each leg of the A-Frame equals 4,250 lbs. From Eqn 5-1 the resulting stress in the T-Bar is 63,900 psi. From Eqn 5-2 the A-Frame stress equals 26,000 psi.

The above stress levels are used to calculate the predicted factors of safety for the T-Bar and the A-Frame. The factor of safety is calculated by dividing the yield stress of the component by the predicted maximum load stress. The yield stress for the T-Bar and A-Frame are 116,000 psi and 50,000 psi, respectively. Based on the maximum predicted stress levels given above, the factor of safety is 1.81 for the T-Bar and 1.92 for the A-Frame. These factors of safety show that both the T-Bar and the A-Frame are strong enough to withstand the stress from the worst case predicted loads.

VI. INSTRUMENTED TEST

An instrumented dynamic test was conducted on the M119 howitzer at Aberdeen Proving Grounds (APG) in April of 1993. The howitzer was instrumented as described below in paragraph A. The dynamic testing was conducted by driving the howitzer over several of the APG courses at various speeds. The calibrated A-Frame described in Chapter V was used to measure the force levels in the A-Frame during the test. In most respects, the test results for A-Frame force are similar to the results obtained from the computer model. However, because certain physical effects were not included in the computer model, there are some differences between the results of the actual test and the results from the computer model. The results of this instrumented test confirmed that the M119 Howitzer could be safely transported in the firing position with the A-Frame attached.

A. INSTRUMENTATION

For this test the howitzer was instrumented with 20 strain gages, two tri-axial accelerometers, and two extensimeters. This instrumentation is explained in the following paragraphs.

1. Accelerometers

The howitzer was instrumented as shown in Figure 6-1. A tri-axial accelerometer was placed on the T-Bar to measure the vertical, longitudinal, and transverse accelerations of the howitzer

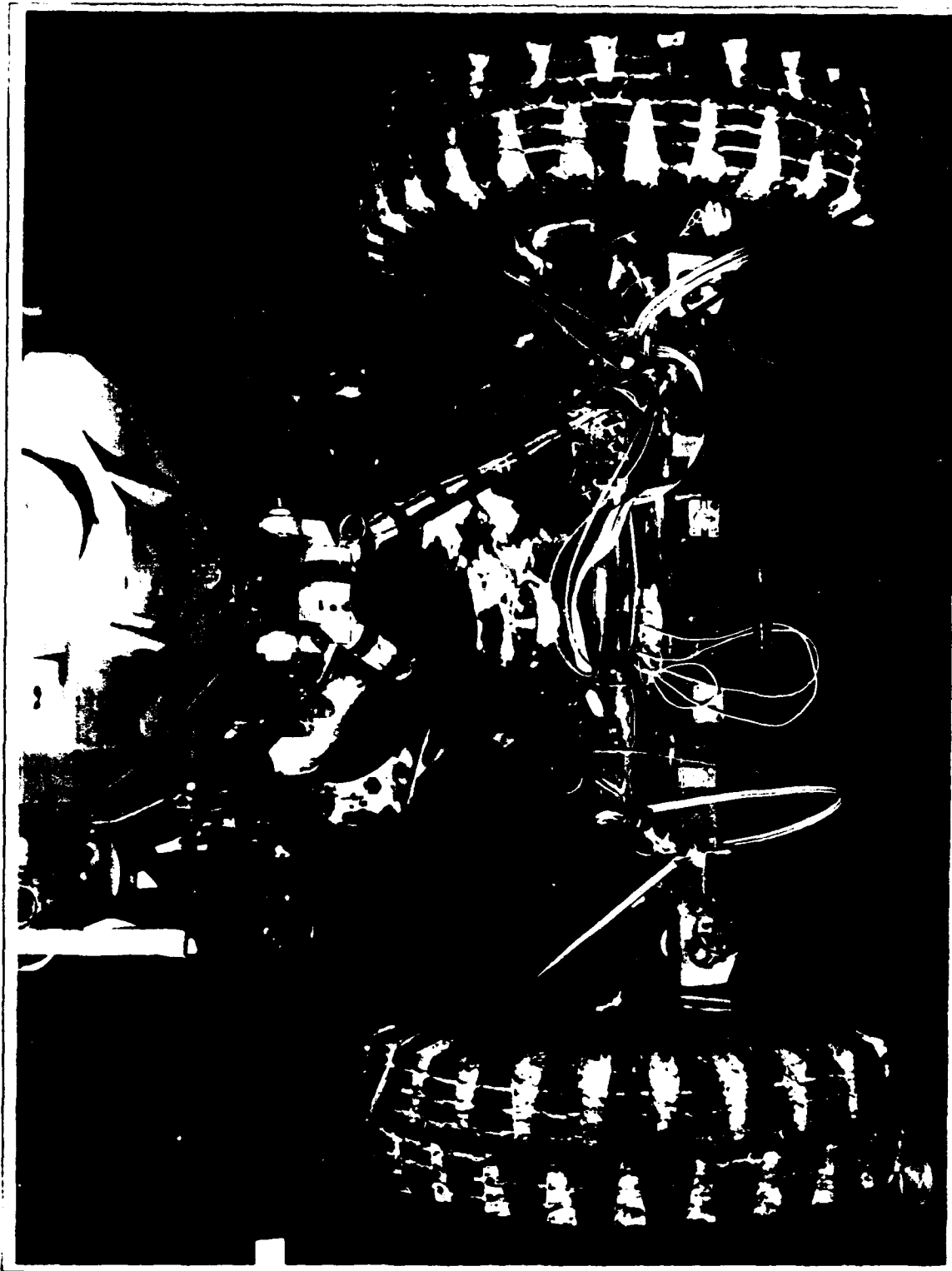


Figure 6-1 Howitzer Instrumentation for APG Test

trail mass. This accelerometer was not placed at the center of gravity of the trail mass because of difficulties in attaching an accelerometer at this point. The location chosen on the T-Bar provided accelerations on the same order of magnitude and representative of the accelerations at the center of gravity of the trail. The other tri-axial accelerometer was attached on the elevating mass near its center of gravity. This location is shown in Figure 6-2.

2. Single Strain Gages

The two pair of single strain gages on the bottom of each leg (gage pair 1 & 4 in Figure 5-6) of the previously calibrated A-Frame were used to measure the strain in the A-Frame legs. The calibration factor determined in Chapter V was used to correlate measured strains in the A-Frame legs to force levels in the A-Frame. Single strain gages were also attached on the top and the bottom of the T-Bar on both sides of the howitzer. The location of these gages is shown in Figure 6-3. Because the highest levels of stress on the T-Bar are at the corners, it was not possible to place the gages at these points. The gages were placed as close to the high stress points as possible. Even though these gages could not be used to determine the maximum stress on the T-Bar, they could be used to roughly judge the level of stress.

3. Other Gages

Strain rosettes were placed on the bottom of the A-Frame legs and on the bottom howitzer trail on each side of the howitzer.

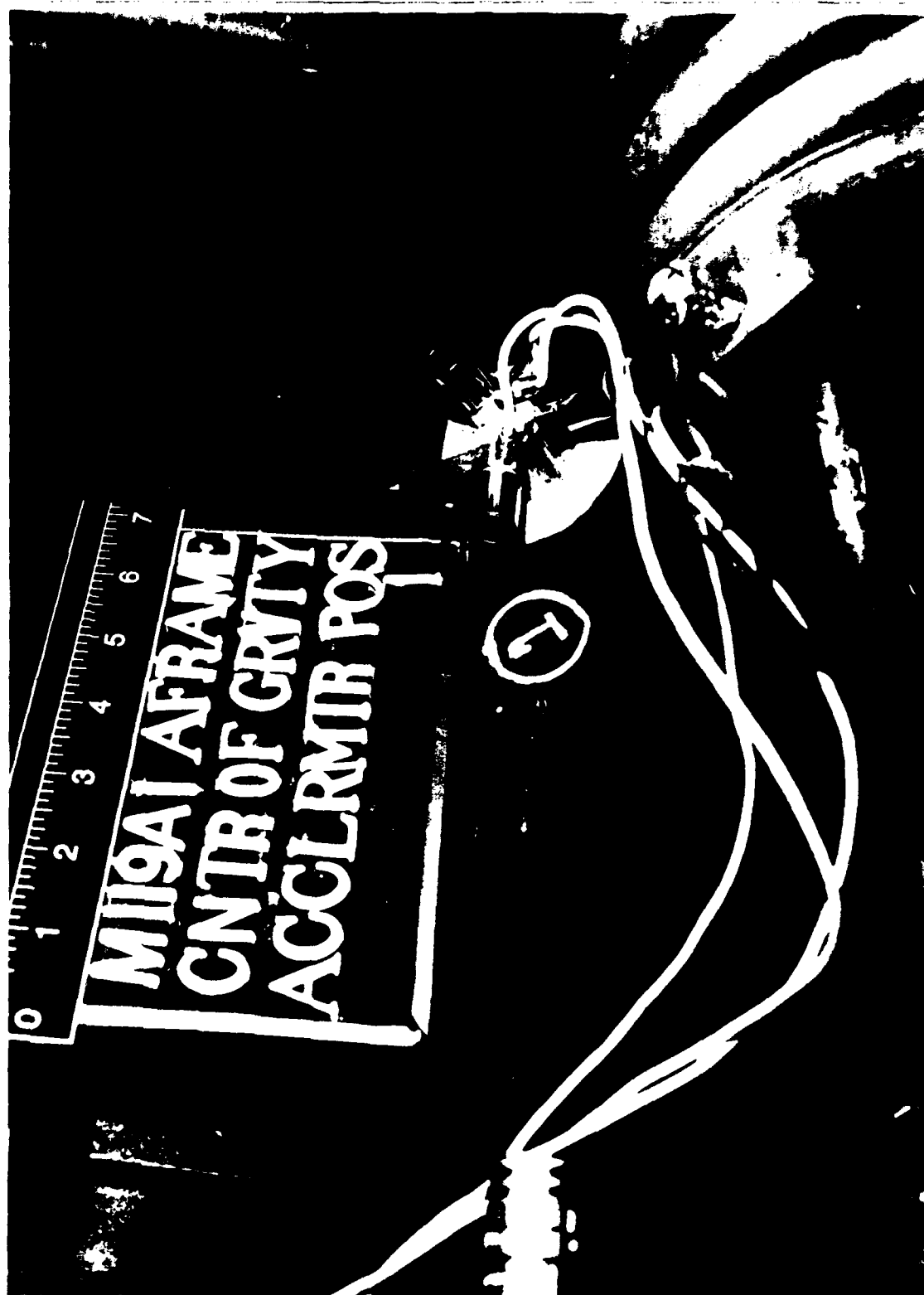


Figure 6.2 Location of Elevating Mass Accelerometer



Figure 6-3 Location of T-Bar Strain Gages

An extensometer was used on each shock absorber to determine if the shocks were extending far enough so that the stiff rubber bump stops would be activated.

B. TEST COURSES

Several of the standard APG test courses were used for the instrumented test. These courses are described below.

1. Belgian Block Course

This course is designed using "Belgian Blocks" to produce a road that has high frequency random bumps. The magnitude of each bump is small. This course is shown in Figure 6-4. During the test this course was traversed at speeds ranging from 10 to 25 MPH.

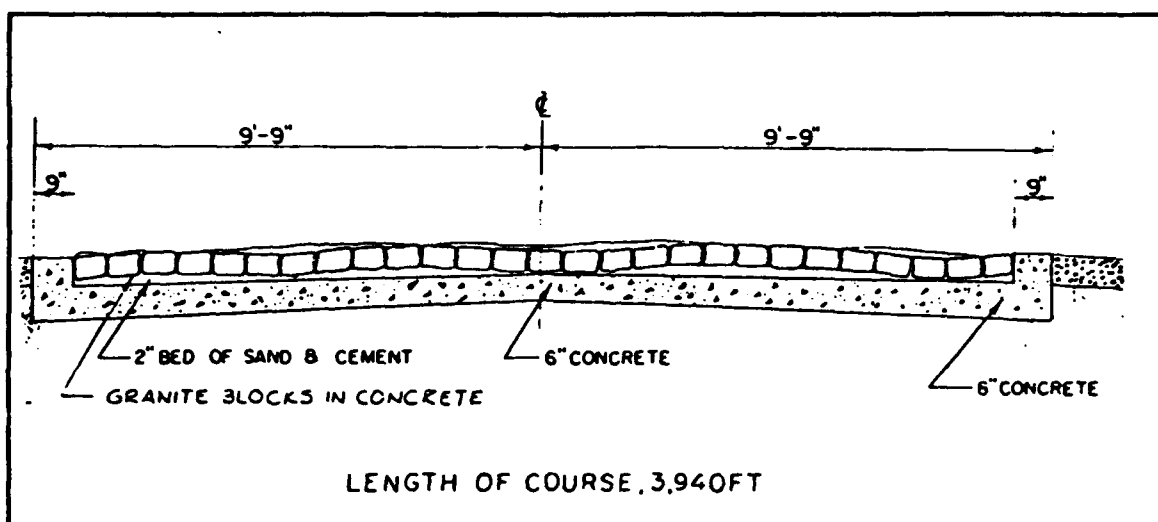


Figure 6-4 APG Belgian Block Course

2. Six Inch Washboard Course

This course has six inch bumps that are evenly spaced six feet or 72 inches apart as shown in Figure 6-5. This course produces

significant heave and pitch effects on wheeled vehicles even at relatively slow speeds. During the test this course was traversed at speeds ranging from three to six MPH.

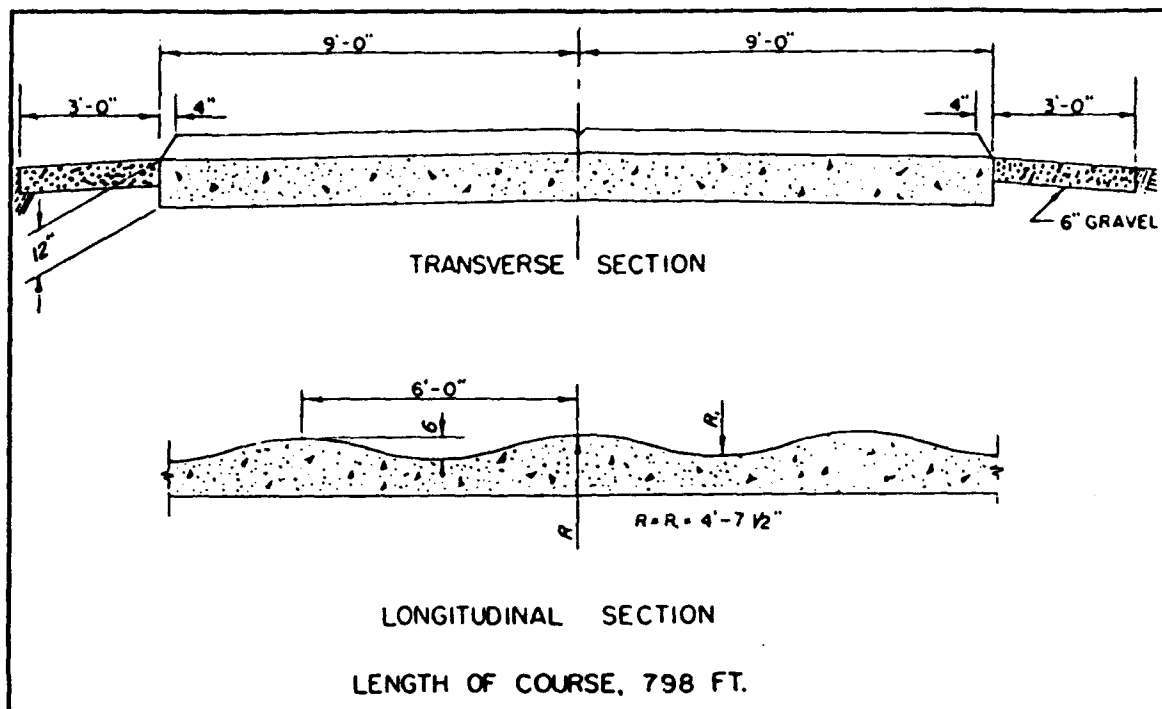


Figure 6-5 APG Six Inch Washboard Course

3. Cross Country Course Number 1

This course is similar to a relatively smooth but winding trail road. This course was traversed at approximately 25 MPH.

4. Cross Country Course Number 3

This is similar to a rough trail road which has random large, medium, and small sized bumps. This course was traversed at speeds ranging from 5 to 15 MPH.

C. TEST PROCEDURES

Each of the above courses were traversed by the howitzer being towed by the HUMMV at speeds within the ranges listed. Data was collected on all the channels described above, using a sampling rate of 2,500 Hertz. Because of memory limitations in the data collection equipment only approximately 30 seconds worth of continuous data could be stored. For each course several data runs were completed using various speeds. For instance, on the Six Inch Washboard Course, six data runs were taken at speeds ranging from three to six MPH.

The speeds for each data run on the Six Inch Washboard Course and Cross Country Course Number 3 were measured using the HUMMV's speedometer, because these courses were too rough to use more accurate devices. For the data runs, on these courses, the driver tried to hold the HUMMV at the specified speed while himself being bounced around. Because of the extremely rough road conditions and inaccuracies in the speedometer, the actual speeds ended up being different than the speeds specified in the test plan. Consequently, the only accurate method of determining the actual speed during a data run on these courses is from the video tape taken during the run.

D. TEST RESULTS AND DISCUSSION

The Belgian Block and Cross Country Course Number 1 showed no significant levels of strain or acceleration even at speeds up 25 MPH. These tests simply proved that the howitzer could traverse

these courses without causing damage to the howitzer. The Six Inch Washboard Course and Cross Country Course Number 3, however, did produce significant levels of strain and acceleration on the howitzer components.

The test results for the Six Inch Washboard Course were analyzed in both the time and frequency domains. Data runs at speeds of 3.75, 5.0 and 5.25 MPH were analyzed for the Six Inch Washboard Course and compared to the predicted results from the computer model. The most severe data run from Cross Country Course Number 3 at 15 MPH was analyzed in the time domain. The procedures used and the analysis of these results are as follows:

1. Time History Results

The time history for vertical "in plane" A-Frame force in each case was produced by first summing the "in plane" axial forces from both of the A-Frame legs. The same calculation procedures as in Chapter V were used for determination of the axial forces in the legs from the strain gage data for strain gage pairs 1 and 4 (see Figure 5-6). The vertical force was determined by multiplying the axial force times the cosine of 28° . This total vertical force in the A-Frame legs was multiplied by the calibration factor of 0.88 that was determined in Chapter V. The A-Frame lateral forces were calculated by determining the difference in the horizontal force components of the axial force in each A-Frame leg. The accelerations were plotted directly from the measured data.

The force and acceleration time histories for the washboard course (Figures 6-6 through 6-11) show that high frequency spikes

occur on the washboard course. These spikes are caused the braking system being activated as the howitzer went over the bumps for all speeds. Also, for the 5.25 MPH data run the spade hit the tops of the bumps. These effects are not included in the computer model and result in differences between the model results and the actual results, particularly, for the 5.25 MPH data because the spade was hitting.

Time histories for A-Frame force for speeds 3.75, 5.0 & 5.25 MPH from the actual test (Figures 6-6, 6-8, & 6-10) are similar to the time histories predicted by the computer model for the same speeds (Figures 4-1, 4-3 & 4-5). The high frequency force spikes do not appear in the model's predicted results, however, the levels of the basic force response in the actual results closely compare to the force response of the model. For example, the actual results for 5.0 MPH (Figure 6-8) has spikes that reach a maximum force of 5,500 lbs. But the basic force response on average reaches approximately 2,400 lbs in tension and 4,300 lbs in compression. The corresponding model prediction (Figure 4-3) shows forces of 2,800 lbs in tension and 4,800 lbs in compression. A similar comparison can be made at the 3.75 and 5.25 MPH speeds. Although the actual results are not exactly the same as the model predictions, they are close enough to conclude that the model is reasonably representative of the actual results.

The A-Frame vertical force results for the most severe portion of the Cross Country Course Number 3 are shown in Figure 6-12. These results show that on a rough trail road the A-Frame force

is not as great as the force that was caused by the Six Inch Washboard Course at a speed of 5.25 MPH.

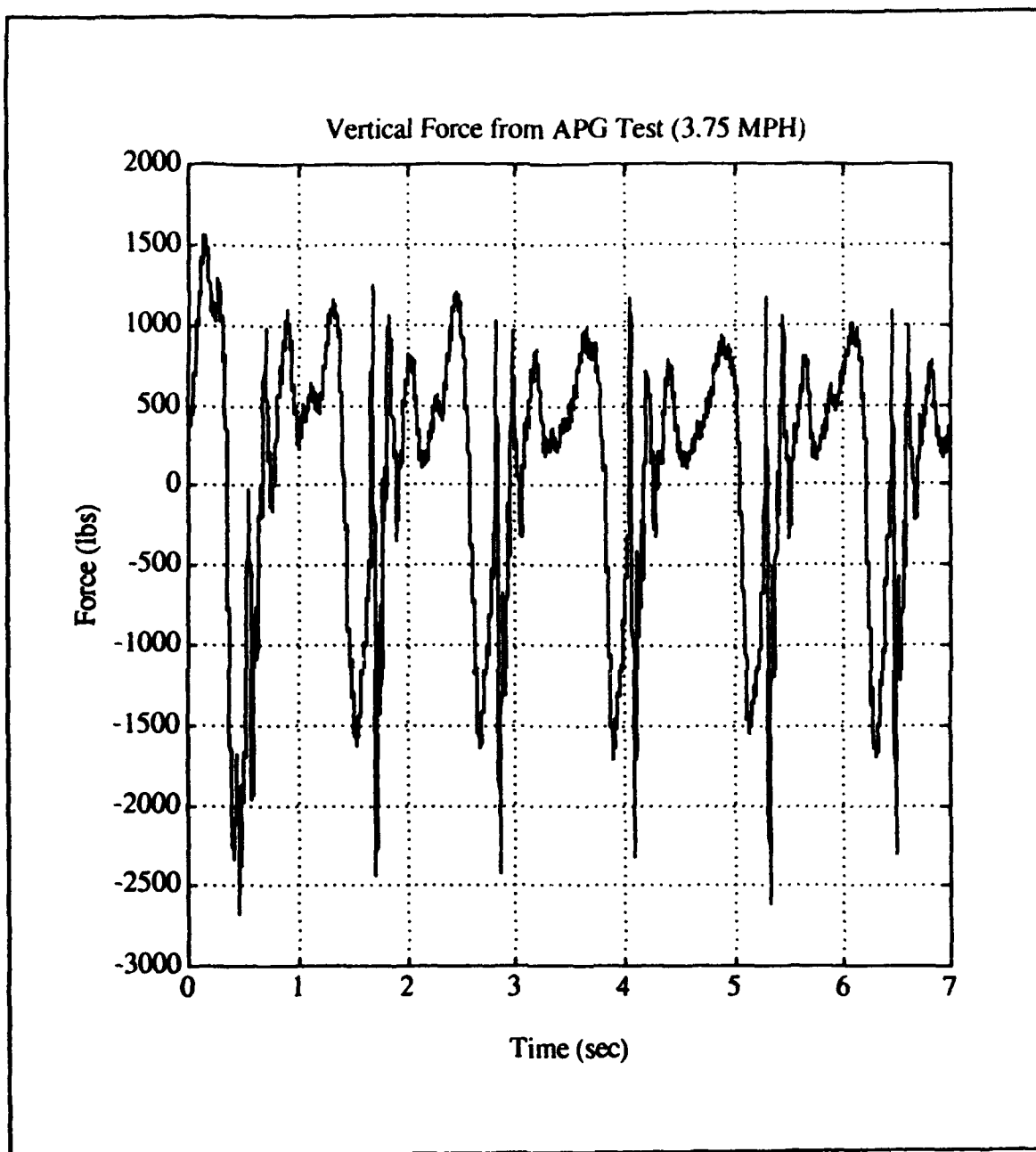


Figure 6-6 A-Frame Force at 3.75 MPH on the Washboard Course

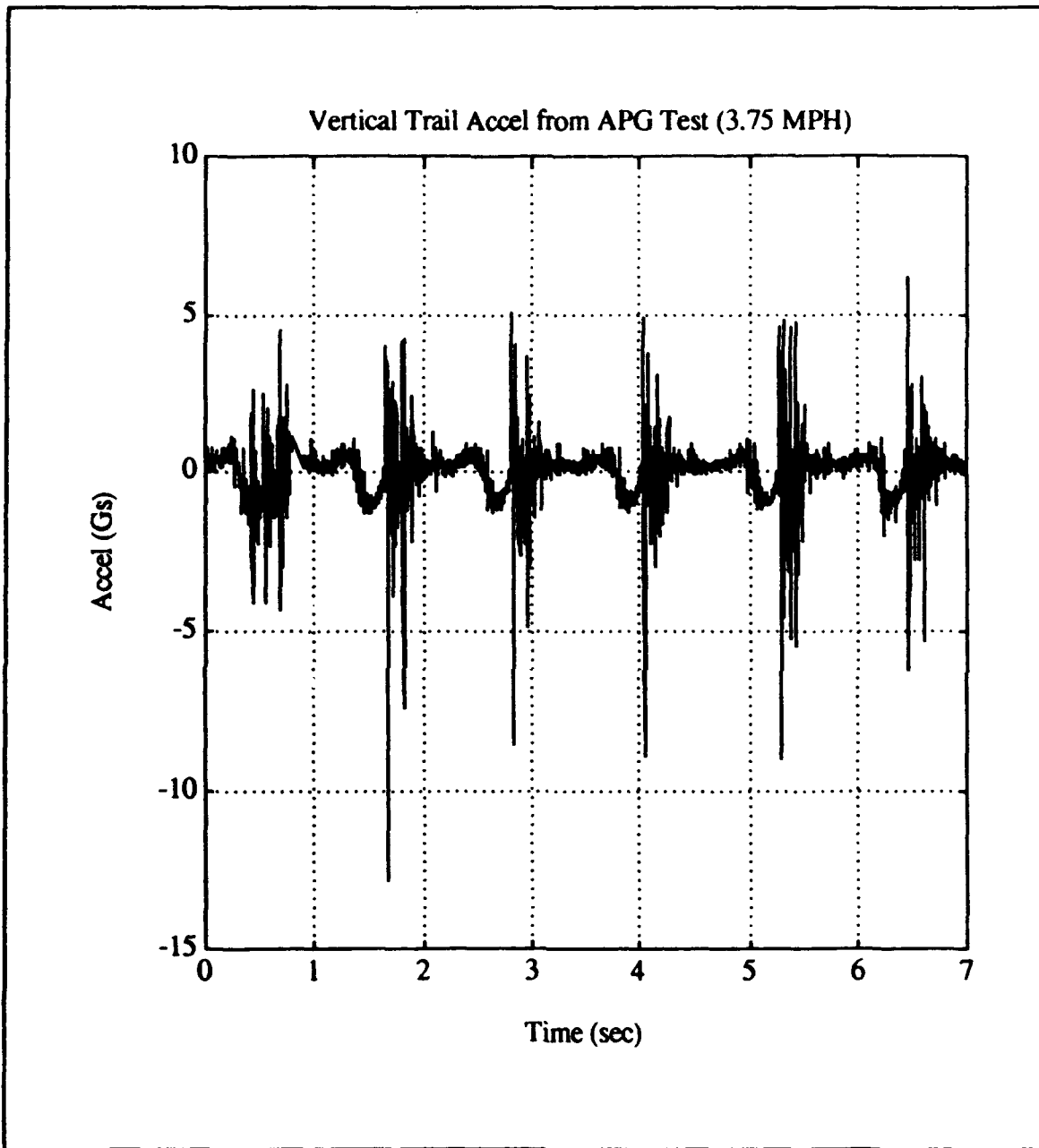


Figure 6-7 Trail Vertical Acceleration at 3.75 MPH on the Washboard Course

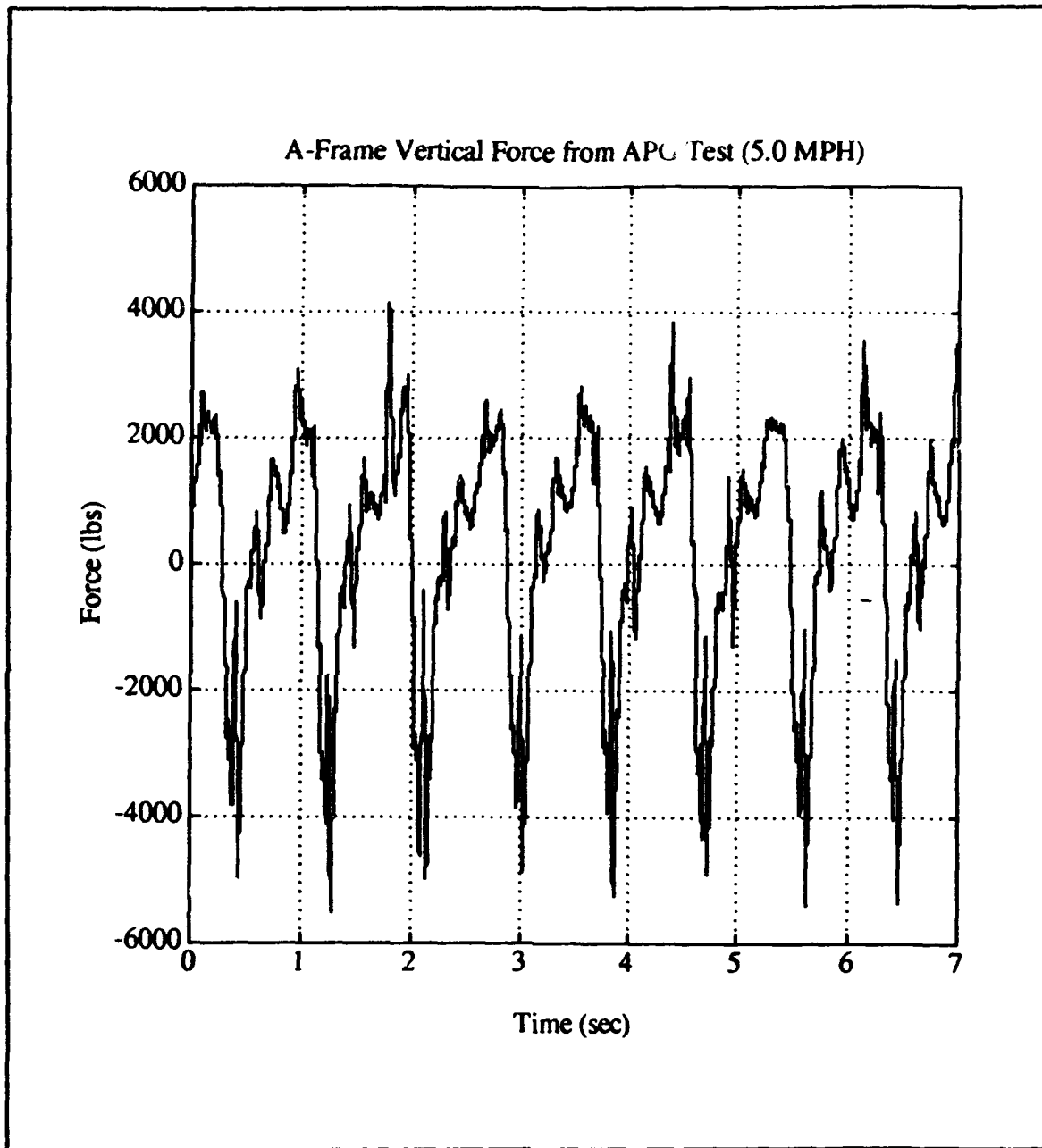


Figure 6-8 A-Frame Force at 5.0 MPH on the Washboard Course

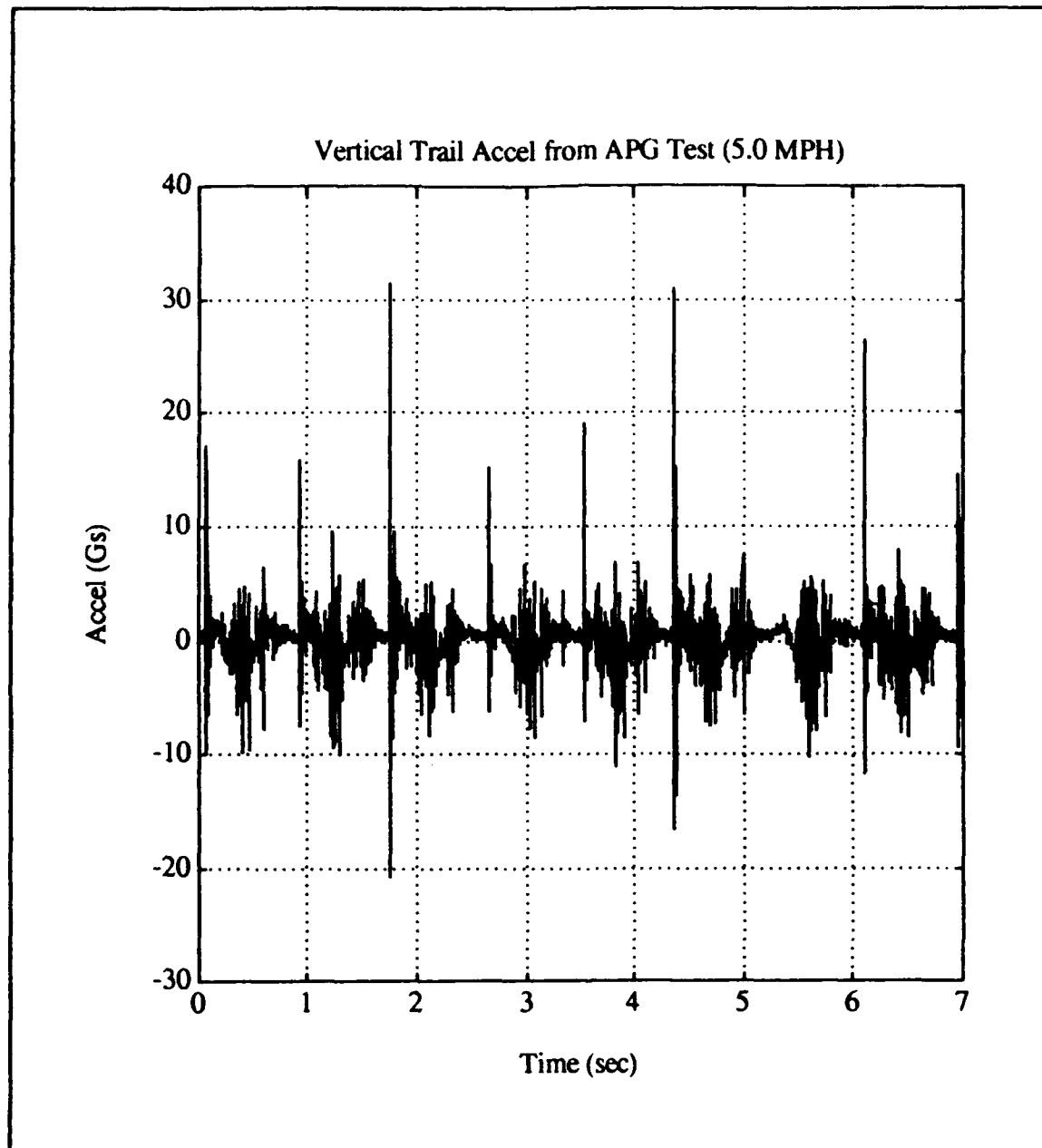


Figure 6-9 Trail Vertical Acceleration at 5.0 MPH on the Washboard Course

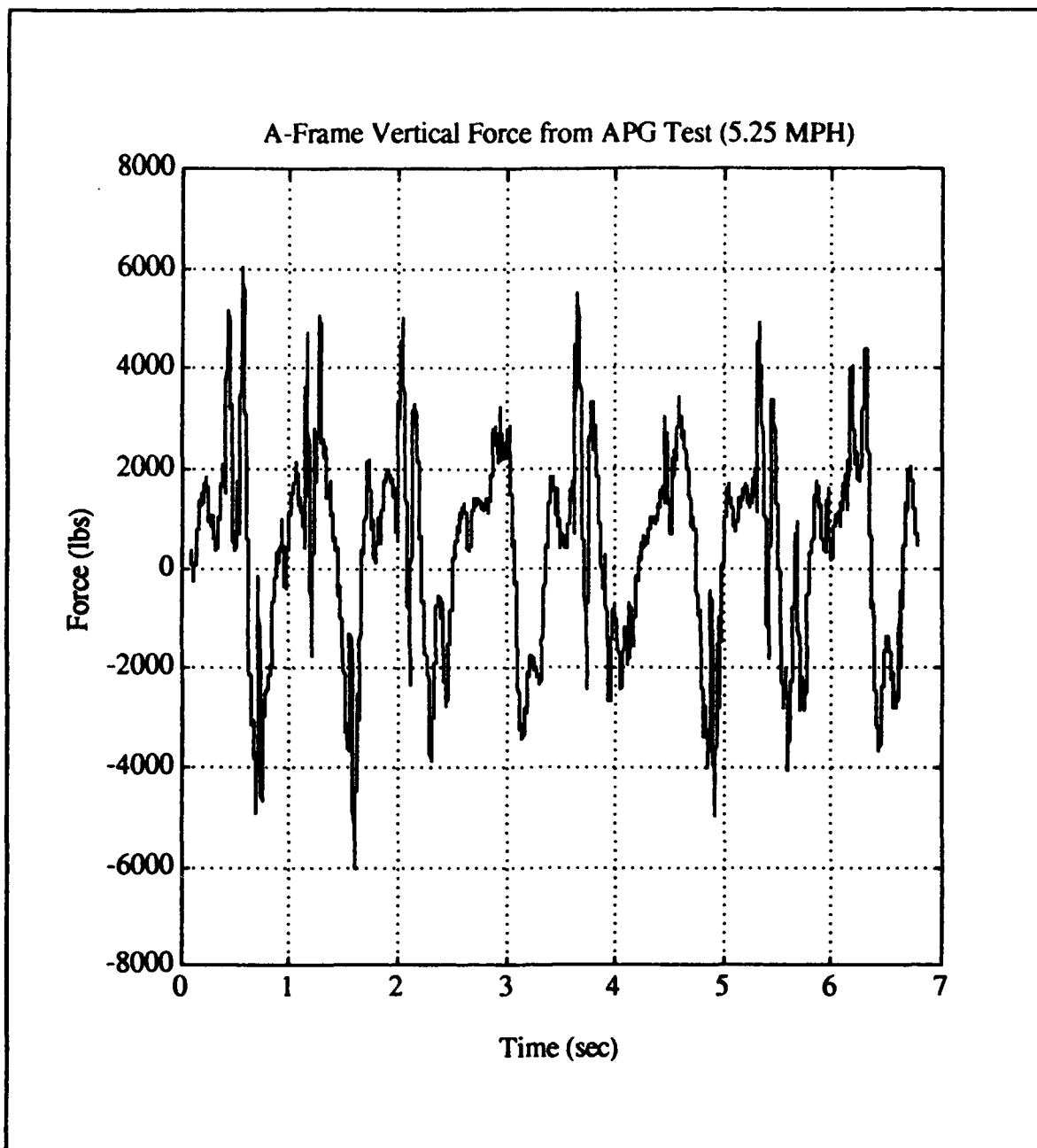


Figure 6-10 A-Frame Force at 5.25 MPH on the Washboard Course

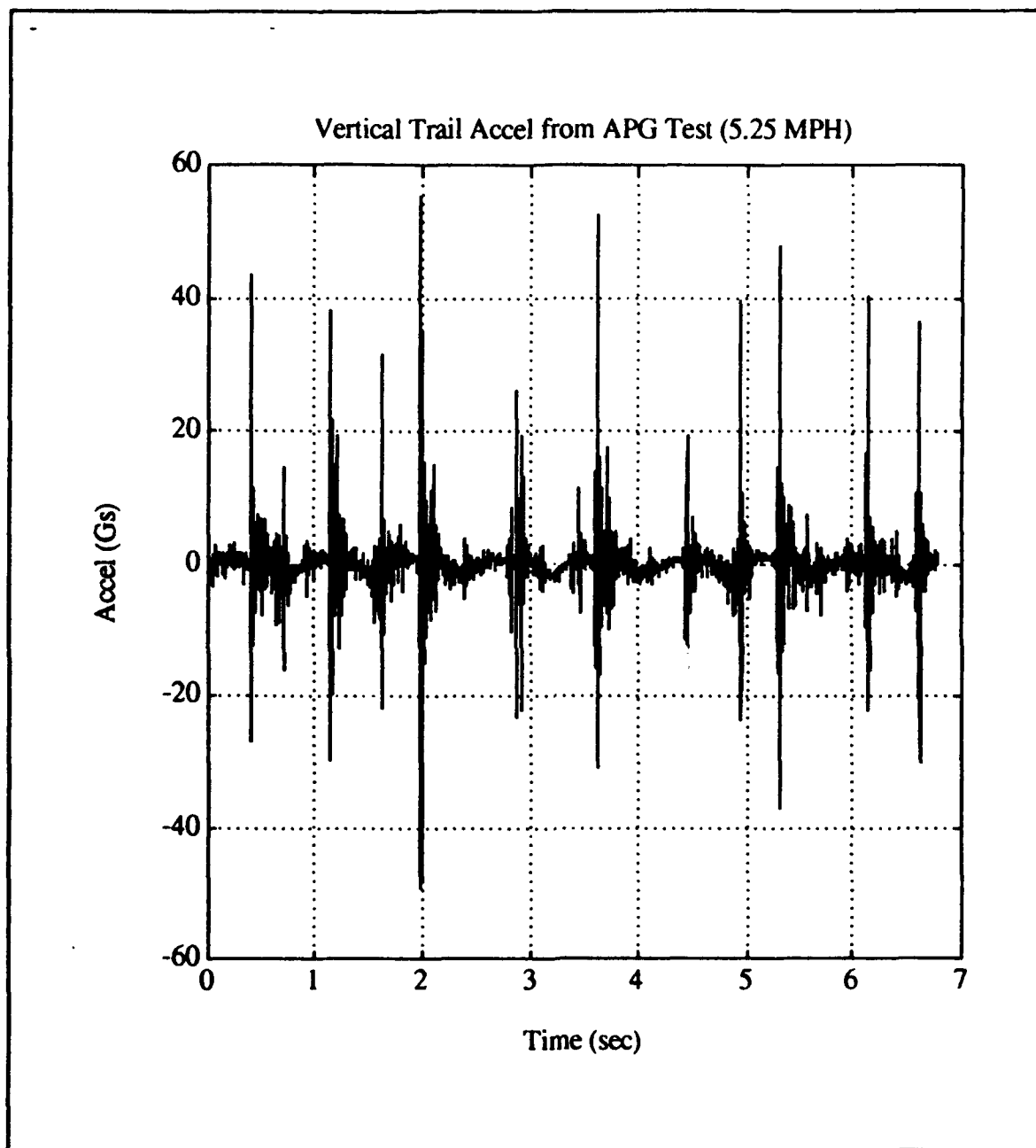


Figure 6-11 Trail Vertical Acceleration at 5.25 MPH on the Washboard Course

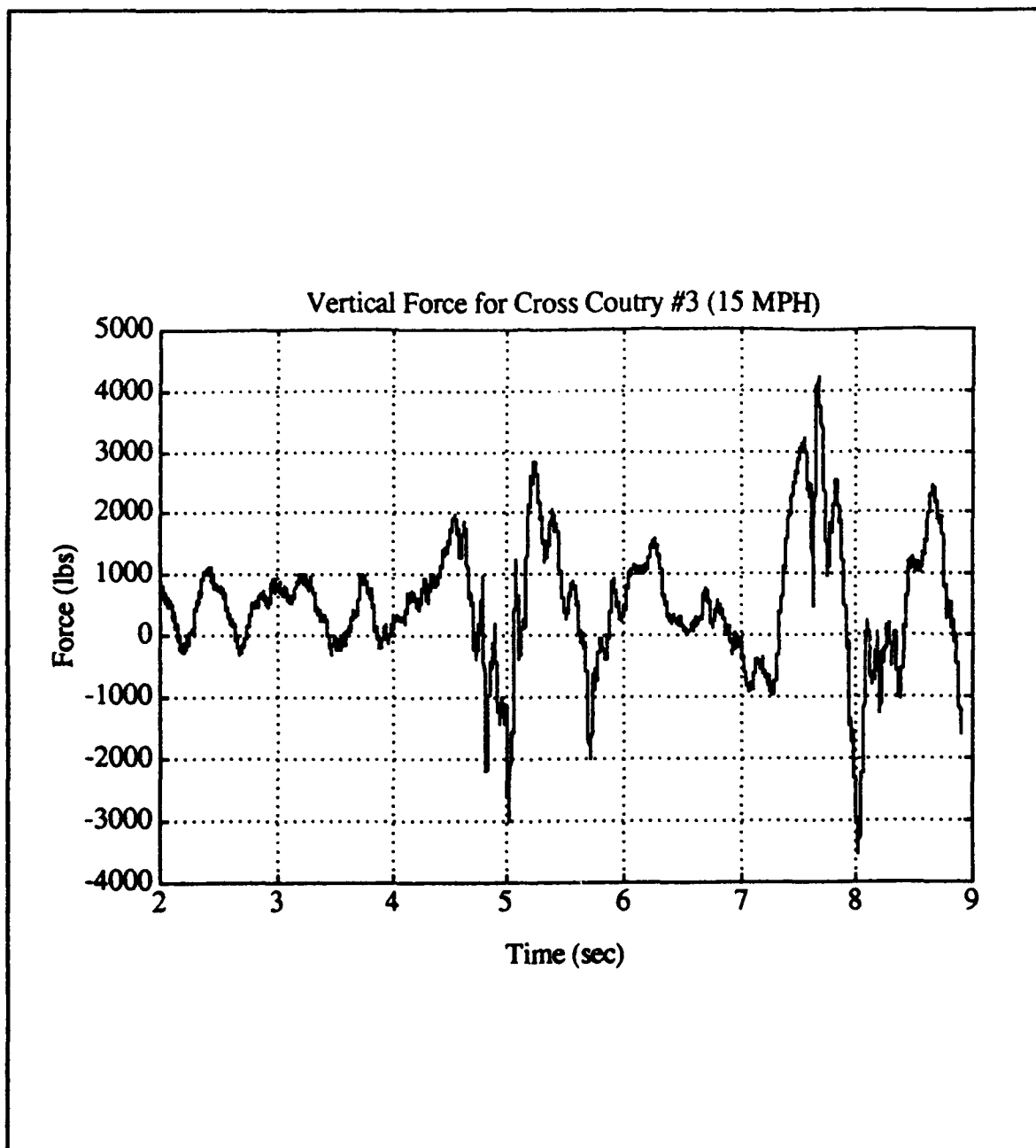


Figure 6-12 A-Frame Force at 15 MPH on Cross Country Course Number 3

2. Frequency Domain

The frequency domain analysis for the actual A-Frame force and trail acceleration results are shown in Figures 6-13 through 6-18. The same procedures using the "FFT" function in Matlab as were used in Chapter IV for the model results were used to perform the frequency analysis on the actual results. The time increment used was 1/1250 seconds and was determined by using every other data point of the original data that was taken at 2500 Hz. 8192 points were used to achieve an adequate frequency discretization. The record length was 8192/1250 and frequency increment was 1250/8192. The FFT analysis of both A-Frame force and trail vertical acceleration for each data run clearly shows two frequency spikes. The lowest frequency and largest spike corresponds to the forcing frequency or road input to the howitzer tires. The second largest spike corresponds to twice the forcing frequency.

The frequency analysis for actual A-Frame force for speeds of 3.75, 5.0, & 5.25 MPH (Figures 6-13, 6-15, & 6-17) compares reasonably well to the corresponding frequency analysis from the model results (Figures 4-2, 4-4, & 4-6). For example, the FFT results from the actual data at 5.25 MPH (Figure 6-17) shows a large force component 1180 lbs at the road input frequency (1.28 Hz) and second large force component of 575 lbs at double the road input (2.56 Hz). Where as the FFT of the model for the corresponding predicted A-frame force (Figure 4-6) shows a large force component of 1375 lbs at the road input frequency (1.28 Hz) and a second large

force component of 500 lbs at twice the input frequency (2.56 Hz). For this case, the total amount of force from the 1.28 and 2.56 Hz spikes for the actual results and the model results are approximately the same (1765 lbs versus 1875 lbs). Although FFT results for the actual data and the model predictions are not exactly the same, they are close enough further to validate the model's predicted results.

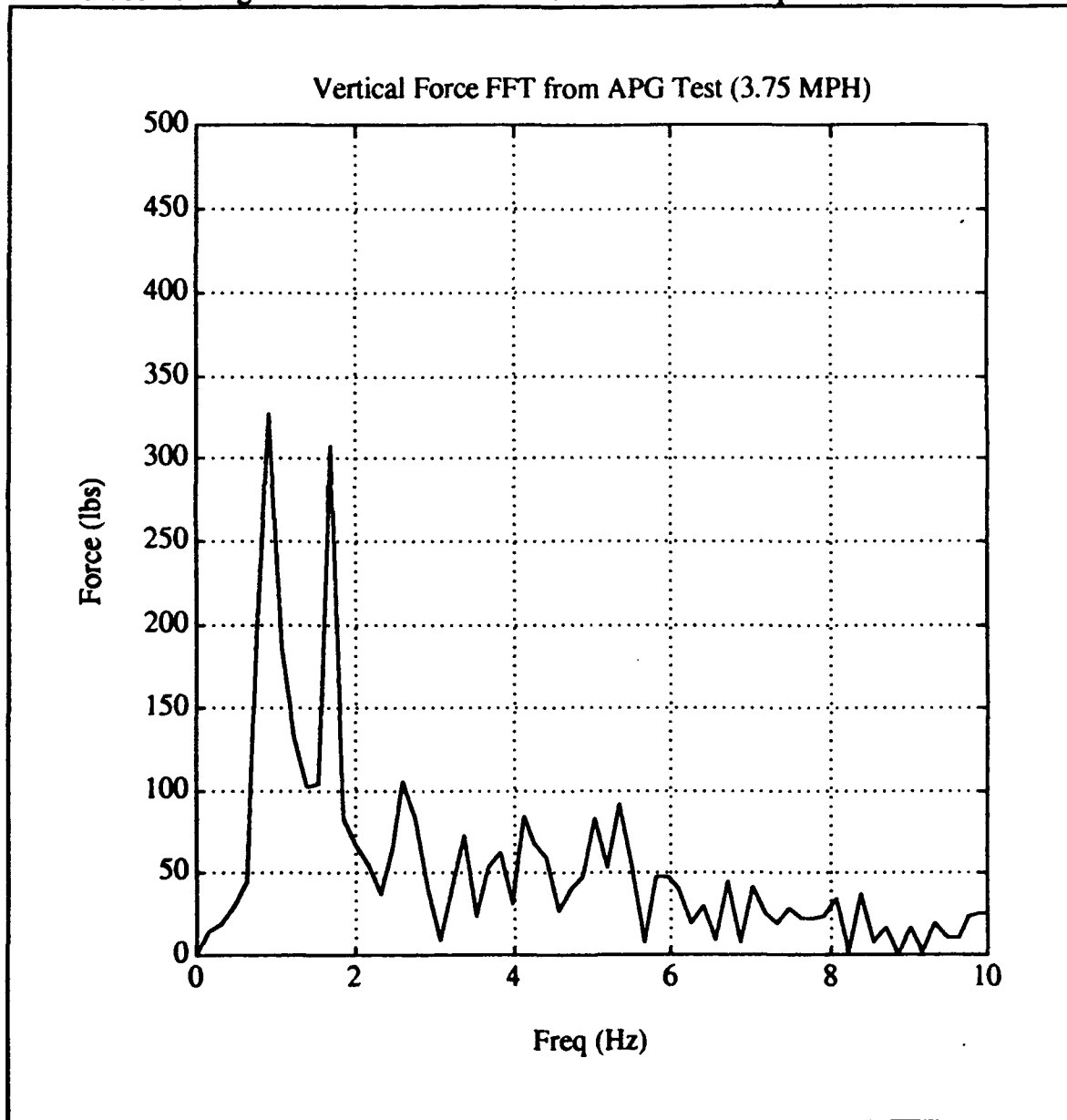


Figure 6-13 FFT of A-Frame Force at 3.75 MPH on the Washboard Course

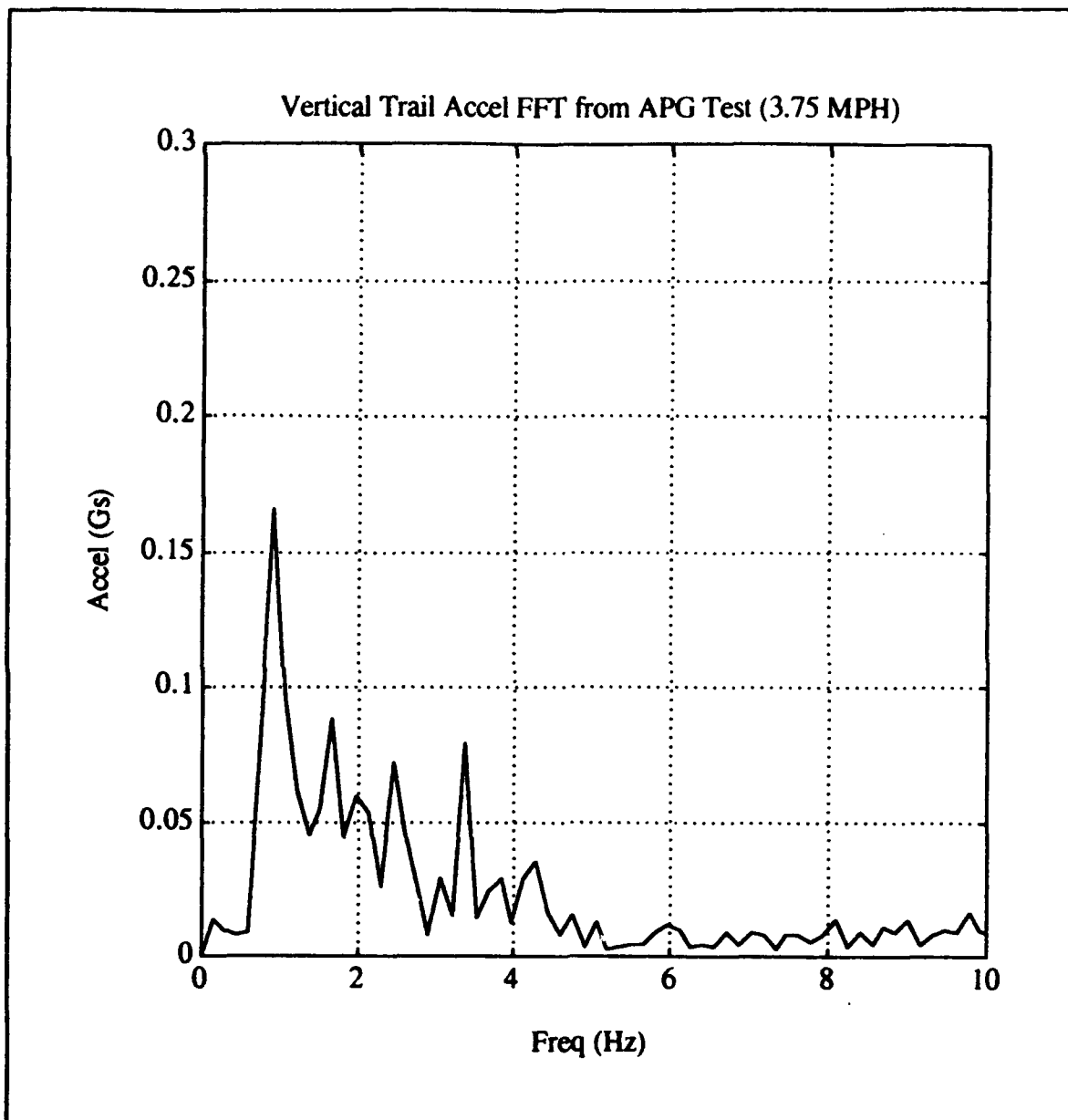


Figure 6-14 FFT of Trail Vertical Acceleration at 3.75 MPH on the Washboard Course

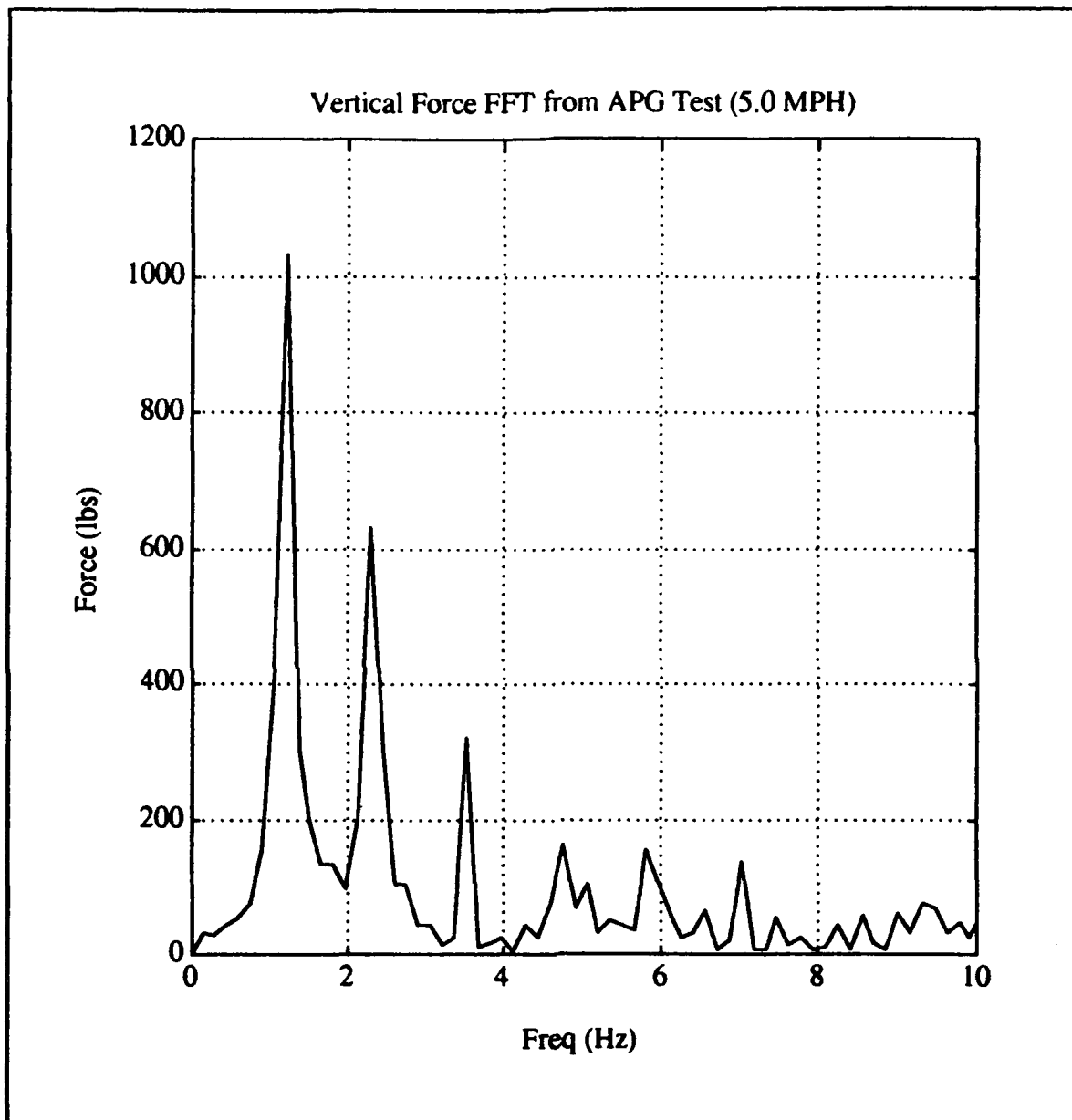


Figure 6-15 FFT of A-Frame Force at 5.00 MPH on the Washboard Course

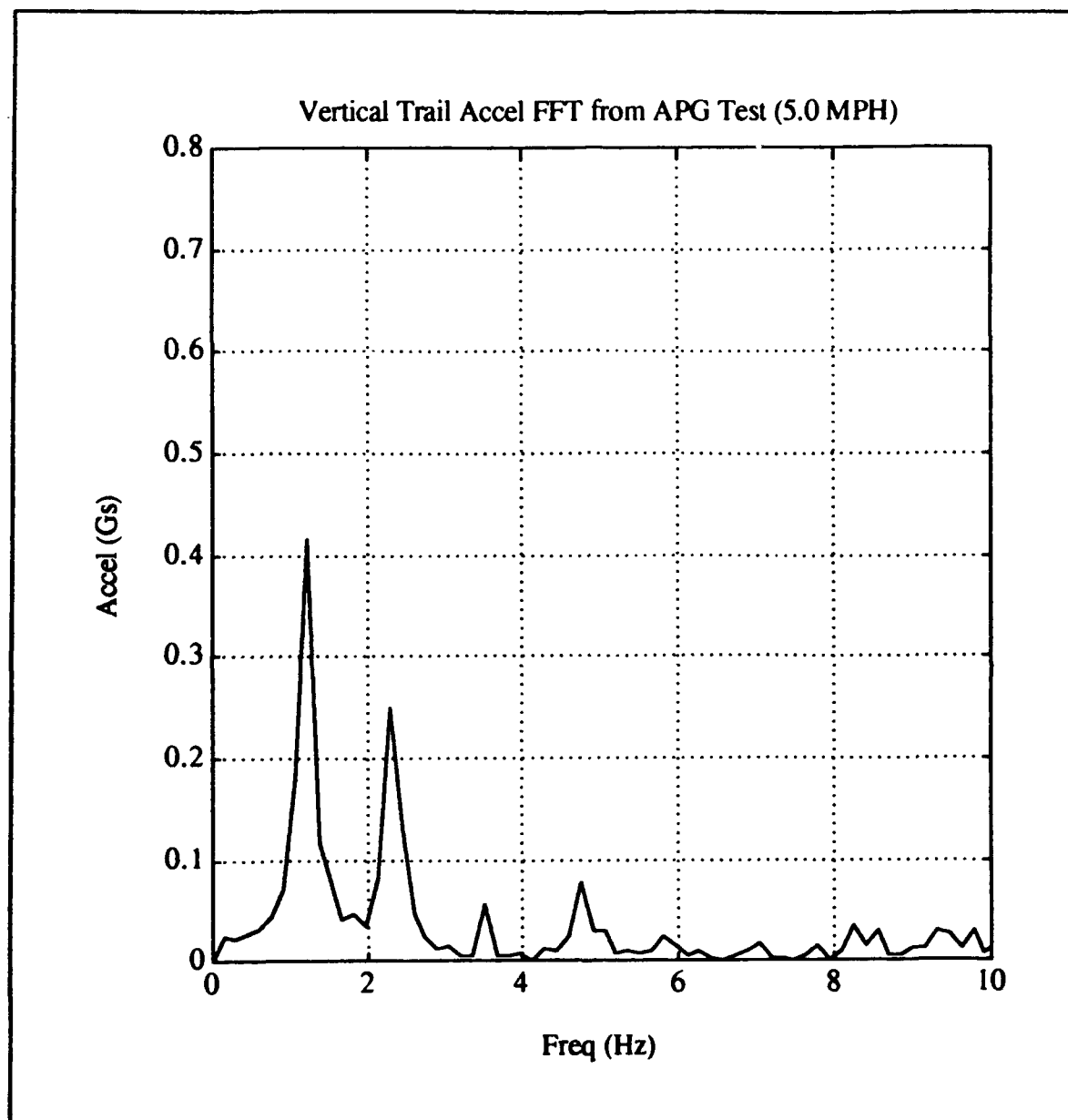


Figure 6-16 FFT of Trail Vertical Acceleration at 5.0 MPH on the Washboard Course

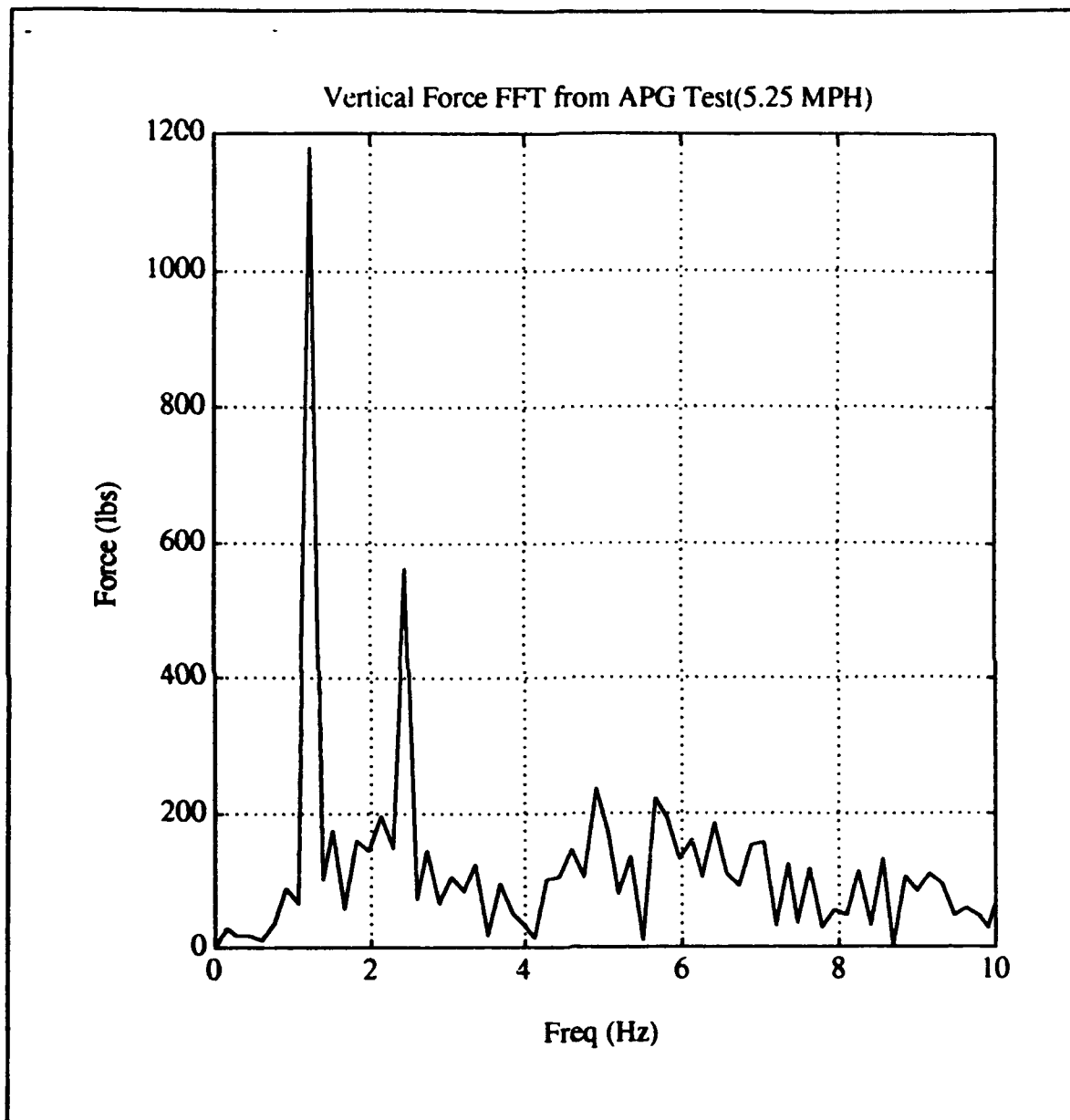


Figure 6-17 FFT of A-Frame Force at 5.25 MPH on the Washboard Course

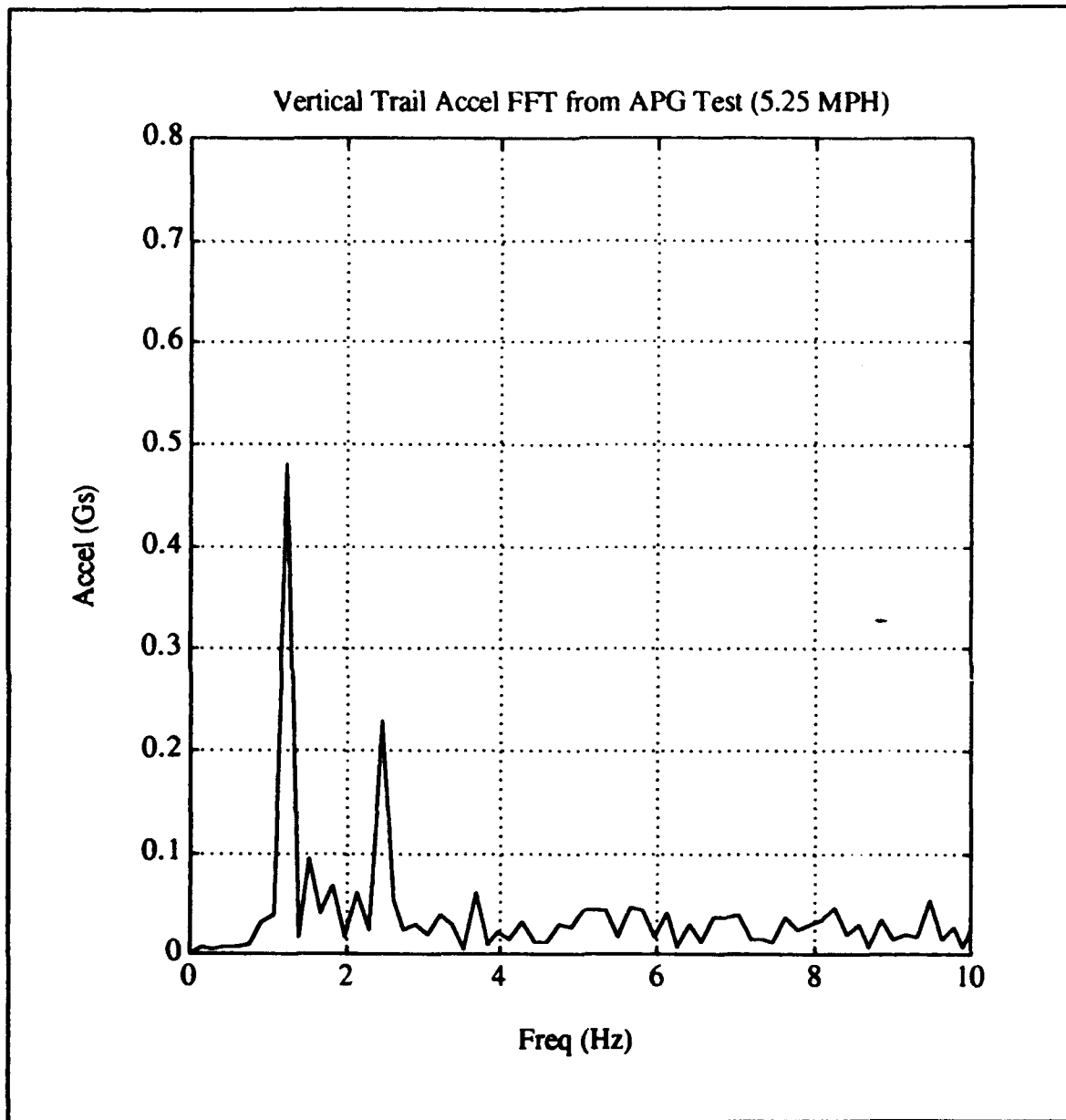


Figure 6-18 FFT of Trail Vertical Acceleration at 5.25 MPH on the Washboard Course

3. Other Results

The strain reading from the strain rosettes that were attached to the bottom the howitzer's trail showed low strain readings for all courses. These low strain readings clearly showed that transporting the howitzer in the firing position with the A-Frame attached produces insignificant levels of stress in the howitzer trail.

Lateral forces in the A-Frame were also determined from the actual test data. Figures 6-19 through 6-21 show the lateral force results for 3.75, 5.0 & 5.25 MPH, respectively. The maximum lateral forces were less than ten percent of the maximum vertical forces for all runs on the washboard course. For the rough terrain Cross Country Course Number Three the maximum lateral force (Figure 6-22) was twenty percent of the maximum vertical force. These relatively low values of lateral force help to show the validity of the modeling technique used, since the computer model only predicts the vertical forces in the A-Frame and assumes that the lateral forces would be comparatively low.

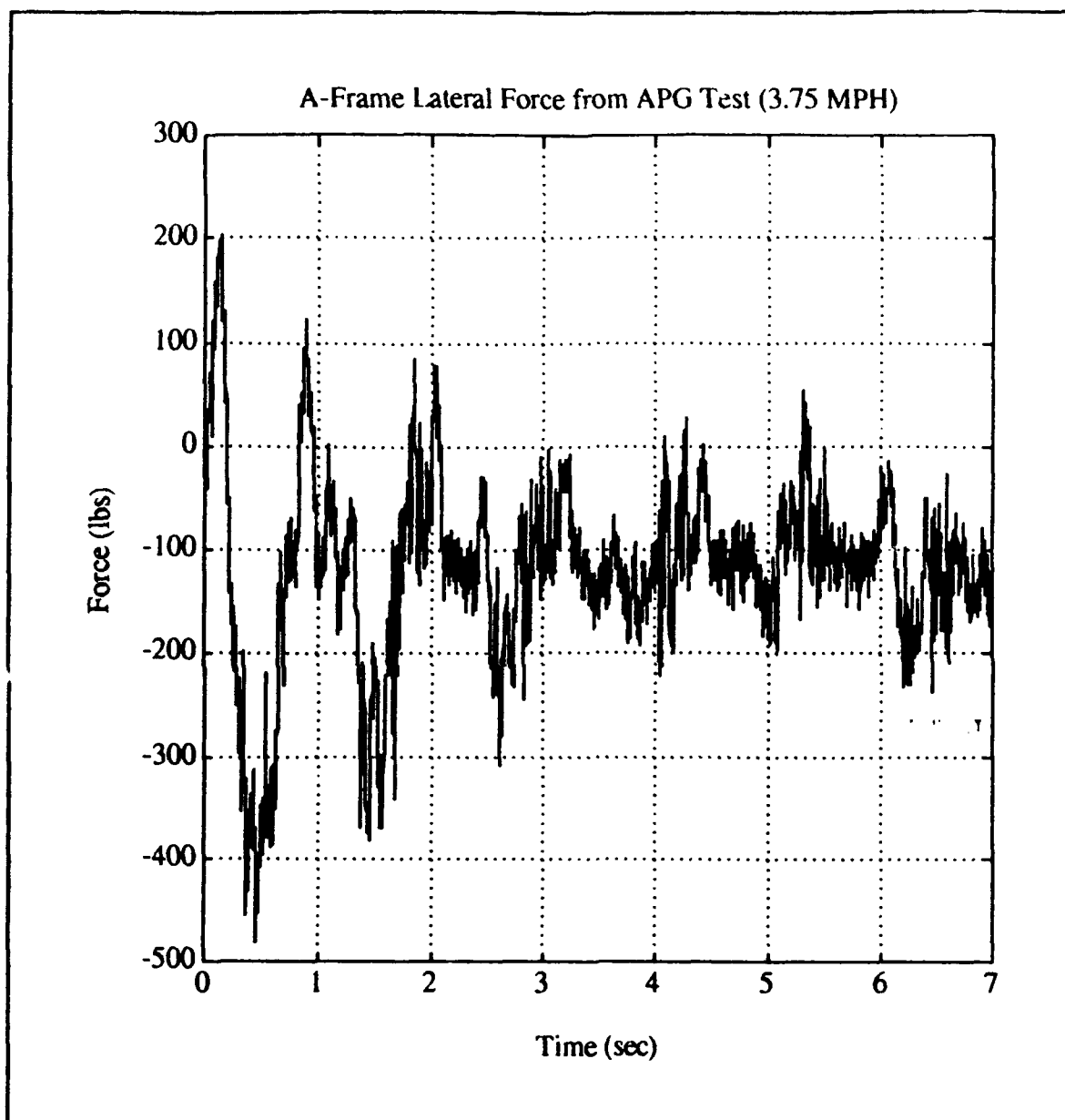


Figure 6-19 Lateral Force from the APG Washboard Course at 3.75 MPH

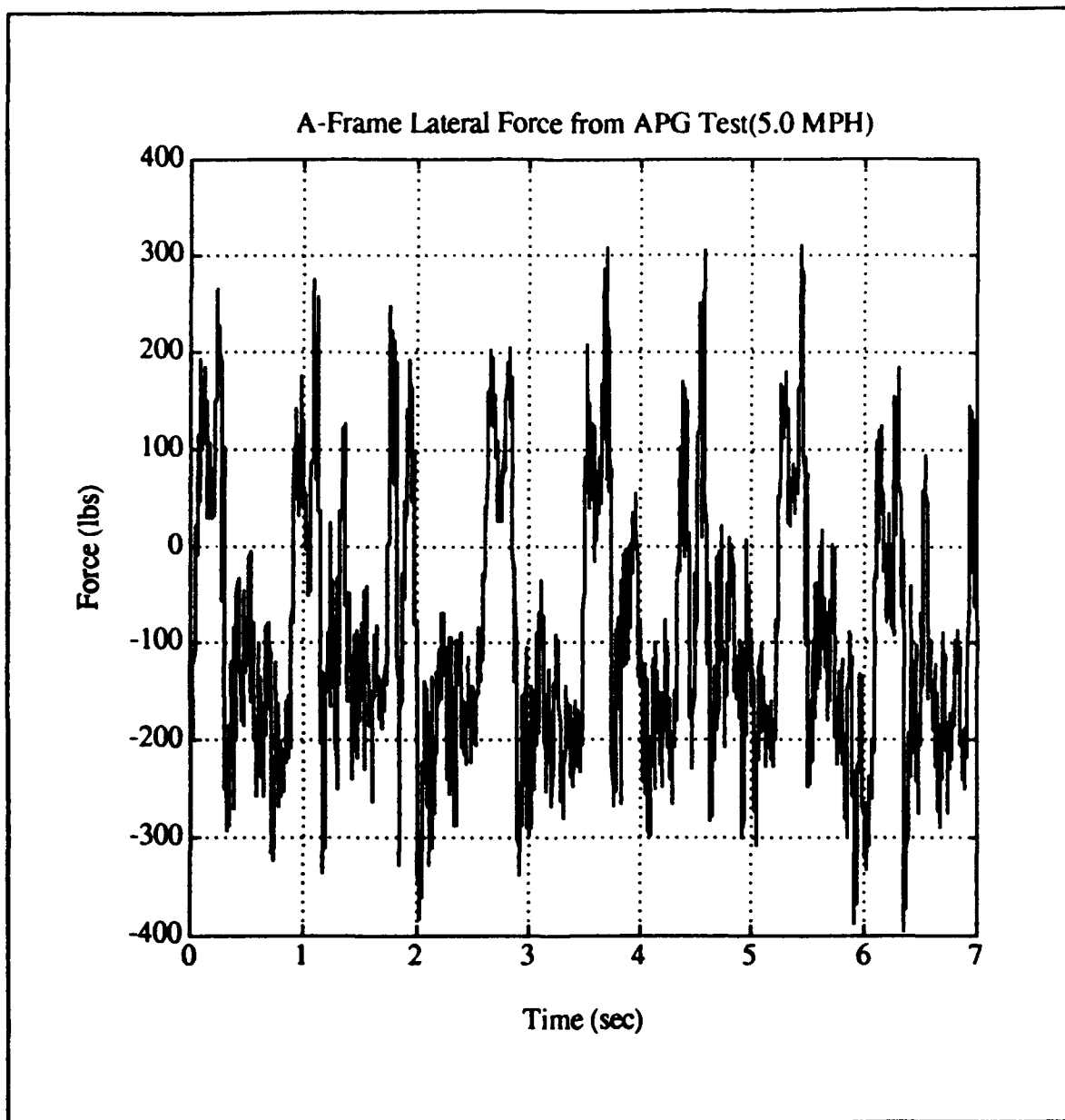


Figure 6-20 Lateral Force from the APG Washboard Course at 5.0 MPH

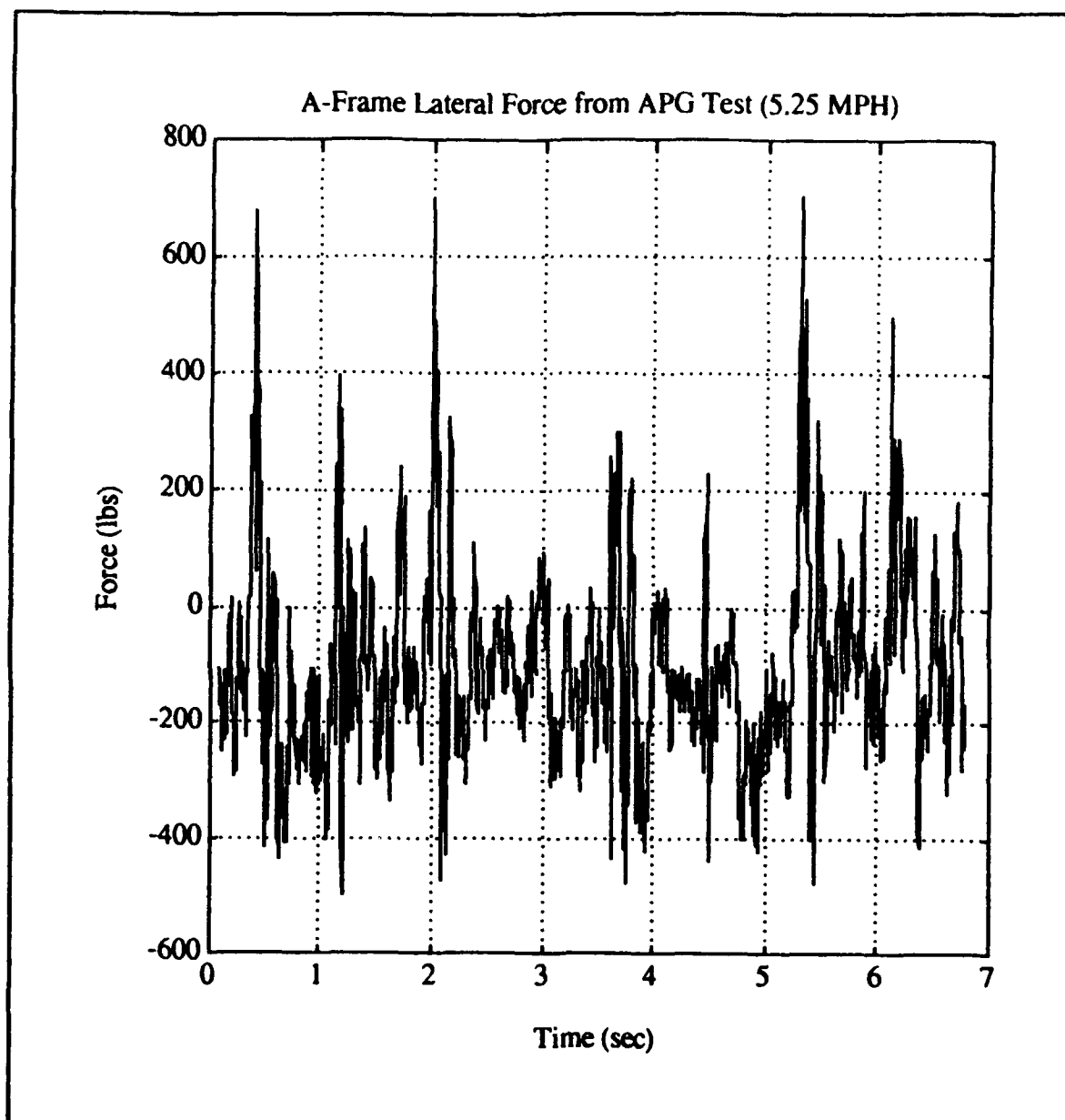


Figure 6-21 Lateral Force from the APG Washboard Course at 5.25 MPH

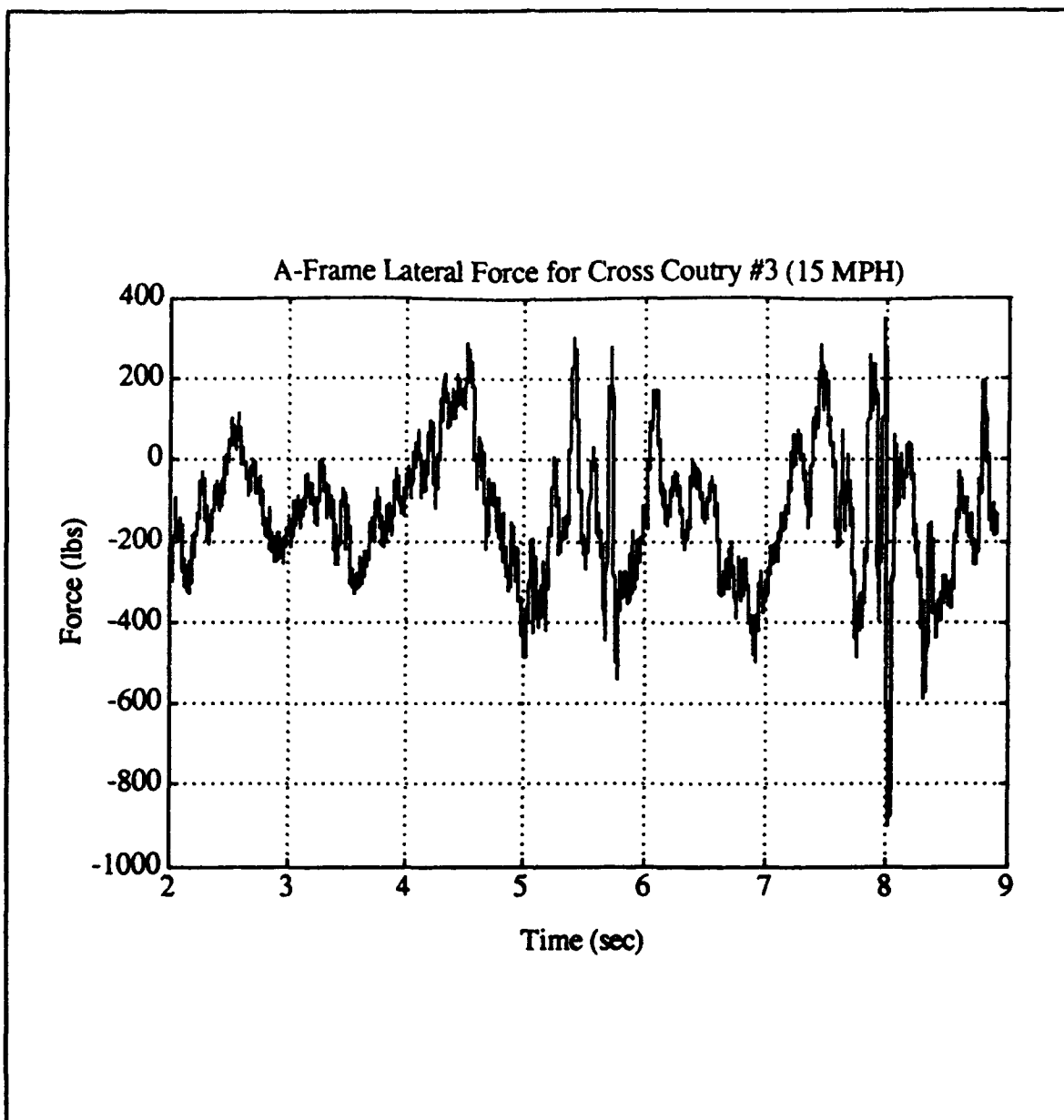


Figure 6-22 Lateral Force from Cross Country Course Number Three at 15 MPH

VII. CONCLUSIONS/RECOMMENDATIONS

A. CONCLUSIONS

The computer model developed, produced output results that are reasonably representative of the actual results for the washboard type road input used at Aberdeen Proving Grounds. Therefore, the model is validated and can be used to predict "worst case" loading on the howitzer's critical parts. These "worst case" predictions for a trench type pothole show the M119 Howitzer can be safely towed in the firing position with the A-Frame attached.

As an additional result of this study, we believe that the T-Bar is the most critical component on the howitzer in regards to mechanical failure when towing in the firing position. The predicted factor of safety for the T-bar based on the "worst case" pothole terrain is 1.81. Due to the high cost of repair, making the T-Bar out of thicker steel would provide an increased factor of safety.

The predicted factor of safety for the A-Frame, from the same "worst case" terrain, is 1.92. This indicates that the A-Frame is strong enough to withstand the worst case expected loads. However, the A-Frame is made out of aluminum and aluminum does not have a fatigue limit. Thus, eventually the A-Frame is expected to fatigue. The A-Frame's fatigue life could be greatly extended by eliminating the holes in its legs.

The strain reading taken from the trail rosettes during the instrumented test at APG show that the stress in the trail is insignificant during towing in the A-Frame position.

B. RECOMMENDATIONS

The US Army should remove the towing restrictions and allow the howitzer to be towed in the firing configuration with the A-Frame attached during tactical operations.

The T-Bar should be made out of thicker steel to provide added assurance that it will not fail.

The A-Frame should be re-configured for manufacture without the hole in its legs.

APPENDIX A

SYSTEM PARAMETER VALUES

The following table defines the HUMMV/Howitzer system parameters using an inches (in), pounds (lbs), and seconds (sec) system of units. Gravity (G) is approximated to be equal to 386.4 in/sec^2 . The nomenclature for the parameters that are identified in this Appendix is the same nomenclature that is used throughout this paper. Refer to Figures 2-1 and 2-2 to identify the parameters defined below. The values listed in the table incorporate the effects of both sides for those components that are identical on the right and left side of the HUMMV or Howitzer. For example, the spring stiffness for each of the front HUMMV tires, K_1 , is 1323.0 lbs/in. This value is multiplied by two to account for the combined effect of both front HUMMV front tires. The value listed in the following table for K_1 is 2646 lbs/in.

TABLE A-1 COMPUTER MODEL PARAMETER VALUES

Symbol	Value/units	How Determined/Notes
K_1	2646.0 lbs/in	Reference 1/HUMMV front tires stiffness
K_2	1908.0 lbs/in	Reference 1/HUMMV front suspension stiffness
K_3	3544.0 lbs/in	Reference 1/ HUMMV rear tires stiffness
K_4	5040.0 lbs/in	Reference 1/ HUMMV rear suspension stiffness
K_6	2000.0 lbs/in	Estimated/Howitzer tires stiffness
K_7	1056.0 lbs/in	Reference 2/Modeled Howitzer vertical suspension stiffness
K_A	200,000.0 lbs/in	Calculated/Combine A-Frame & T-Bar stiffness
B_1	$B_{1C}=171.6$ lbs-sec/in $B_{1T}=308.4$ lbs-sec/in	Reference 1/ B_{1C} is for compression & B_{1T} for tension. Values are 20% more than Ref 1
B_2	$B_{2C}=199.2$ lbs-sec/in $B_{2T}=480.0$ lbs-sec/in	Reference 1/ B_{2C} is for compression & B_{2T} for tension. Values are 20% more than Ref 1
B_3	$B_{3C}=40.0$ lbs-sec/in $B_{3T}=132.0$ lbs-sec/in	Calculated from RIA data/ B_{3C} is for compression & B_{3T} for tension.
B_4	250,000 lbs-in-sec/rad	Estimated/ Torsional Damping in elevating clutch
M_1	1.294 lbm	Reference 1/ Includes mass of HUMMV front wheels, shocks and suspension springs
M_2	1.294 lbm	Reference 1/ Includes mass of HUMMV rear wheels, shocks and suspension springs
M_3	21.22 lbm	Reference 1/ HUMMV Body
M_4	1.035 lbm	Reference 2/Includes howitzer wheels, shocks, and 30% of the road arm masses
M_5	9.834 lbm	Reference 2/ Howitzer trail & saddle mass
M_6	5.952 lbm	Reference 2/ Howitzer elevating mass
I_1	52,680.0 lbs-in-sec ²	Reference 1/ Moment of inertia about HUMMV CG

TABLE A-1 COMPUTER MODEL PARAMETER VALUES (CONT)

Symbol	Value/units	How Determined/Notes
I_2	10,000 lbs-in- sec ²	Estimated/ Moment of inertia of Trail & saddle mass about CG
I_3	15,000 lbs-in-sec ²	Estimated/ Moment of inertia of Elevating mass about CG
L_1	83.8 in	Reference 1/HUMMV CG to front springs & shocks
L_2	46.7 in	Reference 1/HUMMV CG to rear springs & shocks
L_3	75.7 in	Reference 1/HUMMV CG to hitch connecting point
L_7	130.5 in	Measured/ HUMMV front axle to HUMMV rear axle
L_8	294.5 in	Measured/ HUMMV front axle to Howitzer axle
L_{11}	104.4 in	Measured/ Howitzer axle to CG of Trail & Saddle mass
L_{12}	135.0 in	Measured/Howitzer axle to hitch connecting point
L_{13}	38.0 in	Measured/Trunion to where A-Frame connects to the T-Bar
L_{16}	110.3 in	Measured/Trunion to hitch connecting point
L_A	45.0 in	Measured/ Trunion to where A-Frame attaches to the Elevating mass/Gun Tube
L_{CG}	32.5 in	Provide by RIA/ Trunion to CG of Elevating mass
θ_0	12.0 degrees	Measured/ Static angle from horizontal to Gun Tube when A-Frame is Attached
ϕ_A	51.0 degrees	Measured/ Angle from Gun Tube to A-Frame

APPENDIX B

MATRICES FOR EQUATIONS OF MOTION

This Appendix contains the mass, damping, and stiffness matrices for the equations of motion that were developed in Chapter II. The mass system matrix, $[M]$, is as follows:

$$\begin{bmatrix} m_{11} & 0 & 0 & 0 & 0 & 0 & 0 \\ 0 & m_{22} & 0 & 0 & 0 & 0 & 0 \\ 0 & 0 & m_{33} & 0 & m_{35} & m_{36} & m_{37} \\ 0 & 0 & 0 & m_{44} & 0 & 0 & 0 \\ 0 & 0 & m_{53} & 0 & m_{55} & m_{56} & m_{57} \\ 0 & 0 & m_{63} & 0 & m_{65} & m_{66} & m_{67} \\ 0 & 0 & m_{73} & 0 & m_{75} & m_{76} & m_{77} \end{bmatrix}$$

where:

$$m_{11} = M_1 \quad m_{22} = M_2$$

$$m_{35} = M_5 L_3 + M_6 L_3$$

$$m_{37} = M_6 L_{CG} \cos(\theta_0)$$

$$m_{53} = M_5 L_3 + M_6 L_3$$

$$m_{56} = M_5 L_3 L_{11} + M_6 L_3 L_{16}$$

$$m_{63} = M_5 L_{11} + M_6 L_{16}$$

$$m_{66} = I_2 + M_5 L_{11}^2 + M_6 L_{16}^2$$

$$m_{73} = M_6 L_{CG} \cos(\theta_0)$$

$$m_{76} = M_6 L_{CG} L_{16} \cos(\theta_0)$$

$$m_{33} = M_3 + M_5 + M_6$$

$$m_{36} = M_5 L_{11} + M_6 L_{16}$$

$$m_{44} = M_4$$

$$m_{55} = I_1 + M_5 L_3^2 + M_6 L_3^2$$

$$m_{57} = M_6 L_{CG} L_3 \cos(\theta_0)$$

$$m_{65} = M_5 L_3 L_{11} + M_6 L_3 L_{16}$$

$$m_{67} = M_6 L_{CG} L_{16} \cos(\theta_0)$$

$$m_{75} = M_6 L_{CG} L_3 \cos(\theta_0)$$

$$m_{77} = I_3 + M_6 L_{CG}^2$$

Note due to symmetry of $[M]$ the following matrix elements are equal:

$$m_{53} = m_{35}$$

$$m_{63} = m_{36}$$

$$m_{73} = m_{37}$$

$$m_{65} = m_{56}$$

$$m_{75} = m_{57}$$

$$m_{76} = m_{67}$$

The damping matrix for the system is dependent on whether the shock absorber forces are tensile or compressive at a given time. The tensile or compressive state for each of the shock absorbers is determined by the relative velocities of the end connection points for the shock absorber. The damping matrix, $[C(\dot{x})]$, is as follows:

$$\begin{bmatrix} c_{11} & 0 & c_{13} & 0 & c_{15} & 0 & 0 \\ 0 & c_{22} & c_{23} & 0 & c_{25} & 0 & 0 \\ c_{31} & c_{32} & c_{33} & c_{34} & c_{35} & c_{36} & 0 \\ 0 & 0 & c_{43} & c_{44} & c_{45} & c_{46} & 0 \\ c_{51} & c_{52} & c_{53} & c_{54} & c_{55} & c_{56} & 0 \\ 0 & 0 & c_{63} & c_{64} & c_{65} & c_{66} & c_{67} \\ 0 & 0 & 0 & 0 & 0 & c_{76} & c_{77} \end{bmatrix}$$

where:

$c_{11} = B_1$	$c_{13} = -B_1$	$c_{15} = B_1 L_1$
$c_{22} = B_2$	$c_{23} = -B_2$	$c_{25} = -B_2 L_2$
$c_{31} = -B_1$	$c_{32} = -B_2$	$c_{33} = B_1 + B_2 + B_3$
$c_{34} = -B_3$	$c_{35} = -B_1 L_1 + B_2 L_2 + B_3 L_3$	
$c_{36} = B_3 L_{12}$	$c_{43} = -B_3$	$c_{44} = B_3$
$c_{45} = -B_3 L_3$	$c_{46} = -B_3 L_{12}$	$c_{51} = B_1 L_1$
$c_{52} = -B_2 L_2$	$c_{53} = -B_1 L_1 + B_2 L_2 + B_3 L_3$	
$c_{54} = -B_3 L_3$	$c_{55} = B_1 L_1^2 + B_2 L_2^2 + B_3 L_3^2$	
$c_{56} = B_3 L_3 L_{12}$	$c_{63} = B_3 L_{12}$	$c_{64} = -B_3 L_{12}$
$c_{65} = B_3 L_3 L_{12}$	$c_{66} = B_3 L_{12}^2 + B_4$	$c_{67} = -B_4$
$c_{76} = -B_4$	$c_{77} = B_4$	

Note due to symmetry of $[C(\dot{x})]$ the following elements are equal:

$c_{31} = c_{13}$	$c_{32} = c_{23}$	$c_{51} = c_{15}$	$c_{43} = c_{34}$
$c_{52} = c_{25}$	$c_{53} = c_{35}$	$c_{54} = c_{45}$	$c_{63} = c_{36}$
$c_{64} = c_{46}$	$c_{65} = c_{56}$	$c_{76} = c_{67}$	

The system stiffness matrix, $[K]$, is as follows:

$$\begin{bmatrix} k_{11} & 0 & k_{13} & 0 & k_{15} & 0 & 0 \\ 0 & k_{22} & k_{23} & 0 & k_{25} & 0 & 0 \\ k_{31} & k_{32} & k_{33} & k_{34} & k_{35} & k_{36} & 0 \\ 0 & 0 & k_{43} & k_{44} & k_{45} & k_{46} & 0 \\ k_{51} & k_{52} & k_{53} & k_{54} & k_{55} & k_{56} & 0 \\ 0 & 0 & k_{63} & k_{64} & k_{65} & k_{66} & k_{67} \\ 0 & 0 & 0 & 0 & 0 & k_{76} & k_{77} \end{bmatrix}$$

where:

$$\begin{aligned} k_{11} &= K_1 + K_2 & k_{13} &= -K_2 & k_{15} &= K_2 L_1 \\ k_{22} &= K_3 + K_4 & k_{23} &= -K_4 & k_{15} &= -K_4 L_2 \\ k_{31} &= -K_2 & k_{32} &= -K_4 & k_{33} &= K_2 + K_4 + K_7 \\ k_{34} &= -K_7 & k_{35} &= -K_2 L_1 + K_4 L_2 + K_7 L_3 \\ k_{36} &= K_7 L_{12} & k_{43} &= -K_7 & k_{44} &= K_6 + K_7 \\ k_{45} &= -K_7 L_3 & k_{46} &= -K_7 L_{12} & k_{51} &= K_2 L_1 \\ k_{52} &= -K_4 L_2 & k_{53} &= -K_2 L_1 + K_4 L_2 + K_7 L_3 \\ k_{54} &= -K_7 L_3 & k_{55} &= K_2 L_1^2 + K_4 L_2^2 + K_7 L_3^2 \\ k_{56} &= K_7 L_3 L_{12} & k_{63} &= K_7 L_{12} & k_{64} &= -K_7 L_{12} \\ k_{65} &= K_7 L_3 L_{12} & k_{66} &= K_7 L_{12}^2 + K_A L_A L_{13} \cos(\theta_0) \\ k_{67} &= -K_A L_A L_{13} \cos(\theta_0) & k_{76} &= -K_A L_A L_{13} \cos(\theta_0) \\ k_{77} &= K_A L_A L_{13} \cos(\theta_0) \end{aligned}$$

Note due to symmetry of $[K]$ the following matrix elements are equal:

$$\begin{aligned} k_{31} &= k_{13} & k_{32} &= k_{23} & k_{51} &= k_{15} & k_{43} &= k_{34} \\ k_{52} &= k_{25} & k_{53} &= k_{35} & k_{54} &= k_{45} & k_{63} &= k_{36} \\ k_{64} &= k_{46} & k_{65} &= k_{56} & k_{76} &= k_{67} \end{aligned}$$

APPENDIX C

NUMERICAL INTEGRATION COMPUTER CODE

This Appendix contains the computer code used to integrate the equations of motion using the ODE 45 integration routine in Matlab..

1. THE ODE 45 INTEGRATION FUNCTION

```
function xdot=mateqn(t,x)

%Define gravity
G=386.4;

%Define HUMMV Parameters:
L1=83.8;      L2=46.7;      L3=75.7;  L7=130.5;  L8=294.5;
K1=2*1323.0;  K2=2*954.0;    K3=2*1777.0;  K4=2*2520.0;
K5=1000000.0;
B1C=2*1.2*71.5;  B1T=2*1.2*128.25;  B2C=2*1.2*83.0;
B2T=2*1.2*200.0;
W1=2*250.0;      W2=2*250.0;      W3=8200.0;
M1=W1/G;          M2=W2/G;          M3=W3/G;
I1=52680;         RW=5400;          FW=3800;

%Define Gun Parameters:
L4=123.4;      L5=11.6;      LA=45.0;      LS=42.6;      LCG=32.5;
L11=104.4;     L12=135.0;    L13=38.0;      L14=17.0;    L15=9.70;
L16=110.3;
K6=2*1000.0;    K7=2*528;      KA=200000;    KS=300;
B3C=2*20.0;     B3T=2*66.0;     B4=.5*250000.0;
W4=2*200;       W5=1500;      W6=2300;      M4=W4/G;      M5=W5/G;
M6=W6/G;
I2=10000;       I3=15000;
Q0=12.0*pi/180; PHIA=51.0*pi/180;  PHIS=14.0*pi/180;
AW=3800;        TB=88000;  %Define Mass matrice

%Define the mass matrix
M=[zeros(7,7)];
```



```

M(1,1)=M1;   M(2,2)=M2; M(3,3)=M3+M5+M6; M(3,5)=M5*L3+M6*L3;
M(3,6)=M5*L11+M6*L16; M(3,7)=M6*LCG*cos(Q0);
M(4,4)=M4;   M(5,3)=M5*L3+M6*L3; M(5,5)=I1+M5*L3^2+M6^2;
M(5,6)=M5*L3*L11+M6*L3*L16;   M(5,7)=M6*L3*LCG*cos(Q0);
M(6,3)=M5*L11+M6*L16;   M(6,5)=M5*L3*L11+M6*L3*L16;
M(6,6)=I2+M5*L11^2+M6*L16^2+M6*L14^2;
M(6,7)=M6*L16*LCG*cos(Q0);
M(7,3)=M6*LCG*cos(Q0);   M(7,5)=M6*L3*LCG*cos(Q0);
M(7,6)=M6*L16*LCG*cos(Q0);
M(7,7)=I3+M6*LCG^2;

```

%Define Stiffness Matrix

```

K=[zeros(7,7)];
K(1,1)=K1+K2; K(1,3)=-K2; K(1,5)=K2*L1;
K(2,2)=K3+K4; K(2,3)=-K4; K(2,5)=-K4*L2;
K(3,1)=-K2; K(3,2)=-K4; K(3,3)=K2+K4+K7; K(3,4)=-K7; K(3,5)=-
K2*L1+K4*L2+K7*L3; K(3,6)=K7*L12;
K(4,3)=-K7; K(4,4)=K6+K7; K(4,5)=-K7*L3; K(4,6)=-K7*L12;
K(5,1)=K2*L1; K(5,2)=-K4*L2; K(5,3)=-K2*L1+K4*L2+K7*L3; K(5,4)=-
K7*L3;
K(5,5)=K2*L1^2+K4*L2^2+K7*L3^2; K(5,6)=K7*L3*L12;
K(6,3)=K7*L12; K(6,4)=-K7*L12; K(6,5)=K7*L3*L12;
K(6,6)=K7*L12^2+KA*LA*L13*cos(Q0);
K(6,7)=-KA*L13*LA*cos(Q0);
K(7,6)=-KA*L13*LA*cos(Q0);
K(7,7)=+KA*L13*LA*cos(Q0);

```

%Define and velocities:

```

VHF=x(10) - (L1*x(12));   VHB=x(10) + (L2*x(12));
VGB=x(10) + (L3*x(12)) + (L12*x(12));

```

%Define Road Inputs:

```

VMPH=5.0; VEL=VMPH*17.6; PD=72/VEL;
U1=3*(sin(2*pi*t/PD));

```

```

if t < L7/VEL, U2=0;else, T2=t-(L7/VEL);
U2=3*(sin(2*pi*T2/PD)); end

```

```

if t < L8/VEL, U3=0;else, T3=t-(L8/VEL);
U3=3*(sin(2*pi*T3/PD)); end

```

% Determine the shock absorber damping constants based on compression or tension

% HUMMV Front shock

if (VHF - x(8)) > 0.0, B1=B1T; else, B1=B1C; end

% HUMMV Rear shock

if (VHB - x(9)) > 0.0, B2=B2T; else, B2=B2C; end

% GUN shock

if (VGB - x(11)) > 0.0, B3=B3T; else, B3=B3C; end

%Define Damping Matrix

B=zeros(7,7);

B(1,1)=B1; B(1,3)=-B1; B(1,5)=B1*L1;

B(2,2)=B2; B(2,3)=-B2; B(2,5)=-B2*L2;

B(3,1)=-B1; B(3,2)=-B2; B(3,3)=B1+B2+B3; B(3,4)=-B3; B(3,5)=-B1*L1+B2*L2+B3*L3; B(3,6)=B3*L12;

B(4,3)=-B3; B(4,4)=B3; B(4,5)=-B3*L3; B(4,6)=-B3*L12;

B(5,1)=B1*L1; B(5,2)=-B2*L2; B(5,3)=-B1*L1+B2*L2+B3*L3;

B(5,4)=-B3*L3; B(5,5)=B1*L1^2+B2*L2^2+B3*L3^2;

B(5,6)=B3*L3*L12;

B(6,3)=B3*L12; B(6,4)=-B3*L12; B(6,5)=B3*L3*L12;

B(6,6)=B3*L12^2+B4;

B(6,7)=-B4; B(7,6)=-B4; B(7,7)=B4;

%Define Forcing Vector

F=zeros(7,1);

F(1,1)=K1*U1; F(2,1)=K3*U2; F(4,1)=K6*U3;

% CHECK IF FRONT HUMMV WHEEL LOSES CONTACT

if K1*(U1 - x(1)) < -FW, F(2,1)=-FW; K(1,1)=K2; end

% CHECK IF REAR HUMMV WHEEL LOSES CONTACT

if K3*(U2 - x(2)) < -RW, F(2,1)=-RW; K(2,2)=K4; end

% CHECK IF HOWITZER WHEEL LOSES CONTACT

if K6*(U3 - x(4)) < -AW, F(4,1)=-AW; K(4,4)=K7; end

%transform into system of 1st order ode's

id=[1 zeros(1,6);0 1 zeros(1,5);0 0 1 zeros(1,4);zeros(1,3) 1 zeros(1,3)];

id=[id;zeros(1,4) 1 0 0;zeros(1,5) 1 0;zeros(1,6) 1];

```

a=[zeros(7,7) id; -inv(M)*K -inv(M)*B];
f1=inv(M)* F;
f=[[zeros(7,1)]; f1];

```

```

%integrate
xdot=a*x + f;

```

2. THE DRIVER CODE FOR ODE 45

```

% Set the Initial Condition
x01=[zeros(14,1)];

```

```

% Integrate in one second increments
t01=0.00; tf1=0.999; %x01=xn(length(xn),:);
[t1,x1]=ode45('mateqn',t01,tf1,x01,1e-3);
t02=1.0001; tf2=1.999; x02=x1(length(x1),:);
[t2,x2]=ode45('mateqn',t02,tf2,x02,1e-3);
t03=2.0001; tf3=2.999; x03=x2(length(x2),:);
[t3,x3]=ode45('mateqn',t03,tf3,x03,1e-3);
t04=3.0001; tf4=3.999; x04=x3(length(x3),:);
[t4,x4]=ode45('mateqn',t04,tf4,x04,1e-3);
t05=4.0001; tf5=4.999; x05=x4(length(x4),:);
[t5,x5]=ode45('mateqn',t05,tf5,x05,1e-3);
t06=5.0001; tf6=5.999; x06=x5(length(x5),:);
[t6,x6]=ode45('mateqn',t06,tf6,x06,1e-3);
%t07=6.0; tf7=6.999; x07=x6(length(x6),:);
%[t7,x7]=ode45('mateqn',t07,tf7,x07,1e-3);
%t08=7.0; tf8=7.999; x08=x7(length(x7),:);
%[t8,x8]=ode45('mateqn',t08,tf8,x08,1e-3);

```

```

% Combine the solution state matrix
xn=[x1;x2;x3;x4;x5;x6];%x7;x8];
tn=[t1;t2;t3;t4;t5;t6];%t7;t8];
save gh1 xn tn

```

APPENDIX D

POTHOLE COURSE COMPUTER CODE

This Appendix contains the computer code that was developed to model the terrain inputs for a road with a trench type pothole. This program calculates and plots a trace of a pothole profile and the axle path followed by circular wheel rolling through this type pothole. This program works for any pothole that can be model with a flat bottom, and sides that can be approximated as straight lines. The portion of the code shown below only works for potholes that have an entrance height that is equal to the exit height. Additional code to determine the terrain inputs for a any type of pothole is on file at the Naval Postgraduate School. Computer code was also developed to model bump inputs, such a log in a road and maintained on file at the Naval Postgraduate School.

COMPUTER CODE:

```
function [x,y,xa,u]=pothole(xent,depth,theta1,xbot,theta2,farht,xtrail);

% The call statement for this program/function is as %follows:
%       [x,y,xa,u]=pothole(xent,depth,theta1,xbot,theta2,farht,xtrail)

% Input parameters used in the call are defined as follows:
%   depth - the vertical distance from the bottom to the level
%           entrance surface.
%   theta1 - the angle of the decline on the entrance side, measured
%            from an extension of the level entrance surface to the decline.
%   xbot   - the horizontal distance across the bottom.
%   theta2 - the angle decline on the exit side, measured like theta1.
%   farht  - the vertical distance from the bottom to the level exit
%           surface.
%   xent   - the horizontal length of the level entrance region.
%   xtrail - the horizontal length of the level exit region.

% Output parameters
%   x - a column vector containing a discrete amount of evenly spaced 'x'
%       values that were used to calculate the profile and axle path.
%   y - a column vector that contains the 'y' values for the pothole
```

```
%      profile. The bottom of the pothole is defined as "zero" y value.
%      ya - a column vector containing the axle path 'y' values.
%      u   - a column vector containing the height of the bottom of the
%            wheel. 'u' is the input for the simulation model
```

```
% Other parameters assigned in the program:
%      deltax - the 'x' intraval spacing.
%      xent   - the horizontal length of the level entrance region.
%      xtrail - the horizontal length of the level exit region.
%      rad    - the radius of the wheel that is rolling through the pothole.
```

```
% Variables that are calculated based on the above assigned
% parameters:
%
%      rhteta1 & rtheta2 - the theta1 & theta2 in radians.
%      xnear & xfar - the x distance difference from the top to the
%                     bottom for the near & far sides.
%      xcrit1 & xcrit2 - the x value where the wheel can no longer
%                     follow a circular path as it goes around the near & far
%                     corners(near into hole, far out of hole).
%      xcr1 - the x value where the wheel hits the far side or corner
%      xcr2 - the x value from where the wheel hits the the exit region
%                     from the near side or near corner.
%      xch1 - the x value at the bottom corner on the entrance side.
%      xch2 - the x value at the bottom corner on the exit side.
%      xch3 - the x value at the top corner on the exit side.
%      xend - the ending x value of the pothole profile.
%      ycorn1 & ycorn2 - the y values when the axle is following a
%                     circular path around the near & far corners respectively
```

```
%*****assignment of pothole & wheel parameters*****
deltax=.01;      rad=17.0;
```

```
% ***** calculating other variables used *****
rtheta1=theta1*pi/180;      rtheta2=theta2*pi/180;
xnear=depth/tan(rtheta1);,  xfar=farht/tan(rtheta2);
xch1=xnear+xent;,           xch2=xch1+xbot;
xch3=xch2+xfar;,           xend=xch3+xtrail;
xcrit1=xent+rad*sin(rtheta1);,  xcrit2=xch3-rad*sin(rtheta2);
xcrit3=xent+rad*sin(rtheta2);,  xcrit4=xch3-rad*sin(rtheta2);
```

```
% converting/rounding x-switch values to integer increments of
```

```

% deltax; keeps the output x, y,&ya vectors the same size
num=xent/deltax;; num=round(num);,          xent=num*deltax;
num1=xch1/deltax;; num1=round(num1);,        xch1=num1*deltax;
num2=xch2/deltax;; num2=round(num2);,        xch2=num2*deltax;
num3=xch3/deltax;; num3=round(num3);,        xch3=num3*deltax;
num4=xend/deltax;; num4=round(num4);,        xend=num4*deltax;
xd1=xcrit1-xent;; n1=xd1/deltax;; n1=round(n1);,  xcrit1=xent +
n1*deltax;
xd2=xch3-xcrit2;; n2=xd2/deltax;; n2=round(n2);,  xcrit2=xch3 -
n2*deltax;

```

```

% ***** POTHOLE PROFILE *****

```

```

% ***** creating x vectors for pothole regions *****
x1=0:deltax:xent;;          siz1=size(x1);
x2=xent+deltax:deltax:xch1;;
x3=xch1+deltax:deltax:xch2;;          siz3=size(x3);
x4=xch2+deltax:deltax:xch3;;
x5=xch3+deltax:deltax:xend;;          siz5=size(x5);
x=[x1 x2 x3 x4 x5];

```

```

% ***** calculating y values for the pothole profile *****
y1=depth*ones(1:siz1(2));
y2= -tan(rtheta1)*x2 +tan(rtheta1)*xent + depth;
y3=zeros(1:siz3(2));
y4= tan(rtheta2)*x4 - tan(rtheta2)*xch2 ;
y5= farht*ones(1:siz5(2));
y=[y1 y2 y3 y4 y5];

```

```

% ***** AXLE PATH *****

```

```

% *****calculating the axle trace in the entrance region*****
xa1=0:deltax:xent;;siza1=size(xa1);
ya1=(depth+rad)*ones(1:siza1(2));
if xcrit2 <= xcrit1,
    %***checking if the axle motion is only circular****
    if xcrit2 > xent,
        %finding the x intercept of the near & far side circular motion
        for xint=xcrit2:deltax:xch3,
            y1=depth + sqrt((rad.^2) - ((xint-xent).^2));
            y2=farht + sqrt((rad.^2) - ((xint-xch3).^2));
            if y1<=y2; break,end
        end
    end
end

```

```

        end
    else
        for xint=xent+deltax:deltax:xch3,
            y1=depth + sqrt((rad.^2) - ((xint-xent).^2));
            y2=farht + sqrt((rad.^2) - ((xint-xch3).^2));
            if y1<=y2; break,end
        end
    end
    % calculating the near and far side y values for the axle path
    xa2=xent+deltax:deltax:xint;
    ya2=depth + sqrt((rad.^2) -((xa2-xent).^2));
    xa3=xint+deltax:deltax:xch3;
    ya3=farht + sqrt((rad.^2) -((xa3-xch3).^2));
    yac=[ya2 ya3] ;
    xa4=xch3+deltax:deltax:xend,,    siza4=size(xa4);
    ya4=(farht+rad)*ones(1:siza4(2));
    ya=[ya1 yac ya4];
    %checking & calculating axle path when its not just circular
else
    %****initializes a counter & the vector yac****
    n=0,,    nnum=(xch3-xent)/deltax,,    yac=zeros(1,nnum);
    %*****checks & determination of axle path*****
    for xa=xent+deltax:deltax:xch3,
        if xa <= xcrit1,
            ycorn1=depth + sqrt((rad.^2) - ((xa-xent).^2));
            yfar=tan(rtheta2)*xa-tan(rtheta2)*xch2+rad/cos(rtheta2);
            if ycorn1 > rad & ycorn1 > yfar, yac1=ycorn1;
            elseif yfar > rad, yac1=yfar;
            else yac1=rad; end
        elseif xa >= xcrit2,
            ycorn2=farht + sqrt((rad.^2) - ((xa-xch3).^2));
            ynear=-tan(rtheta1)*xa+tan(rtheta1)*xent...
                +depth+rad/cos(rtheta1);
            if ycorn2 > rad & ycorn2 > ynear, yac1=ycorn2;
            elseif ynear > rad, yac1=ynear;
            else yac1=rad; end
        else
            ynear=-tan(rtheta1)*xa+tan(rtheta1)*xent...
                +depth+rad/cos(rtheta1);
            yfar=tan(rtheta2)*xa-tan(rtheta2)*xch2+rad/cos(rtheta2);
            if ynear > yfar & ynear > rad, yac1=ynear;
            elseif yfar > rad, yac1=yfar;

```

```

        else yac1=rad; end
    end
    n=n+1;;      yac(1,n)=yac1;
end
    %***** axle y values in the exit region *****
    xa4=xch3+deltax:deltax:xend;;    size4=size(xa4);
    ya4=(farht+rad)*ones(1:size4(2));
    ya=[ya1 yac ya4];
end
%***** PLOT OF POTHOLE PROFILE & AXLE PATH *****

ax=[0,xend,-50,yplot];
y=y-depth; ya=ya-depth;u=ya-17;
x=x';y=y';ya=ya';u=u';
matrix=[x y ya u];
save road2dat.m matrix
axis(ax);
plot(x,y); hold on ; plot(x,ya) ,pause,hold off

```


APPENDIX E **NATURAL FREQUENCIES AND MODE SHAPES**

Table E-1 below contains the natural frequencies and mode shapes of the HUMMV/Howitzer system. They were calculated using the procedures described in Chapter IV. In Table E-1 the system's natural frequencies are listed in the top row. The positional coordinate values of the mode shape which corresponds to a particular natural frequency are listed in the column below the natural frequency. The natural frequencies shown in Table E-1 have units of hertz. The positional coordinates have units of inches for Z_1 , Z_2 , Z_3 , and Z_4 , and radians for the rotational coordinates θ_1 , θ_2 , and θ_3 .

TABLE E-1 NATURAL FREQUENCIES AND MODE SHAPES

<u>Coordi- nates</u>	<u>Natural Frequencies</u>						
	<u>1.286</u>	<u>1.870</u>	<u>3.328</u>	<u>12.26</u>	<u>13.61</u>	<u>18.51</u>	<u>23.80</u>
Z_1	-.0001	.0783	-.2392	-.0212	1.217	.0130	.0342
Z_2	.0130	.1293	.1425	.0076	.0364	-1.222	-.1221
Z_3	.0140	.2057	-.0408	.0018	-.0221	.0138	.0277
Z_4	-.1064	.0168	.0202	-1.385	-0.221	-.0097	.0341
θ_1	.0002	.0003	.0059	.0001	.0011	.0005	.0025
θ_2	-.0025	-.0013	-.0026	.0001	-.0003	-.0001	-.0036
θ_3	-.0025	-.0013	-.0027	.0003	-.0006	-.0011	.0063

APPENDIX F

A-FRAME CALIBRATION DATA

The following tables contain the load versus strain data that was recorded during the A-Frame calibration procedures that are described in Chapter V. The locations of the strain gages is shown on Figures 5-1 and 5-6. Tables F-1 and F-2 contain the data from the vertical load tests and Tables F-3 and F-4 contain the data from the lateral load tests. The method used to calculate stress values from the strain gage readings is described in Chapter V.

TABLE F-1 VERTICAL TEST #1 A-FRAME CALIBRATION DATA

A-FRAME VERTICAL LOAD TEST 1													
FORCE (LBS)	2000	3020	4000	5020	6000	7000	8000	9000	10000	8500	6500	4500	2500
STRAIN GAGES													
STRAIN GAGE PAIR 1													
GAGE 1	-280	-423	-548	-666	-758	-848	-950	-1060	-1175	-957	-663	-354	-72
GAGE 2	-118	-164	-224	-321	-405	-501	-599	-702	-800	-700	-588	-515	-401
AVG STRAIN 1&2	-199	-294	-386	-494	-582	-675	-775	-881	-988	-829	-626	-435	-237
AXIAL STRESS (KSI)	1.99	2.94	3.86	4.94	5.82	6.75	7.75	8.81	9.88	8.29	6.25	4.34	2.37
BENDING STRESS (KSI)	0.81	1.30	1.62	1.72	1.77	1.74	1.76	1.79	1.88	1.29	0.38	0.81	1.65
STRAIN GAGE PAIR 2													
GAGE 5	-93	-192	-286	-397	-487	-577	-672	-782	-892	-727	-517	-271	-88
GAGE 8	-323	-420	-511	-614	-700	-793	-882	-970	-1055	-923	-748	-618	-422
AVG STRAIN 5 & 8	-208	-306	-399	-506	-594	-685	-777	-876	-974	-825	-633	-445	-255
AXIAL STRESS (KSI)	2.08	3.06	3.99	5.05	5.94	6.85	7.77	8.76	9.73	8.25	6.33	4.44	2.55
BENDING STRESS (KSI)	1.15	1.14	1.13	1.08	1.06	1.08	1.05	0.94	0.82	0.98	1.16	1.74	1.67
STRAIN GAGE PAIR 3													
GAGE 6	-310	-428	-550	-687	-809	-948	-1083	-1217	-1356	-1186	-932	-721	-421
GAGE 7	-203	-297	-382	-485	-561	-637	-713	-796	-880	-749	-580	-370	-226
AVG STRAIN 6 & 7	-257	-363	-466	-586	-685	-793	-898	-1007	-1118	-968	-756	-546	-324
AXIAL STRESS (KSI)	2.57	3.63	4.66	5.86	6.85	7.93	8.98	10.08	11.18	9.68	7.56	5.40	3.24
BENDING STRESS (KSI)	0.53	0.66	0.84	1.01	1.24	1.56	1.85	2.11	2.38	2.19	1.76	1.76	0.98
STRAIN GAGE PAIR 4													
GAGE 9	52	-86	-230	-398	-529	-669	-789	-925	-1047	-826	-522	-223	35
GAGE 10	-534	-602	-669	-745	-810	-884	-968	-1055	-1143	-1050	-933	-801	-628
AVG STRAIN 9 & 10	-241	-344	-450	-571	-670	-777	-884	-990	-1095	-938	-728	-512	-297
AXIAL STRESS (KSI)	2.41	3.44	4.50	5.71	6.70	7.77	8.84	9.90	10.95	9.38	7.27	5.12	2.97
BENDING STRESS (KSI)	2.83	2.58	2.20	1.75	1.41	1.07	0.85	0.65	0.48	1.12	2.06	2.89	3.31

TABLE F-1 VERTICAL TEST #1 A-FRAME CALIBRATION DATA (CONT)

A-FRAME VERTICAL LOAD TEST 1 (CONT)														
FORCE (LBS)	2000	3020	4000	5020	6000	7000	8000	9000	10000	8500	6500	4500	2500	
<u>STRAIN GAGES</u>														
GAGE 3 (CLAMP)	-3	14	20	27	35	44	53	61	69	40	4	-21	-31	
CLAMP STRESS (KSI)	-0.03	0.14	0.2	0.27	0.35	0.44	0.53	0.61	0.69	0.4	0.04	-0.21	-0.31	
GAGE 4 (CROSS BAR)	-68	-78	-86	-99	-108	-119	-129	-142	-155	-144	-129	-112	-93	
CROSS BAR STRESS (KSI)	-0.68	-0.78	-0.86	-0.99	-1.08	-1.19	-1.29	-1.42	-1.55	-1.44	-1.29	-1.12	-0.93	
<u>STRAIN ROSETTE</u>														
GAGE 11 (TRANSVERSE)	35	55	78	110	146	191	244	305	368	303	233	160	85	
GAGE 12 (45 DEGREE)	-129	-194	-250	-312	-347	-372	-401	-433	-459	-381	-286	-191	-116	
GAGE 13 (AXIAL)	-187	-292	-391	-502	-612	-740	-882	-1054	-1226	-989	-683	-426	-157	

TABLE F-2 VERTICAL TEST #2 A-FRAME CALIBRATION DATA

A-FRAME VERTICAL LOAD TEST 2														
FORCE (LBS)	2500	3500	4500	5500	6500	7500	8500	9500	10500	9000	7500	6000	4500	3000
STRAIN GAGES														
STRAIN GAGE PAIR 1														
GAGE 1	-186	-331	-478	-629	-780	-908	-1033	-1151	-1255	-1031	-811	-580	-347	-128
GAGE 2	-317	-367	-415	-466	-515	-577	-655	-747	-851	-752	-660	-589	-532	-452
AVG STRAIN 1&2	-252	-349	-447	-548	-648	-743	-844	-949	-1053	-892	-736	-585	-440	-289
AXIAL STRESS (KSI)	2.51	3.49	4.48	5.48	6.48	7.43	8.44	9.49	10.53	8.92	7.36	5.95	4.40	2.89
BENDING STRESS (KSI)	0.66	0.18	0.32	0.82	1.33	1.66	1.89	2.02	2.02	1.40	0.76	0.05	0.92	1.63
STRAIN GAGE PAIR 2														
GAGE 5	-235	-340	-433	-529	-639	-737	-864	-998	-1124	-947	-779	-614	-452	-283
GAGE 8	-284	-372	-471	-569	-660	-740	-814	-880	-938	-810	-686	-562	-438	-318
AVG STRAIN 5 & 8	-260	-356	-452	-549	-650	-739	-839	-939	-1031	-879	-733	-588	-445	-300
AXIAL STRESS (KSI)	2.60	3.56	4.52	5.49	6.50	7.39	8.39	9.39	10.31	8.78	7.33	5.98	4.45	3.00
BENDING STRESS (KSI)	0.24	0.16	0.19	0.20	0.11	0.02	0.25	0.59	0.93	0.69	0.47	0.26	0.07	0.17
STRAIN GAGE PAIR 3														
GAGE 6	-183	-305	-444	-587	-721	-845	-963	-1071	-1175	-1007	-826	-641	-461	-274
GAGE 7	-278	-365	-437	-509	-598	-677	-774	-880	-984	-840	-712	-578	-448	-317
AVG STRAIN 6 & 7	-231	-335	-441	-548	-660	-761	-869	-976	-1080	-924	-769	-610	-455	-296
AXIAL STRESS (KSI)	2.31	3.35	4.40	5.48	6.60	7.61	8.68	9.76	10.80	9.23	7.69	6.10	4.55	2.96
BENDING STRESS (KSI)	0.48	0.30	0.04	0.39	0.62	0.84	0.95	0.96	0.96	0.84	0.57	0.32	0.07	0.21
STRAIN GAGE PAIR 4														
GAGE 9	-16	-147	-282	-428	-576	-711	-838	-966	-1090	-866	-651	-429	-220	-43
GAGE 10	-448	-523	-599	-672	-740	-812	-893	-977	-1062	-961	-868	-774	-669	-436
AVG STRAIN 9 & 10	-232	-335	-441	-550	-659	-762	-866	-972	-1076	-914	-760	-602	-445	-240
AXIAL STRESS (KSI)	2.32	3.35	4.40	5.50	6.59	7.62	8.66	9.72	10.76	9.14	7.60	6.02	4.44	2.40
BENDING STRESS (KSI)	2.16	1.88	1.58	1.22	0.81	0.51	0.28	0.06	0.14	0.48	1.08	1.72	2.24	1.96

TABLE F-2 VERTICAL TEST #2 A-FRAME CALIBRATION DATA (CONT)

A-FRAME VERTICAL LOAD TEST 2 (CONT)														
FORCE (LBS)	2000	3020	4000	5020	6000	7000	8000	9000	10000	8500	6500	4500	2500	
<u>STRAIN GAGES</u>														
GAGE 3 (CLAMP)	67	72	79	87	95	105	113	112	127	98	73	50	39	30
CLAMP STRESS (KSI)	0.67	0.72	0.79	0.87	0.95	1.05	1.13	1.12	1.27	0.98	0.73	0.5	0.39	0.3
GAGE 4 (CROSS BAR)	-81	-89	-96	-102	-111	-116	-127	-140	-156	-143	-128	-120	-108	-92
CROSS BAR STRESS (KS)	-0.81	-0.89	-0.96	-1.02	-1.11	-1.16	-1.27	-1.4	-1.56	-1.43	-1.28	-1.2	-1.08	-0.92
<u>STRAIN ROSETTE</u>														
GAGE 11 (TRANSVERSE)	63	91	123	158	193	235	284	340	406	341	275	219	168	111
GAGE 12 (45 DEGREE)	-155	-193	-227	-262	-300	-333	-370	-408	-440	-362	-291	-244	-162	-109
GAGE 13 (AXIAL)	-235	-338	-454	-618	-754	-899	-1047	-1210	-1396	-1157	-923	-706	-500	-291

TABLE F-3 LATERAL TEST #1 A-FRAME CALIBRATION DATA

A-FRAME LATERAL LOAD TEST 1																
FORCE (LBS)	540	1025	2040	2520	3090	3580	4100	3475	2990	2465	1910	1610	960	480		
STRAIN GAGES																
STRAIN GAGE PAIR 1																
GAGE 1	108	71	-96	-182	-280	-371	-482	-381	-306	-224	-131	-101	-12	14		
GAGE 2	-305	-443	-631	-715	-815	-894	-999	-856	-770	-681	-555	-493	-311	-188		
AVG STRAIN 1&2	-99	-186	-384	-449	-548	-633	-741	-619	-538	-453	-343	-297	-162	-87		
AXIAL STRESS (KSI)	0.98	1.86	3.64	4.49	5.48	6.33	7.41	6.19	5.38	4.53	3.43	2.97	1.62	0.87		
BENDING STRESS (KSI)	2.07	2.57	2.88	2.67	2.88	2.62	2.59	2.38	2.32	2.28	2.12	1.96	1.50	1.01		
STRAIN GAGE PAIR 2																
GAGE 5	-129	-188	-320	-389	-470	-540	-622	-510	-441	-365	-274	-234	-115	-52		
GAGE 8	-76	-204	-437	-548	-673	-775	-888	-749	-647	-540	-416	-360	-212	-128		
AVG STRAIN 5 & 8	-103	-196	-379	-469	-572	-658	-755	-630	-544	-453	-345	-297	-164	-90		
AXIAL STRESS (KSI)	1.03	1.96	3.79	4.69	5.72	6.58	7.55	6.30	5.44	4.53	3.45	2.97	1.64	0.90		
BENDING STRESS (KSI)	0.26	0.08	0.58	0.79	1.02	1.17	1.33	1.19	1.03	0.88	0.71	0.63	0.49	0.38		
STRAIN GAGE PAIR 3																
GAGE 6	109	229	424	519	611	700	800	765	595	511	403	357	221	143		
GAGE 7	97	165	350	448	568	668	779	743	547	449	327	275	131	60		
AVG STRAIN 6 & 7	103	197	387	483	588	683	789	754	571	480	365	316	176	101		
AXIAL STRESS (KSI)	1.03	1.97	3.67	4.63	5.68	6.63	7.69	7.54	5.71	4.80	3.65	3.16	1.76	1.01		
BENDING STRESS (KSI)	0.06	0.32	0.37	0.36	0.23	0.17	0.11	0.11	0.24	0.31	0.38	0.41	0.45	0.42		
STRAIN GAGE PAIR 4																
GAGE 9	-91	34	298	412	525	620	740	636	564	489	393	349	232	152		
GAGE 10	294	355	463	535	630	720	824	668	564	455	318	264	100	33		
AVG STRAIN 9 & 10	102	194	380	473	577	670	782	651	584	472	355	306	166	92		
AXIAL STRESS (KSI)	1.02	1.94	3.80	4.73	5.77	6.70	7.82	6.51	5.64	4.72	3.55	3.06	1.66	0.92		
BENDING STRESS (KSI)	1.93	1.61	0.83	0.62	0.52	0.50	0.42	0.15	0.00	0.17	0.38	0.43	0.66	0.59		

TABLE F-3 LATERAL TEST #1 A-FRAME CALIBRATION DATA (CONT)

A-FRAME LATERAL LOAD TEST 1 (CONT)																
FORCE (LBS)	540	1025	2040	2520	3090	3580	4100	3475	2990	2465	1910	1610	860	480		
STRAIN GAGES																
GAGE 3 (CLAMP)	20	25	27	30	35	36	37	22	13	6	5	7	0	0		
CLAMP STRESS (KSI)	0.2	0.25	0.27	0.3	0.35	0.36	0.37	0.22	0.13	0.06	0.05	0.07	0	0		
GAGE 4 (CROSS BAR)	-30	-36	-30	-24	-18	-8	0	-2	-6	-8	-11	-14	-15	-16		
CROSS BAR STRESS (KSI)	-0.3	-0.38	-0.3	-0.24	-0.18	-0.08	0	-0.02	-0.06	-0.08	-0.11	-0.14	-0.15	-0.16		
STRAIN ROSETTE																
GAGE 11 (TRANSVERSE)	49	77	120	129	152	178	230	218	204	188	149	126	75	37		
GAGE 12 (45 DEGREE)	8	-71	-120	-144	-176	-200	-235	-213	-191	-168	-128	-111	-71	-50		
GAGE 13 (AXIAL)	-23	-82	-204	-242	-314	-394	-543	-502	-455	-403	-294	-237	-118	-46		

TABLE F-4 LATERAL TEST #2 A-FRAME CALIBRATION DATA

A-FRAME LATERAL LOAD TEST 2													
FORCE (LBS)	590	975	1500	2060	2925	3575	3000	2450	2000	1500	970	500	
STRAIN GAGES													
STRAIN GAGE PAIR 1													
GAGE 1	16	-45	-111	-197	-330	-431	-332	-246	-166	-98	-34	10	
GAGE 2	-250	-326	-445	-560	-730	-855	-745	-649	-562	-457	-331	-200	
AVG STRAIN 1&2	-117	-186	-278	-379	-530	-643	-539	-448	-364	-276	-183	-95	
AXIAL STRESS (KSI)	1.17	1.85	2.78	3.79	5.30	6.43	5.39	4.48	3.64	2.78	1.83	0.95	
BENDING STRESS (KSI)	1.33	1.41	1.87	1.82	2.00	2.12	2.07	2.01	1.98	1.80	1.49	1.05	
STRAIN GAGE PAIR 2													
GAGE 5	-99	-160	-242	-330	-462	-560	-458	-377	-306	-233	-150	-73	
GAGE 8	-142	-226	-331	-447	-630	-768	-650	-534	-431	-330	-225	-126	
AVG STRAIN 5 & 8	-121	-193	-287	-389	-546	-664	-554	-456	-369	-282	-188	-100	
AXIAL STRESS (KSI)	1.20	1.93	2.87	3.89	5.46	6.64	5.54	4.56	3.69	2.82	1.88	1.00	
BENDING STRESS (KSI)	0.21	0.33	0.45	0.58	0.84	1.04	0.96	0.78	0.63	0.49	0.38	0.26	
STRAIN GAGE PAIR 3													
GAGE 6	127	204	300	406	585	674	561	488	384	295	201	111	
GAGE 7	98	169	266	378	551	681	567	460	365	266	168	80	
AVG STRAIN 6 & 7	113	187	284	393	559	678	567	468	377	283	187	98	
AXIAL STRESS (KSI)	1.13	1.87	2.84	3.93	5.56	6.78	5.67	4.68	3.77	2.83	1.87	0.98	
BENDING STRESS (KSI)	0.15	0.18	0.17	0.14	0.07	0.04	0.03	0.04	0.10	0.15	0.17	0.16	
STRAIN GAGE PAIR 4													
GAGE 9	125	188	279	378	520	631	536	455	360	301	209	120	
GAGE 10	107	191	295	414	598	726	594	474	373	266	160	72	
AVG STRAIN 9 & 10	116	190	290	399	580	678	573	471	383	290	191	104	
AXIAL STRESS (KSI)	1.16	1.90	2.90	3.99	5.60	6.78	5.73	4.71	3.83	2.90	1.91	1.04	
BENDING STRESS (KSI)	0.09	0.02	0.08	0.16	0.39	0.46	0.29	0.10	0.04	0.18	0.24	0.24	

TABLE F-4 LATERAL TEST #2 A-FRAME CALIBRATION DATA (CONT)

A-FRAME LATERAL LOAD TEST 2 (CONT)													
FORCE (LBS)	590	975	1500	2060	2925	3575	3000	2450	2000	1500	970	500	
STRAIN GAGES													
GAGE 3 (CLAMP)	12	21	28	34	40	42	28	16	11	6	4	5	
CLAMP STRESS (KSI)	0.12	0.21	0.28	0.34	0.4	0.42	0.28	0.16	0.11	0.06	0.04	0.05	
GAGE 4 (CROSS BAR)	-6	-6	-5	-3	8	12	10	6	1	-5	-4	-2	
CROSS BAR STRESS (KSI)	-0.06	-0.06	-0.05	-0.03	0.08	0.12	0.1	0.06	0.01	-0.05	-0.04	-0.02	
STRAIN ROSETTE													
GAGE 11 (TRANSVERSE)	38	57	87	113	155	192	176	164	144	112	77	40	
GAGE 12 (45 DEGREE)	-25	-57	-86	-118	-167	-206	-179	-154	-126	-97	-69	-46	
GAGE 13 (AXIAL)	-45	-101	-175	-249	-370	-470	-418	-330	-304	-220	-136	-59	

APPENDIX G

HOWITZER ORIENTATION PICTURES AND DIAGRAMS

This Appendix contains pictures and diagrams that identify the key components of the M119 Howitzer that were important for this study.

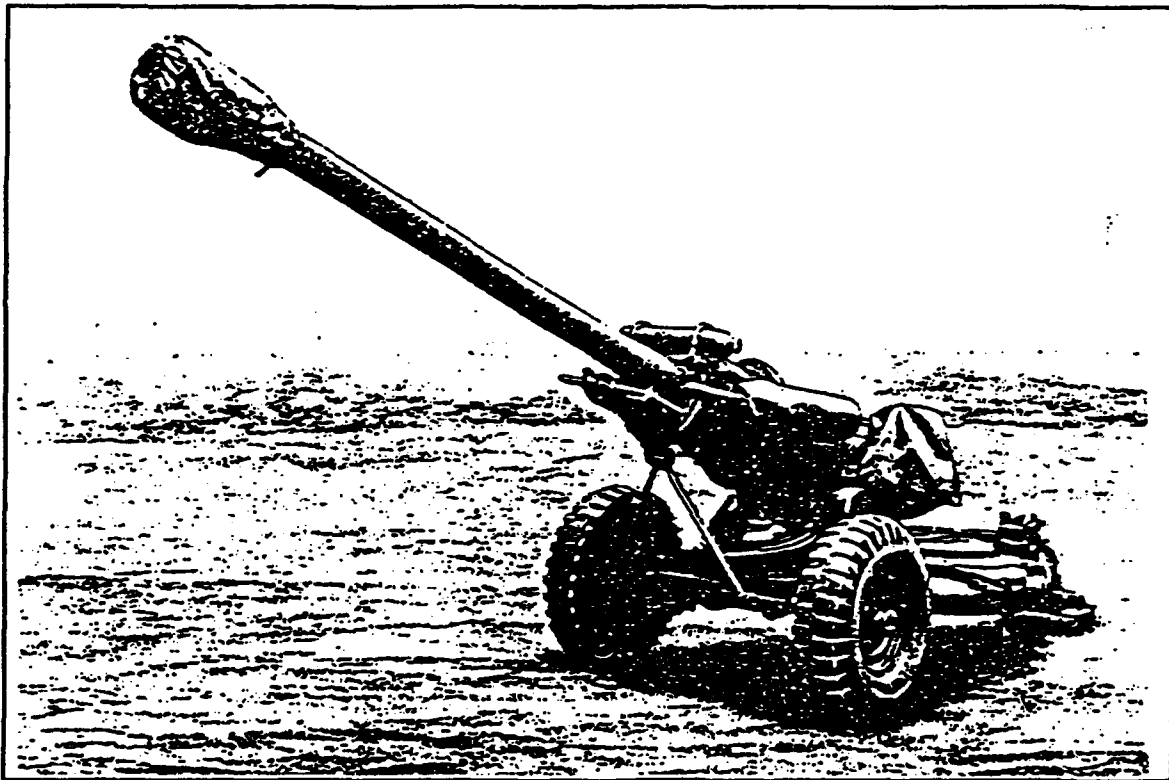


Figure G-1 Towing in Firing Position

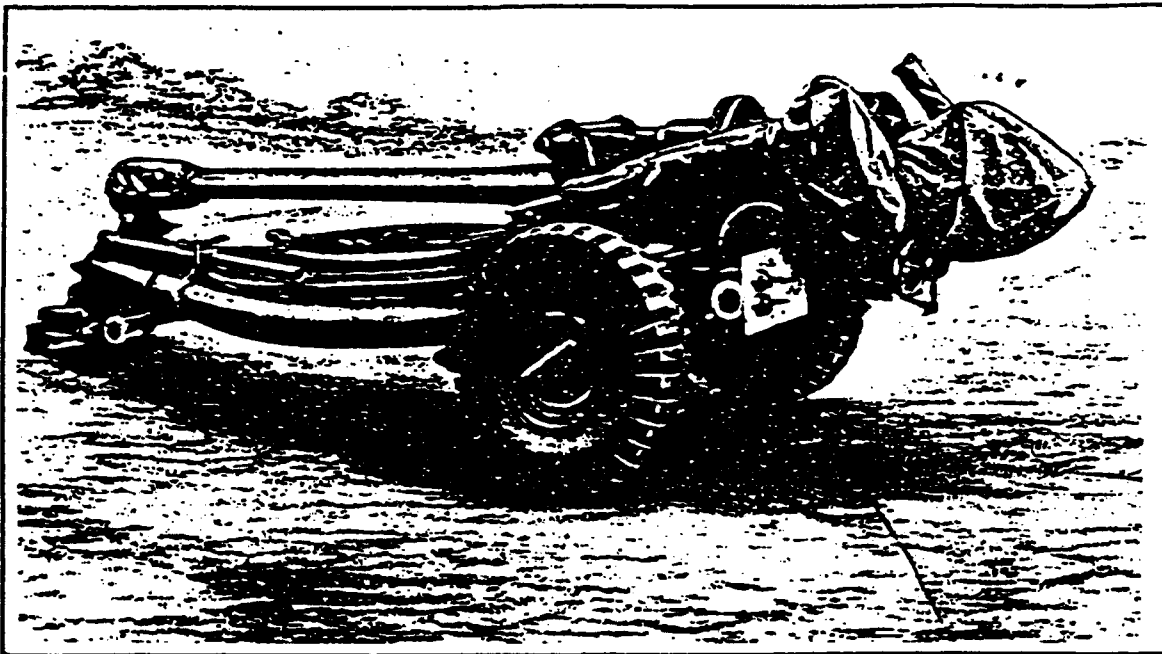


Figure G-2 Towing in Stowed Position

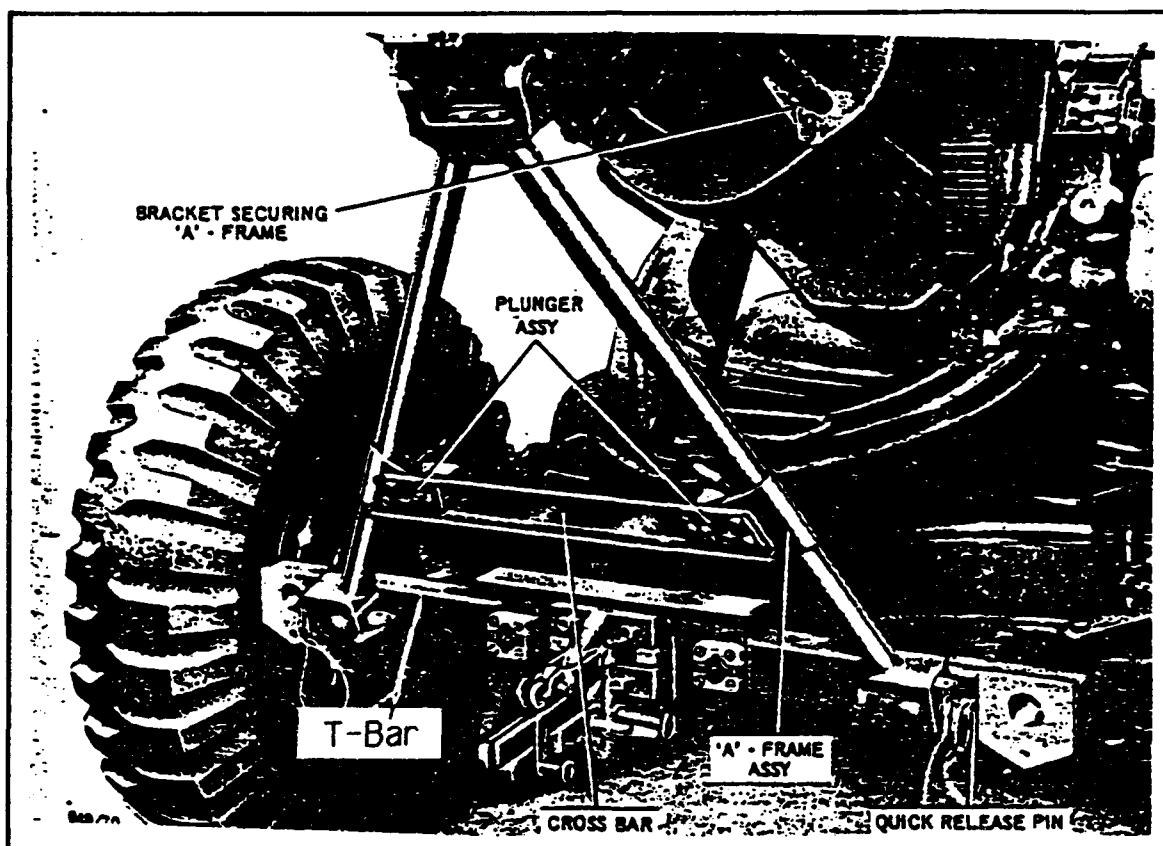


Figure G-3 A-Frame/T-Bar Support

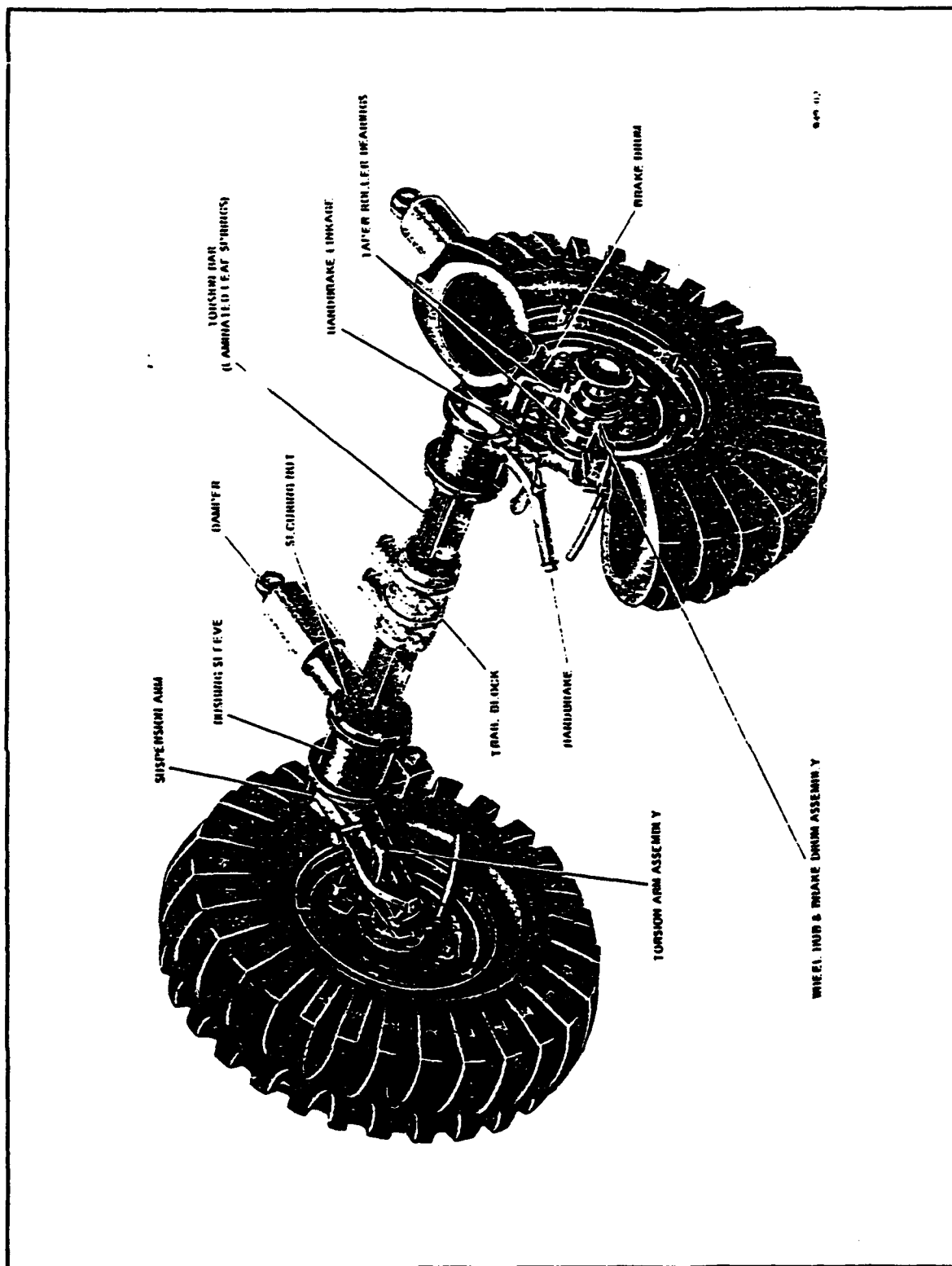


Figure G-5 Howitzer Wheels and Suspension

LIST OF REFERENCES

1. US Army Tank-Automotive Command Technical Report Number 13337, "Failure Analysis of the Lower Ball Joint on the High-Mobility Multipurpose Wheeled Vehicle (HUMMV)", Warren, MI, August 1988.
2. US Army Combat Systems Test Activity Report, Test Record Number: P-83179, "Physical Properties of the 105mm M119 Howitzer", Aberdeen Proving Grounds, MD, January, 1990.
3. Roark, Raymond J. and Young, Warren C., Formulas for Stress and Strain, McGraw-Hill Company, 1982.

INITIAL DISTRIBUTION LIST

1. Defense Technical Information Center 2
Cameron Station
Alexandria, VA 22304-6145
2. Library, Code 052 2
Naval Postgraduate School
Monterey, CA 93943-5000
3. Chairman Code ME/KK 1
Department of Mechanical Engineering
Naval Postgraduate School
Monterey, CA 93943-5000
4. Naval Engineering Curricular Office, Code 34 1
Naval Postgraduate School
Monterey, CA 93943-5000
5. Dr. Anthony J. Healey, Code ME/HY 1
Department of Mechanical Engineering
Naval Postgraduate School
Monterey, CA 93943-5000
6. CPT Ole Knudson 1
Office of the Product Manager, Paladin
Picatinny Arsenal, NJ 07806-5000
7. Commander, AMCCOM 1
Weapons Systems Management Directorate
ATTN: AMSMC-ASA-H
Rock Island, IL 61299-6000
8. Headquarters, US Army ARDEC 1
Fire Support Armaments Center
ATTN: SMCAR-FSA-T
Picatinny Arsenal, NJ 07806-5000
9. Commander, US Army Field Artillery School 1
Gunnery Department
ATTN: Concepts and Procedures
Fort Sill, OK 73503

- | | |
|---|---|
| 10. CPT David Anderson
Department of Mechanical Engineering
West Point NY 10996 | 1 |
| 11. CPT Stephen A. Rogers
Office of the Product Manager, Paladin
Picatinny Arsenal, NJ 07806-5000 | 1 |
| 12. LTC (Ret) Melvin Miller
2790 Hickory Hill Court
Bettendorf, IA 52722 | 1 |
| 13. Dr. Joshua Gordis, Code ME/GO
Department of Mechanical Engineering
Naval Postgraduate School
Monterey, CA 93943-5000 | 1 |